



**HAL**  
open science

## A fusion peptide in preS1 and the human protein-disulfide isomerase ERp57 are involved in HBV membrane fusion process

Jimena Pérez-Vargas, Elin Teppa, Fouzia Amirache, Bertrand Boson, Rémi Pereira de Oliveira, Christophe Combet, Anja Böckmann, Floriane Fusil, Natalia Freitas, Alessandra Carbone, et al.

### ► To cite this version:

Jimena Pérez-Vargas, Elin Teppa, Fouzia Amirache, Bertrand Boson, Rémi Pereira de Oliveira, et al.. A fusion peptide in preS1 and the human protein-disulfide isomerase ERp57 are involved in HBV membrane fusion process. *eLife*, 2021, 10, 10.7554/eLife.64507 . hal-03275938

**HAL Id: hal-03275938**

<https://hal.sorbonne-universite.fr/hal-03275938v1>

Submitted on 1 Jul 2021

**HAL** is a multi-disciplinary open access archive for the deposit and dissemination of scientific research documents, whether they are published or not. The documents may come from teaching and research institutions in France or abroad, or from public or private research centers.

L'archive ouverte pluridisciplinaire **HAL**, est destinée au dépôt et à la diffusion de documents scientifiques de niveau recherche, publiés ou non, émanant des établissements d'enseignement et de recherche français ou étrangers, des laboratoires publics ou privés.

1 **A fusion peptide in preS1 and the human protein-disulfide isomerase ERp57 are involved in**  
2 **hepatitis B virus membrane fusion process**

3  
4 **Authors:**

5 Jimena Pérez-Vargas<sup>1,\*</sup>, Elin Teppa<sup>2,3,\*</sup>, Fouzia Amirache<sup>1</sup>, Bertrand Boson<sup>1</sup>, Rémi Pereira de  
6 Oliveira<sup>1</sup>, Christophe Combet<sup>4</sup>, Anja Böckmann<sup>5</sup>, Floriane Fusil<sup>1</sup>, Natalia Freitas<sup>1,\*\*</sup>, Alessandra  
7 Carbone<sup>2,\*\*,\$</sup> and François-Loïc Cosset<sup>1,\*\*,\$</sup>

8  
9 **Affiliations:**

10 <sup>1</sup>CIRI – Centre International de Recherche en Infectiologie, Univ Lyon, Université Claude Bernard  
11 Lyon 1, Inserm, U1111, CNRS, UMR5308, ENS Lyon, 46 allée d'Italie, F-69007, Lyon, France.

12 <sup>2</sup>Sorbonne Université, CNRS, IBPS, Laboratoire de Biologie Computationnelle et Quantitative (LCQB)  
13 - UMR 7238, 4 place Jussieu, 75005 Paris, France.

14 <sup>3</sup>Sorbonne Université, Institut des Sciences du Calcul et des Données (ISCD), 4 place Jussieu, 75005  
15 Paris, France.

16 <sup>4</sup>Cancer Research Center of Lyon (CRCL), UMR Inserm 1052 - CNRS 5286 mixte CLB – UCBL1, F-  
17 69008 Lyon, France.

18 <sup>5</sup>Molecular Microbiology and Structural Biochemistry, UMR5086 CNRS-Université Lyon 1, 7 passage  
19 du Vercors, 69367 Lyon, France.

20  
21 \*These authors contributed equally to the work.

22 \*\*These senior authors contributed equally to the work.

23  
24 <sup>\$</sup>Corresponding authors: Address: ENS Lyon, 46 allée d'Italie, F-69007, Lyon, France ; tel:  
25 +33472728732; e-mail: [flcosset@ens-lyon.fr](mailto:flcosset@ens-lyon.fr)

26 Address: LCQB, Sorbonne Université, 4 place Jussieu, 75005 Paris,  
27 France; tel: +33144277345; e-mail: [alessandra.carbone@sorbonne-universite.fr](mailto:alessandra.carbone@sorbonne-universite.fr)

28  
29 **Short title:**

30 Hepatitis B virus membrane fusion determinants

31 **Summary**

32

33 Cell entry of enveloped viruses relies on the fusion between the viral and plasma or endosomal  
34 membranes, through a mechanism that is triggered by a cellular signal. Here we used a combination  
35 of computational and experimental approaches to unravel the main determinants of hepatitis B virus  
36 (HBV) membrane fusion process. We discovered that ERp57 is a host factor critically involved in  
37 triggering HBV fusion and infection. Then, through modelling approaches, we uncovered a putative  
38 allosteric cross-strand disulfide (CSD) bond in the HBV S glycoprotein and we demonstrate that its  
39 stabilization could prevent membrane fusion. Finally, we identified and characterized a potential fusion  
40 peptide in the preS1 domain of the HBV L glycoprotein. These results underscore a membrane fusion  
41 mechanism that could be triggered by ERp57, allowing a thiol/disulfide exchange reaction to occur and  
42 regulate isomerization of a critical CSD, which ultimately leads to the exposition of the fusion peptide.

43

44

## 45 Introduction

46

47 Hepatitis B is a major public health problem; it affects over 250 million people worldwide and 850,000  
48 deaths occur each year as a result of hepatitis B complications (WHO, March 2015). The structure of  
49 its etiological agent, the hepatitis B virus (HBV), features a nucleocapsid that is surrounded by a lipid  
50 bilayer containing the envelope glycoproteins (GPs) designated as the small (S), medium (M) and  
51 large (L), which are the product of a single open reading frame. They share the C-terminal S-domain  
52 that contains four putative transmembrane domains. The L and M proteins have N-terminal extensions  
53 (preS1/prS2 and preS2, respectively) that mediate diverse functions in nucleocapsid binding and  
54 receptor recognition (Baumert et al., 2014). The first 2-75 amino acids sequence of the preS1 domain  
55 of the L protein (Blanchet and Sureau, 2007; Bremer et al., 2011; Le Seyec et al., 1999) and the  
56 antigenic loop (AGL) of the S domain (Le Duff et al., 2009; Salisse and Sureau, 2009; Schulze et al.,  
57 2007) have been identified as essential determinants for infectivity of HBV and hepatitis delta virus  
58 (HDV).

59 Entry of enveloped viruses into cells can be defined as the sequence of events occurring from the  
60 attachment of the virus to the host cell until the release of the genome in the cytoplasm, *via* fusion  
61 between viral and cellular membrane. Like for most enveloped viruses, HBV entry into cells is a finely  
62 regulated and complex process consisting in different steps, in which several viral and cellular factors  
63 are involved. Its first step involves low-affinity binding to heparan sulfates proteoglycans (HSPGs)  
64 residing on the hepatocytes' surface (Leistner et al., 2008; Schulze et al., 2007). This attachment is  
65 mediated by the preS1 region of the L protein and/or the antigenic loop of the S protein (Ni et al.,  
66 2014; Schulze et al., 2007). Afterwards, the virus interacts with its high-affinity receptor, the sodium  
67 taurocholate-cotransporting polypeptide (NTCP) (Ni et al., 2014; Yan et al., 2012) through the amino-  
68 terminal end of the L protein preS1 domain (Glebe et al., 2005a; Gripon et al., 2005; Yan et al., 2012).  
69 NTCP is an integral membrane protein, expressed at the basolateral membrane of hepatocytes, which  
70 explains the tropism of HBV for the liver.

71 The post-binding entry steps of HBV occur through endocytosis; however, the exact mechanism is still  
72 unclear and somehow controversial. One early study showed that HBV in HepaRG cells is internalized  
73 *via* caveolin-mediated endocytosis (Macovei et al., 2010). Nevertheless, inhibition of caveolin-  
74 mediated endocytosis or silencing of caveolin-1 did not impair HBV infection in Tupaia hepatocytes  
75 (Bremer et al., 2009) or in HepaG2-NTCP cells (Herrscher et al., 2020). Contrastingly, several other  
76 studies presented evidence that HBV endocytosis is clathrin-dependent (Herrscher et al., 2020; Huang  
77 et al., 2012; Umetsu et al., 2018). Recent studies reported that HBV infection of HepaRG cells  
78 depends on Rab5 and Rab7 (Macovei et al., 2013), which are GTPases involved in the biogenesis of  
79 endosomes, and that the epidermal growth factor receptor (EGFr) is a host-entry cofactor that  
80 interacts with NTCP and mediates HBV internalization (Iwamoto et al., 2019). These findings support

81 the hypothesis that HBV is transported from early to mature endosomes. After the early endosome  
82 stage, translocation is associated with a gradually decreasing pH, from about 6.2 in early endosomes  
83 to close to 5.5 in late endosomes, which allows fusion of many enveloped viruses with the endosomal  
84 membrane. However, in the case of HBV, pharmacological agents that raise or neutralize the pH in  
85 the endocytic pathway do not affect infection (Macovei et al., 2010, 2013; Rigg and Schaller, 1992).  
86 Furthermore, treatment with protease inhibitors have no effect on infection (Macovei et al., 2013),  
87 suggesting that HBV transport into the degradative branch of the endocytic pathway is not required  
88 *per se* to initiate this process.

89 Virus entry by membrane fusion involves interactions between viral fusion proteins and host receptors,  
90 which results in conformational changes of the virus envelope proteins. However, the molecular  
91 determinants and mechanism of membrane fusion of HBV remain to be defined. Previous results  
92 indicated the essential role of the cysteine residues of the antigenic loop, as shown by the reduction of  
93 virus entry levels by inhibitors of thiol/disulfide exchange reaction (Abou-Jaoudé and Sureau, 2007),  
94 hence suggesting a redox state responsible for conformational changes that can have a role during  
95 the fusion step.

96 Here, using a combination of computational and experimental approaches, we sought to better  
97 understand how HBV induces the fusion of its lipid membrane with that of the infected cell.  
98 Specifically, using a coevolution analysis of HBV GPs and molecular modelling combined with  
99 experimental investigations *ex vivo* in molecular virology and *in vivo* in liver humanized mice, we  
100 provide evidence that the mechanism triggering HBV membrane fusion involves ERp57, a cellular  
101 protein disulfide isomerase. Furthermore, our results highlight the role of specific cysteines in the AGL  
102 determinant and well as a sequence (aa 48 to 66) in the preS1 determinant that could ultimately act as  
103 a fusion peptide mediating HBV membrane fusion.

104

105

## 106 **Results**

107

108 **HBV membrane fusion is independent of acid pH and receptor expression.** To investigate the  
109 fusion activation mechanism and to identify the fusion determinants of HBV, we designed a cell-cell  
110 fusion assay whereby Huh7 “donor” cells, expressing a luciferase reporter gene under control of the  
111 HIV-1 promoter, were co-cultured with either Huh7-tat or Huh7-NTCP-tat “indicator” cells, expressing  
112 the HIV-1 transactivator of transcription (Tat) protein, which induces luciferase expression only in  
113 fused donor and indicator cells (Lavillette et al., 2007). We transfected donor cells with pT7HB2.7  
114 (Sureau et al., 1994), an expression plasmid encoding the wild-type HBV glycoproteins L, M and S.  
115 The transfected donor cells were then co-cultivated with Huh7-tat or Huh7-NTCP-tat indicator cells  
116 for 1 day. The medium of the co-cultures was then acidified at pH4 for 3 min to trigger fusion and the

117 next day, the luciferase activity in the lysates of co-cultured cells was measured as a read-out of  
118 membrane fusion (Figure 1A). The GPs of vesicular stomatitis virus (VSV) or of Crimean-Congo  
119 hemorrhagic fever virus (CCHFV) were used as controls for viruses that need acidic pH to promote  
120 membrane fusion. We found that HBV GPs induced similar levels of fusion in co-cultures that were  
121 exposed to either acidic or neutral pH, as well as in co-cultures lacking or expressing the NTCP  
122 receptor (Figure 1A; see raw data in Figure 1-figure supplement 1). Since HBV entry requires HSPG  
123 to mediate the capture of its viral particles through HBsAg (Leistner et al., 2008; Schulze et al., 2007),  
124 we addressed whether blocking of HBsAg/HSPG interaction could inhibit cell-cell fusion using heparin  
125 as competitor. Yet, while the applied doses of heparin could prevent cell-free entry, as shown  
126 previously (Schulze et al., 2007), addition of soluble heparin to the co-cultures did not prevent HBsAg  
127 mediated fusion, whether the indicator cells expressed or not NTCP (Figure 1B). We confirmed these  
128 results by using CHO and CHO-pgsB618 (Richard et al., 1995) cells as donor and/or indicator cells.  
129 While both cell types do not express NTCP, only the former expresses HSPGs. We found that cell-cell  
130 fusion could be detected for either indicator cell type to the same extent as for Huh7 cells (Figure 1C).  
131 Altogether, these results indicated that cell-cell fusion mediated by HBV GPs is independent of acid  
132 pH and requires neither HSPG nor NTCP receptor, which underscores an alternative fusion trigger.

133

134 **The preS1 domain of HBsAg harbors a critical determinant of membrane fusion.** The L, M and S  
135 GPs of HBV are produced by a single open reading frame and share a common C-terminal S-domain.  
136 M and L proteins harbor additional N-terminal extensions (preS2 and preS1/preS2, respectively), with  
137 preS1 harboring the NTCP-binding determinant (Glebe et al., 2005b; Gripon et al., 2005). Noteworthy,  
138 the fusion determinants of HBV GPs and, particularly, the fusion peptide that could induce merging of  
139 viral and endosomal membranes has not yet been functionally identified in infection or cell-cell fusion  
140 assays.

141 First, to address which GP is responsible for HBV membrane fusion, we evaluated the role of either  
142 proteins in cell-cell fusion assays (Figure 1D). Huh7 cells were transfected with plasmids encoding wt  
143 HBV GPs, *i.e.*, L, M and S (pT7HB2.7 plasmid), vs. only L, M or S (using pCiL, pCiM and pCiS  
144 plasmids, respectively) (Komla-Soukha and Sureau, 2006). To analyze the expression of either protein  
145 at the cell surface, transfected cells were labeled with sulfo-NHS-SS-biotin, a chemical compound that  
146 is unable to penetrate biological membranes. After lysis and immuno-precipitation of biotinylated  
147 proteins, we found that the individually expressed L, M or S proteins were detected at similar levels as  
148 compared to HBV GPs (L, M and S) expressed simultaneously, as in cells transfected with the wt  
149 pT7HB2.7 plasmid (Figure 1E, 1F). Then, to determine the fusion activity of either protein, we  
150 performed cell-cell fusion assays as described above. We found that none of the L, M or S proteins  
151 expressed alone were able to induce membrane fusion (Figure 1D). Furthermore, when we tested the  
152 pT7HB2.7Mless plasmid, which induces co-expression of S and L only (“noM” in Figure 1D-1F), we

153 detected a cell-cell fusion activity at the same level than for wt HBV GPs (Figure 1D). This indicated  
154 that M is not necessary for membrane fusion, in agreement with previous results (Ni et al., 2010;  
155 Sureau et al., 1994) showing that M is dispensable for infectivity of viral particles (Figure 1-figure  
156 supplement 3).

157 Altogether, these results suggested that the determinants of membrane fusion are harbored within L  
158 and S GPs.

159

160 Next, aiming to identify a fusion peptide in either protein, we used a computational approach to  
161 pinpoint regions of the HBV GPs that may potentially interact with membrane bilayers. Using  
162 Membrane Protein Explorer (MPEX), a tool based on the Wimley-White Interfacial Hydrophobicity  
163 Scale (Snider et al., 2009), five regions of high interfacial hydrophobicity were identified (Figure 2-  
164 figure supplement 1A). Two out of the five hydrophobic regions did not correspond to HBV GP  
165 transmembrane regions (TM1, TM2, and TM3/TM4), and therefore were considered as candidate  
166 fusion peptides (Figure 2A, 2B). The first predicted segment comprised amino acids 48 to 66 that  
167 partially overlap with the preS1 domain. The second segment, which includes amino acids 127 to 145,  
168 is included in the preS2 region. Our prediction analyzes indicated that the first segment ( $\Delta G = -3.38$ )  
169 was more likely to be a fusion peptide than the second one ( $\Delta G = -0.85$ ) (Figure 2-figure supplement  
170 1B). Considering the Wimley-White scale, a set of mutants was designed to alter the hydrophobicity of  
171 the two predicted segments (Figure 2B and Figure 2-figure supplement 1B). In the first segment, three  
172 mutants were studied by changing the aromatic residues to an alanine or glutamate: F52A, F56A,  
173 W66A, F52A/W66A (FW/AA) and F52E/W66E (FW/EE), or a glycine to an alanine (G53A). In the  
174 second segment, four mutants were considered: Y129A, F130A, S136E, L144A; while the first two  
175 mutants targeted aromatic residues, S136 and L144 were also considered important because they are  
176 at the center of the predicted region and have a relatively high hydrophobicity.

177 To evaluate the role of these two sequences in HBV fusion, we introduced these single or double  
178 mutations in both regions and inserted them in the pT7HB2.7 HBV GP expression plasmid. Each  
179 mutant was compared to wt HBV GPs in both infection assays, using HDV particles (Sureau, 2010;  
180 Perez-Vargas et al., 2019), and cell-cell fusion assays, as above-described. We found that HDV  
181 particles carrying these mutant GPs were produced by Huh7 cells at levels similar to those produced  
182 with wt GPs (Figure 2C, 2D), hence ruling out gross misfolding induced by the mutations that would  
183 otherwise prevent HBV GPs incorporation on viral particles (Abou-Jaoudé and Sureau, 2007).  
184 Interestingly, no infectivity could be detected for most of the mutations introduced in the preS1 peptide  
185 (Figure 2E), whereas the HDV particles with mutations in the preS2 peptide showed levels of  
186 infectivity that were similar to those obtained with the wt GPs (Figure 2F). Correlating with the results  
187 of these infection assays, we found that the mutants in the preS1 peptide that prevented HDV  
188 infectivity also abrogated cell-cell fusion activity (Figure 2G) in a manner unrelated to the levels of GPs

189 cell surface expression (Figure 2I and Figure 2-figure supplement 2). In contrast, mutations in the  
190 preS2 peptide displayed the same levels of cell-cell fusion activity as compared to wt (Figure 2H, 2J).  
191 Altogether, these results indicated that the preS1 region harbors a potential fusion peptide.

192

193 **Stabilizing cross-strand disulfide exchanges in HBV S protein prevents membrane fusion.** Next,  
194 we sought to investigate the mechanisms that could induce fusion-activating conformational changes  
195 in the HBV GPs, leading to exposure of the fusion peptide. As neither the HBV receptor interaction nor  
196 the acidic pH could trigger membrane fusion (Figure 1), we thought that conformational rearrangement  
197 of HBV GPs might involve reshuffling of their disulfide bonds. Indeed, previous studies showed that  
198 cysteine residues of the HBV S antigenic loop are essential for HDV infectivity and that viral entry is  
199 blocked by inhibitors of thiol/disulfide exchange reactions, such as TCEP, DTT, DTNB or AMS (Abou-  
200 Jaoudé and Sureau, 2007). Thus, to extend the notion that thiol/disulfide exchange reactions are  
201 implicated during membrane fusion and entry, we performed HBV infection and fusion assays in the  
202 presence of DTNB, an alkylator agent. First, using different DTNB concentrations that were added  
203 either at the onset of infection or at 16h post-infection, we confirmed that DTNB could block HDV  
204 infection in a dose-dependent manner, but only when it was added at the onset of infection (Abou-  
205 Jaoudé and Sureau, 2007) (Figure 3-figure supplement 1). Second, using time-of-addition  
206 experiments, we found that DTNB could inhibit infection only if added within the first 2 hours after  
207 inoculation with HDV particles (Figure 3A). These results suggested that DTNB blocks a thiol/disulfide  
208 exchange reaction that could be necessary at an early step of infection, such as a trigger of the fusion  
209 mechanism, though not at a later stage of the entry process. Third, to evaluate the effect of DTNB in  
210 membrane fusion, we performed cell-cell fusion assays in presence of DTNB, which was added at the  
211 onset of cell co-cultures vs. at 16h after seeding the cell co-cultures. We showed that DTNB added  
212 during the co-culture neither induced cytotoxicity (Figure 1-figure supplement 2) nor affected  
213 expression of HBV glycoproteins on the cell surface (Figure 3C, 3D). Yet, we found a dose-dependent  
214 reduction of the level of cell-cell fusion when DTNB was added immediately after cell-cell contact,  
215 whereas we detected a much lower effect in fusion activity when DTNB was added at 16h after cell  
216 contact (Figure 3B).

217 Altogether, these results suggested a role of the disulfide bonds network during HBV membrane  
218 fusion steps, perhaps at the level of the fusion trigger.

219

220 To address this possibility and to identify potential mechanisms involved in fusion triggering, we  
221 focused on the “a” determinant of protein S that exhibits eight conserved Cys, which, for some of  
222 them, are in strong proximity in the sequence (Figure 4A). To avoid trivial contact predictions between  
223 consecutive Cys, we defined four Cys-containing regions in a way that Cys pairs that are potentially in  
224 contact should have a sequence separation of at least four amino acids. The first Cys-containing



225 region includes C270, the second C284 and 287, the third C300, C301 and C302, and the last one  
226 C310 and C312 (Figure 4A). We applied secondary and tertiary structure prediction methods together  
227 with the contact prediction method RaptorX (Ma et al., 2015; Wang et al., 2017), based on coevolution  
228 signals, to predict disulfide connectivity in the “a” determinant, which may identify which Cys forms  
229 disulfide bonds. Notably, RaptorX predicted structural contacts between either region (Figure 4-figure  
230 supplement 1) and we highlighted pairs of residues in contact in the four Cys-regions, with the  
231 strongest signal detected between the third and fourth regions (Figure 4B). Next, applying the JPred  
232 secondary structure prediction method (Cole et al., 2008), we predicted two  $\beta$ -strands in the Cys-rich  
233 regions delimited by the S segments 298-303 and 310-313 (Figure 4A). Then, considering the  
234 secondary structure prediction and the contact prediction, we built a three-dimensional model for the  
235 region 294-317 (Figure 4C), which indicated that this sequence is compatible with a  $\beta$ -hairpin  
236 structural motif containing a cross-strand disulfide (CSD) between C301 and C310. Finally, through  
237 the analysis of its five  $\chi$  dihedral angles (Figure 4-figure supplement 2), this disulfide bond was  
238 classified in a “-HStaple conformation”, which is a particular type of disulfide geometry associated with  
239 allosteric functions by triggering a conformational change upon switching between the reduced and  
240 oxidized states (Chiu and Hogg, 2019; Hogg, 2003).

241 We therefore hypothesized that the redox state of this disulfide may act as an allosteric switch that  
242 could contribute to control conformational rearrangements of the S protein. Thus, we used our  
243 structural model of the C301-C310 disulfide bond to design a mutant of S that could disrupt this  
244 hypothetical allosteric function, *i.e.*, the T303C/G308C double mutant that induces an additional C303-  
245 C308 disulfide bond (Figure 4C). Further molecular dynamics (MD) simulations (1,000 frames per MD  
246 trajectory) carried out to differentiate between allosteric and structurally stabilizing disulfides, where  
247 the disulfides can be classified based on their angles (Figure 4-figure supplement 2), showed that the  
248 T303C/G308C mutant predominantly forms a structural disulfide bond.

249 Aiming to validate our prediction that an additional disulfide bond between the two  $\beta$ -strands could, by  
250 stabilizing the 298-313  $\beta$ -hairpin motif, prevent membrane fusion from occurring, we produced HDV  
251 particles carrying the individual (T303C or G308C) and double (T303C/G308C) mutations in HBV  
252 GPs. By measuring HDV RNAs in cell supernatants, we found that all mutants could produce  
253 comparable levels of viral particles relative to wt virus (Figure 5A), suggesting absence of gross  
254 alterations of HBV GP conformation that would otherwise preclude virion assembly (Abou-Jaoudé and  
255 Sureau, 2007). Importantly, we found that while HDV particles generated with GPs harboring the  
256 individual mutations were as infectious as wt, those that were produced with the T303C/G308C double  
257 mutation (noted TG/CC in Figure 5) and the putative additional C303-C308 CSD bond were not  
258 infectious (Figure 5B). Moreover, we found that HDV particles harboring GPs with this T303C/G308C  
259 mutation had similar binding levels on Huh7 cells than those generated with wt GPs (Figure 6A),  
260 underscoring a post-binding defect. Then, to address this possibility, we performed cell-cell fusion

261 assays with either HBV GP mutant, which were readily expressed at the cell surface (Figure 5C). We  
262 found that whereas the single mutations displayed similar fusion activity as compared to wt HBV GPs,  
263 the T303C/G308C double mutation completely prevented HBV GP-induced cell-cell fusion activity  
264 (Figure 5D).

265 Altogether, these results suggested that the putative C303-C308 additional disulfide bond stabilizing  
266 the loop containing the C301-C310 CSD bond inhibited HBV entry and fusion, perhaps by preventing  
267 conformational rearrangements of HBV GPs that are required for promoting membrane fusion.

268

269 **ERp57 is a protein disulfide isomerase that promotes HBV entry and infectivity *in vivo*.** We  
270 reasoned that isomerization of the C301-C310 CSD (Figure 4) or of another CSD of the AGL  
271 determinant with allosteric functions could facilitate some conformational rearrangements required to  
272 promote membrane fusion. We therefore hypothesized that such an isomerization could be induced by  
273 a host factor from the Protein Disulfide Isomerase (PDI) family, which are enzymes that can both  
274 reduce and oxidize disulfide bonds.

275 To address if PDIs are involved in HBV entry, we tested the effect of inhibitors (NTZ, EGCG, Rutin,  
276 Bacitracin, PX-12) that target different PDI species (PDIA1, ERp5, ERp57, TMX1) for their effect in cell  
277 entry of viral particles. First, through binding assays of viral particles to Huh7 or Huh7-NTCP cells  
278 performed in the presence of either inhibitor, we found that none of these inhibitors affected binding of  
279 HDV particles generated with either wt or T303C/G308C mutant GPs (Figure 6A). Second, using  
280 infection assays with Huh7-NTCP cells pre-incubated with either inhibitor, we found that HDV particles  
281 had strongly reduced infectivity in presence of NTZ and EGCG inhibitors that both target ERp57  
282 (Figure 6B). Third, we confirmed these results using infection assays with authentic HBV particles  
283 (Figure 6C). Finally, to demonstrate that the inhibitors acted at the level of membrane fusion, we  
284 performed cell-cell fusion assays, as above-described, whereby either inhibitor was added at the onset  
285 of co-cultures of HBV GP-expressing Huh7 donor and Huh7-NTCP-Tat indicator cells, and was kept  
286 throughout the assay period. Remarkably, we found a strong reduction of the levels of cell-cell fusion  
287 with the same drugs that inhibited HDV infection (Figure 6D). Hence, these results suggested a  
288 potential role of ERp57 in HBV membrane fusion.

289

290 Next, aiming to confirm and extend these findings, we selected a subset of the above PDIs, *i.e.*,  
291 ERp46, ERp57 and ERp72, that displayed low but significant expression at the surface of Huh7 cells  
292 (Figure 7A), in agreement with a previous report (Turano et al., 2002). We down-regulated either PDI  
293 in target cells *via* transduction of Huh7-NTCP cells with shRNA-expressing lentiviral vectors (Figure 7-  
294 figure supplement 1 and Figure 7-figure supplement 2). We found that down-regulation of ERp57,  
295 though not ERp46 or ERp72, strongly reduced the levels of HDV (Figure 7B) and HBV infection  
296 (Figure 7C) and of cell-cell fusion (Figure 7D). Finally, through confocal microscopy analysis of Huh7-

297 NTCP cells (Figure 8A), we investigated the co-localization between ERp57 and Rab5 (early  
298 endosomes), Rab7 (late endosomes), Rab11 (recycling endosomes) or Lamp1 (lysosomes). The  
299 quantifications of these results showed that ERp57 could be detected in late endosomes but poorly in  
300 the other above-tested locations (Figure 8B), in line with the notion that fusion of HBV particles occurs  
301 in late endosomes (Macovei et al., 2013). Thus, ERp57 can be found at locations compatible for both  
302 cell-cell fusion and cell-free entry by internalization.

303 Altogether, these results indicated that ERp57 is likely a protein disulfide isomerase that promotes  
304 HBV entry at a membrane fusion step.

305

306 Finally, we sought to demonstrate that ERp57 inhibition may prevent HBV propagation *in vivo* using  
307 NTZ, which has a short half-life of about 1.5h (Ruiz-Olmedo et al., 2017; Stockis et al., 1996). We  
308 generated a cohort of liver humanized mice (HuHep-mice) derived from the NFRG mouse model  
309 (Azuma et al., 2007) (Figure 9A). We retained the animals that displayed >15 mg/mL of human serum  
310 albumin (HSA), which corresponds to 40-70% of human hepatocytes in the liver (Calattini et al., 2015).  
311 In agreement with previous reports (Perez-Vargas et al., 2019), these animals supported HBV  
312 infection (Group#1) for several weeks/months (Figure 9B; see Figure 9-figure supplement 1 for  
313 individual mice). The second group of HuHep mice was treated with NTZ 30min prior to inoculation  
314 with HBV, and then, treated again with NTZ 1h later. We found that viremia in this group was delayed  
315 by about 4 weeks, as compared to Group#1 for which HBV could disseminate immediately after  
316 inoculation. This indicated that the blocking of ERp57 could prevent HBV infection *in vivo*.

317

318

## 319 **Discussion**

320

321 The entry process of enveloped viruses into cells is the series of all events that take place from the  
322 attachment of the virus to the host cell until the release of its genome in the cytoplasm. It is a finely  
323 regulated and complex process with several steps, in which many viral and cellular factors are  
324 involved. The first interaction often occurs with HSPGs. It may lack specificity but serves to give a  
325 virus an initial catch hold from which it can recruit specific receptors and entry co-factors that drive the  
326 reactions leading to entry. Fusion is the last step of enveloped virus entry and allows the release of the  
327 viral capsid in the cytoplasm following the merging of the viral membrane with a membrane of the  
328 infected cell. The interactions with the target cell that trigger conformational changes of the viral  
329 surface glycoproteins, ultimately leading to the insertion of their fusion peptide into the cell membrane,  
330 vary widely for enveloped viruses and can be divided into different scenarios. In a first one (*e.g.*, HIV),  
331 fusion is triggered directly by the interaction of the viral glycoprotein with its cellular receptor, through  
332 allosteric conformational rearrangements. In some cases, a sequential interaction with additional host

333 factors is required to trigger the conformational changes required for fusion. In a second scenario  
334 (e.g., influenza virus), the interactions with the receptor at the cell surface leads to the endocytosis of  
335 viral particles, which is followed by GP protonation in the low pH environment of the intracellular  
336 endosomal organelles that triggers the fusogenic conformational change. In a third scenario (e.g.,  
337 Ebola virus), the initial interactions of the virion with the cell surface trigger its endocytosis followed by  
338 a second interaction with an internal receptor, often found in late endosomes, which is preceded by  
339 proteolytic cleavage of the fusion protein by an endosomal protease, leading to fusion activation  
340 (Harrison, 2015; White and Whittaker, 2016). Finally, for certain viruses (e.g., Sindbis virus), the fusion  
341 protein requires an activating redox reaction involving disulfide bonds of their glycoproteins to induce  
342 membrane fusion (Key et al., 2015; Rey and Lok, 2018).

343

344 Using a cell-cell fusion assay, we found that HBV fusion activity reached similar levels whether  
345 indicator cells expressed or not HSPG and/or NTCP but was not increased when the cell co-cultures  
346 were exposed at low pH, in contrast to *bona fide* pH-dependent GPs such as VSV-G or CCHFV  
347 Gn/Gc (Figure 1). That both HSPG and NTCP, which are respectively HBV virion membrane capture  
348 molecules (Leistner et al., 2008; Schulze et al., 2007) and specific entry factors (Ni et al., 2014; Yan et  
349 al., 2015), are not required for cell-cell fusion highlights that this fusion assay reveals late entry events,  
350 such as those occurring after virus interaction with either factor. Similarly, for other viruses such as  
351 e.g., influenza virus or hepatitis C virus (HCV), binding to their cell entry receptor is not a requirement  
352 in both cell-cell fusion (Lin and Cannon, 2002) and liposome fusion (Lavillette et al., 2006) assays  
353 triggered by low pH treatment. Thus, while it is clear that cell-cell fusion does not recapitulate *per se*  
354 all the events required to promote cell entry of viral particles since it bypasses the step of  
355 internalization that subsequently allows membrane fusion in endosomes that are required for entry of  
356 the above-mentioned viruses and of HBV (Macovei et al., 2013; Iwamoto et al., 2019), it a suitable  
357 experimental tool for investigating some of the structural and functional determinants that promote  
358 envelope glycoprotein membrane-fusion activity (Earp et al., 2004). Accordingly, our results indicate  
359 that the trigger for the HBV membrane fusion mechanism not only is independent of an allosteric  
360 interaction of its GPs with the NTCP receptor but also is independent of GPs protonation that is  
361 induced by the low pH environment of endosomes. That low pH does not increase HBV cell-cell fusion  
362 agrees with previous results indicating that pharmacological agents that raise or neutralize the pH of  
363 the endocytic pathway had no effect on HBV infection (Macovei et al., 2010, 2013; Rigg and Schaller,  
364 1992).

365 Previous results from the group of Camille Sureau showed that cysteine residues of the HBV antigenic  
366 loop are essential for HDV infectivity and that viral entry is blocked by inhibitors of thiol/disulfide  
367 exchange reaction (Abou-Jaoudé and Sureau, 2007). Our results extend this notion as they indicate  
368 that such reactions seem to be necessary to mediate a critical early post-binding event but not at a

369 later stage of the infection process since no effect in virus infectivity could be detected when DTNB  
370 was added at 4h post-infection (Figure 3). Since isomerization of disulfide bonds has been shown to  
371 be crucial for conformational rearrangements of GPs from other enveloped viruses leading to fusion  
372 (Fenouillet et al., 2007), we sought to investigate if and how such reactions could be implicated during  
373 the membrane fusion step of HBV entry. Here, using our cell-cell fusion assay, we found that DTNB  
374 blocked HBV GP-mediated membrane fusion (Figure 3B). Altogether, these results indicated a role of  
375 disulfide bond network of S GP during HBV membrane fusion.

376

377 Capitalizing on the above-mentioned experimental information that inhibitors of thiol/disulfide  
378 exchange reactions alter virus entry, we sought to examine how disulfide bonds of the HBV GPs, or  
379 rather, how a potential reshuffling of its disulfide bonds profile, could be important for HBV entry.  
380 Indeed, cross-strand disulfides occurring in some viral surface GPs are believed to play a role in virus  
381 entry (Barbouche et al., 2003; Jain et al., 2007; Rosenthal et al., 1998; Wouters et al., 2004).  
382 Particularly, allosteric disulfide bonds can modulate the activity of the proteins in which they reside by  
383 mediating a structural change when they are reduced or oxidized (Hogg, 2003; Schmidt et al., 2006).  
384 Allosteric control of protein function is defined as a change in one site (the allosteric site) that  
385 influences another site by exploiting the protein's flexibility; an allosteric disulfide bond represents the  
386 "allosteric site" and the conformational change triggered by cleavage of such bonds alters protein  
387 function. For the HBV S protein, we used the contact prediction method RaptorX (Ma et al., 2015,  
388 Wang et al., 2017) to predict contacts between four Cys-rich regions of the AGL determinant (Figure  
389 4), which highlighted that two of these regions may likely interact: *i.e.*, the Cys-rich regions III and IV  
390 (Figure 4-figure supplement 1). Using the secondary structure prediction method JPred (Cole et al.,  
391 2008), we proposed that these regions organize in two  $\beta$ -strands and we constructed a three-  
392 dimensional model of the region 294-317 of the HBV S GP, which indicated that this sequence is  
393 compatible with a  $\beta$ -hairpin structural motif containing a CSD bond between C301 and C310 (Figure  
394 4). Interestingly, the analysis of the signs of the five  $\chi$  dihedral angles defined by the Cys residues  
395 allowed to classify this particular disulfide bond in a -HStaple conformation, which is a particular type  
396 of disulfide geometry associated with allosteric functions that is known to trigger conformational  
397 changes upon switching between the reduced and oxidized states (Chiu and Hogg, 2019; Schmidt et  
398 al., 2006). Hence, we hypothesized that the redox state of the C301-C310 disulfide bond may act as  
399 an allosteric switch controlling conformational rearrangements of the HBV GP leading, ultimately, to  
400 exposure of the fusion peptide. Of note, the  $\beta$ -hairpin region with the predicted CSD lies at the surface  
401 of the S protein according to a three-dimensional *in silico* model (van Hemert et al., 2008), which may  
402 allow interactions with other HBs subunits and/or cellular factors. Yet, to test our structural and  
403 dynamic model involving a C301-C310 CSD bond in S GP (Figure 4), we reasoned that creating an  
404 additional, neighboring disulfide bond between positions 303 and 308 may stabilize the  $\beta$ -hairpin motif

405 (Figure 4), which may prevent molecular rearrangements and thus, membrane fusion to occur. The *in*  
406 *silico* analysis indicates that the T303C/G308C double mutant most probably generates two structural  
407 CSD according to our JPred-based (Cole et al., 2008) structural modelling, which affects the structural  
408 conformation of the C301-C310 CSD that is no longer classified as an allosteric bond. When we tested  
409 the T303C/G308C mutation in functional assays, we found that the mutant HBV GPs induced an  
410 almost complete loss of infection and fusion activity (Figure 5), hence suggesting that by stabilizing  
411 cross-strand disulfide exchange, the putative additional disulfide bond prevented conformational  
412 rearrangements of HBV GPs that are required for promoting membrane fusion. One possibility is that  
413 such stabilization could prevent an isomerization of the C301-C310 CSD bond that generates  
414 alternative disulfide bond(s) such as, for example, between C284 and C310 that was proposed in a  
415 previous study (Mangold et al., 1995). Yet, the antigenic loss of S induced by these mutations did not  
416 allow us to design an assay that would detect the additional disulfide bond in the T303C-G308C  
417 mutant nor the block of conformational rearrangements that is suggested by its phenotype.

418

419 Assuming that the isomerization of the C301-C310 allosteric CSD or of other thiols/disulfides of the  
420 AGL determinant could facilitate the conformational rearrangements of HBs required to promote HBV  
421 membrane fusion, we hypothesized that such isomerization could be induced by a host factor from the  
422 PDI family, which are enzymes that can both reduce and oxidize disulfide bonds. Protein disulfide  
423 isomerases consist of a family of 21 structurally related proteins with a thioredoxin-like domain. Most  
424 of these isomerases have a CXXC motif that catalyzes formation, reduction and rearrangement of the  
425 disulfide bonds in proteins (Abell and Brown, 1993). These isomerases are primarily involved in the  
426 folding of proteins in the ER, catalyzing formation of their disulfide bonds, and most of these  
427 isomerases have ER retention signals. However, some isomerases from the PDI family have also  
428 been shown to be present at the cell surface, both in functional and in biochemical assays (Turano et  
429 al., 2002). Accordingly, cell surface-localized PDIs are involved in processes such as cell adhesion,  
430 nitric oxide signaling, and in cell entry of different viruses (Diwaker et al., 2013; Fenouillet et al., 2007).  
431 In support of the notion that PDIs are involved in HBV entry, we found that inhibitors that target  
432 different PDI members could block infection and cell-cell fusion though not the binding of viral particles  
433 to the cell surface. Of note, we found that bacitracin, which targets PDIA1, did not inhibit HBV entry  
434 and membrane fusion, in line with a previous study showing that it could not inhibit HDV entry (Abou-  
435 Jaoudé and Sureau, 2007). While the above ruled out PDIA1 as an entry co-factor of HBV, we found a  
436 strong reduction of the levels of HBV and HDV infection as well as of HBV-induced cell-cell fusion  
437 when we used the NTZ and EGCG inhibitors (Figure 6), which target ERp57 (Müller et al., 2008;  
438 Pacello et al., 2016). Consistently, we detected a low but significant expression of ERp57 as well as of  
439 ERp46 and ERp72 at the cell surface (Figure 7), in agreement with a previous study (Turano et al.,  
440 2002). Furthermore, we detected ERp57 in late endosomes (Figure 8), which is meaningful since

441 previous reports showed that HBV infection of HepaRG cells depends on Rab5 and Rab7 (Macovei et  
442 al., 2013), which are GTPases involved in the biogenesis of endosomes, and that the epidermal  
443 growth factor receptor is a host-entry cofactor that interacts with NTCP and mediates HBV  
444 internalization (Iwamoto et al., 2019). Using a gene silencing approach, we confirmed that down-  
445 regulation of ERp57 but not of these alternative PDIs could decrease the levels of HDV and HBV  
446 infection as well as of cell-cell fusion (Figure 7). Importantly, we showed that a short time treatment of  
447 liver humanized mice with NTZ could delay HBV infection by ca. 2-4 weeks (Figure 9). Since NTZ has  
448 a short half-life of about 1.5h *in vivo* (Ruiz-Olmedo et al., 2017; Stockis et al., 1996) and since NTZ  
449 was administrated at very short times before and after HBV inoculation, we calculated that less than  
450 10% of the drug was still present in those mice at 7h post-infection, which likely precludes an effect on  
451 HBV post-entry steps (Korba et al., 2008). Altogether, these results support the role of ERp57 at early  
452 steps of HBV infection and validate this PDI as a therapeutic target. Note that our results did not  
453 discard the possibility that some other PDIs could also play a role during HBV entry into cells.

454

455 The fusion-mediating GPs of enveloped viruses contain a sequence, termed fusion peptide that  
456 interacts with and destabilizes the cellular target membrane. Such an event is finely controlled so as to  
457 occur at the appropriate time and location and to prevent fortuitous inactivation of GP fusion activity  
458 and virus infectivity. Hence, a conformational change in these GPs is a requirement to induce the  
459 accessibility and function of the fusion peptide segment. Candidate fusion peptides are generally  
460 identified as hydrophobic sequences, of ca. 16 to 26 residues in length, that are conserved within a  
461 virus family and that may adopt  $\alpha$ -helical conformation with strongly hydrophobic faces. They can be  
462 internal or located at the amino-terminus of fusion GP subunits (Apellániz et al., 2014; Epand, 2003;  
463 Martin et al., 1999). There are a number of criteria that characterize fusion peptide segments and,  
464 while none of these criteria taken individually are absolute to define a fusion peptide segment, they are  
465 sufficiently restrictive to predict if a given region of a protein presents features of a fusion peptide  
466 segment (Delos and White, 2000; Delos et al., 2000), which needs to be further functionally tested.

467 Previously, a conserved peptide comprising 23 amino acids at the N-terminal end of the HBV S protein  
468 and overlapping its TM1 sequence was shown to interact with model membranes, causing liposome  
469 destabilization in a pH-dependent manner (Berting et al., 2000; Rodríguez-Crespo et al., 1994, 1995,  
470 1999). However, it was also demonstrated that hydrophobic residues in TM1 were critical for S protein  
471 expression as well as for infectivity (Siegler and Bruss, 2013). An essential role of TM1 in fusion  
472 mechanism, albeit in a pH-independent manner, could be shown for the duck hepatitis B virus (DHBV)  
473 (Chojnacki et al., 2005; Grgacic and Schaller, 2000), although there is also evidence for the  
474 involvement of the preS domain of DHBV at an early step of infection, likely during the fusion process  
475 (Delgado et al., 2012).

476 Here, through a computational hydropathy analysis of the HBV GPs, we identified two potential short  
 477 sequences within the preS1 and preS2 regions that may potentially interact with membrane bilayers.  
 478 To validate these predictions, we characterized in both infection and cell-cell fusion assays HBV GP  
 479 mutants in key positions in either sequence. We found that while none of the mutations in the preS2  
 480 segment altered infection or membrane fusion activities, mutations in the preS1 sequence induced an  
 481 almost complete loss of infectivity and cell-cell fusion (Figure 2). Note that these mutants had similar if  
 482 not identical levels of cell surface expressed L, M and S proteins and/or capacity to induce the  
 483 formation of HDV particles. These results suggested that the preS1 region harbors a fusion peptide in  
 484 addition to the NTCP binding determinant.

485  
 486 Overall, our study characterizes some crucial determinants of HBV entry and membrane fusion. The  
 487 mechanism by which fusion proteins are activated and undergo conformational rearrangements or  
 488 fusion intermediates is a particularly complex process involving several regions of viral surface GPs.  
 489 Our results suggest that for HBV, this mechanism could be triggered by ERp57, allowing a  
 490 thiol/disulfide exchange reaction to occur and regulate isomerization of critical CSD(s), which  
 491 ultimately results in the exposition of the fusion peptide that seems to be located within the preS1  
 492 region.

493  
 494

495 **Material and Methods**

496

497 **Key Resources Table**

Reagent type (species) or resource	Designation	Source or reference	Identifiers	Additional information
strain, strain background ( <i>M. musculus</i> , females and males)	NOD-FRG mice	DOI: 10.1038/nbt1326 DOI : 10.1074/jbc.M115.662999		Breeding and experimentation in PBES – Originally purchased to YEcureis corporation
strain, strain background (HBV)	Hepatitis B virus (HBV)	This paper		HBV, genotype D, produced by co-transfection of HepG2.2.15 cells with plasmids pCiHB(env-) and pT7HB2.7



strain, strain background (HDV)	Hepatitis D virus (HDV)	This paper		HDV, genotype 1, produced by co-transfection of Huh7 cells with plasmids pSVLD3 and pT7HB2.7, or variant constructs
cell line ( <i>Homo-sapiens</i> )	Huh7 - hepatocarcinoma cells	PMID: 6286115		
cell line ( <i>Homo-sapiens</i> )	Huh7-NTCP	This paper		Generated by transduction with pLX304NTCP retroviral vector and selection with blasticidin
cell line ( <i>Homo-sapiens</i> )	Huh7-Tat (H-tat) cells	This paper		Generated by transduction with LXSNTat retroviral vector and selection with G418
cell line ( <i>Homo-sapiens</i> )	H-tat cells down regulated for ERp46, ERp57 or ERp72	This paper		Generated by transduction of H-tat cells with shRNA lentiviral vectors against ERp46, ERp57 or ERp72 followed by selection with puromycin
cell line ( <i>Homo-sapiens</i> )	Huh7-NTCP-Tat (N-tat) cells	This paper		Generated by transduction of Huh7-NTCP cells with LXSNTat retroviral vector
cell line ( <i>Homo-sapiens</i> )	N-tat cells down regulated for ERp46, ERp57 or ERp72	This paper		Generated by transduction of N-tat cells with shRNA lentiviral vectors against ERp46, ERp57 or ERp72 followed by selection with puromycin
cell line ( <i>Homo-sapiens</i> )	HepG2.2.15 human hepatoma cells	From David Durantel lab		Production of HBV particles

cell line ( <i>Homo-sapiens</i> )	293T human kidney cells	ATCC	CRL-1573	Production of retro- and lentiviral particles
cell line ( <i>Cricetulus griseus</i> , female)	CHO-K1 Chinese hamster ovary cells	ATCC	CCL-61	Cell-cell fusion assays
transfected construct (human)	pLX304NTCP	DNASU plasmid repository	HQ447437	retroviral construct to transfect and express NTCP
transfected construct (HBV)	pSVLD3	DOI: 10.1128/JVI.63.5.1945-1950.1989		Harbors a trimer of the HDV, genotype 1 genome. Used for production of HDV particles
transfected construct (HBV)	pT7HB2.7	DOI: 10.1128/JVI.68.6.4063-4066.1994		Gift from Camille Sureau, used for production of HBV and HDV particles and expression of HBV envelope proteins
transfected construct (HBV)	pT7HB2.7Mles s (noM)	This paper		Generated for expression of HBV L and S proteins (M protein is silenced)
transfected construct (HBV)	pCiL	doi: 10.1128/JVI.77.9.5519-5523.2003		Encodes only the L-HBsAg protein
transfected construct (HBV)	pCiS	doi: 10.1128/JVI.80.10.4648-4655.2006		Encodes only the S-HBsAg protein
transfected construct (CCHFV)	pCAGGS_GP/wt-M	DOI: 10.1128/JVI.03691-14		Major open reading frame of CCHFV M-segment subcloned into pCAGGS
transfected construct (HBV)	pCIHB(env-)	DOI: 10.1128/JVI.00621-06		Gift from Camille Sureau, used for production of HBV particles
transfected construct (HIV1-Tat)	LXSN-tat retroviral vector	DOI: 10.1128/JVI.73.3.1956-1963.1999		HIV-1 <i>tat</i> gene cloned into the LXSN retroviral vector

transfected construct (HIV1-LTR)	pLTR-luc	DOI: 10.1016/0378-1119(90)90032-m		gift from Olivier Schwartz, contains a 722-base pair <i>Xho</i> I (-644)- <i>Hind</i> III (+78) fragment from HIV-1 placed in front of the luciferase reporter gene
transfected construct (VSV)	phCMV-VSV-G	DOI: 10.1016/s0091-679x(08)60600-7		To express the envelope protein of VSV
transfected construct (human)	shRNA against ERp46 (ERp46-shRNA 1)	Sigma	NM_022085 / TRCN00000 64353 / PLKO.1	Lentiviral construct to transfect and express the shRNA.
transfected construct (human)	shRNA against ERp46 (ERp46-shRNA 2)	Sigma	NM_022085 / TRCN00000 64354 / PLKO.1	Lentiviral construct to transfect and express the shRNA.
transfected construct (human)	shRNA against ERp57 (ERp57-shRNA 3)	Sigma	NM_005313 / TRCN00003 19038 / PLKO	Lentiviral construct to transfect and express the shRNA
transfected construct (human)	shRNA against ERp57 (ERp57-shRNA 4)	Sigma	NM_005313 / TRCN00001 47738 / PLKO.1	Lentiviral construct to transfect and express the shRNA
transfected construct (human)	shRNA against ERp72 (ERp72-shRNA 3)	Sigma	NM_004911 / TRCN00002 89676 / PLKO.1	Lentiviral construct to transfect and express the shRNA
transfected construct (human)	shRNA against ERp72 (ERp72-shRNA 4)	Sigma	NM_004911 / TRCN00000 49334 / PLKO.1	Lentiviral construct to transfect and express the shRNA

transfected construct (human)	shRNA against ERp72 (ERp72-shRNA 5)	Sigma	NM_004911 / TRCN00003 07107 / PLKO.1	Lentiviral construct to transfect and express the shRNA
biological sample ( <i>M. musculus</i> )	Blood samples	PBES (Plateau de Biologie Experimentale de la Souris) SFR Biosciences Lyon		isolated from NOD-FRG mice
antibody	anti-HBsAg antibody, HPR conjugated (goat polyclonal)	DiaSorin	9F80-01	WB(1:400)
antibody	anti-human calnexin (rabbit polyclonal)	Enzo	ADI-SPA-865-F	WB(1:1000)
antibody	anti-mouse TXNDC5/ERp46 (rabbit polyclonal)	Abcam	Ab10292	FACS(1:20) WB(1:1000)
antibody	anti-human ERp57 (mouse monoclonal)	Abcam	Ab13506	FACS(2 $\mu$ g/10 <sup>6</sup> cells) WB(1:10000) IF(1:100)
antibody	anti-human ERp72 (rabbit polyclonal)	Abcam	Ab155800	FACS(1:100) WB(1:1000)
antibody	anti-human NTCP/SLC10A1 antibody, PE conjugated (rabbit polyclonal)	Bioss Antibodies	bs-1958R-PE	FACS(1:100)
antibody	anti-human Rab5 (rabbit monoclonal)	Cell Signaling Technology	(C8B1):3547	IF(1:200)

antibody	anti-human Rab7 (rabbit monoclonal)	Cell Signaling Technology	(D95F2):9 367	IF(1:100)
antibody	anti-human Rab11 (rabbit monoclonal)	Cell Signaling Technology	(D4F5):55 89	IF(1:50)
antibody	anti-human Lamp1 (rabbit monoclonal)	Cell Signaling Technology	(D2D11):9 091	IF(1:200)
sequence-based reagent	F52A	This paper	preS1 mutagenesis is PCR primers	GTAGGAGCTGGAGC AG CCGGGCTGGGTTTC AC
sequence-based reagent	F52E	This paper	preS1 mutagenesis is PCR primers	GTAGGAGCTGGAGC AGA AGGGCTGGGTTTCA C
sequence-based reagent	G53A	This paper	preS1 mutagenesis is PCR primers	CTGGAGCATTGCGG CT GGGTTTCAC
sequence-based reagent	F56A	This paper	preS1 mutagenesis is PCR primers	TTCGGGCTGGGTGC C ACCCACCGCA
sequence-based reagent	W66A	This paper	preS1 mutagenesis is PCR primers	GAGGCCTTTTGGGG GCG AGCCCTCAGGCTC
sequence-based reagent	W66E	This paper	preS1 mutagenesis is PCR primers	GAGGCCTTTTGGGG GAG AGCCCTCAGGCTC
sequence-based reagent	Y129A	This paper	preS2 mutagenesis is primers	GAGTGAGAGGCCTG GCTT TCCCTGCTGGTG

sequence-based reagent	F130A	This paper	preS2 mutagenesis primers	GAGAGGCCTGTATG CCCC TGCTGGTGG
sequence-based reagent	S136E	This paper	preS2 mutagenesis primers	CCCTGCTGGTGGCT CCGAA TCAGGAACAGTAA C
sequence-based reagent	L144A	This paper	preS2 mutagenesis primers	CAGTAAACCCTGTT GCGACT ACTGCCTCTCC
sequence-based reagent	T303C	This paper	CSD mutagenesis primers	CCTCCTGTTGCTGT TGCAA CCTTCGGACG
sequence-based reagent	G308C	This paper	CSD mutagenesis primers	GTACCAAACCTTCG GACTGT AATTGCACCTGTATT CCC
sequence-based reagent	TG/CC	This paper	CSD mutagenesis primers	GTTGCAAACCTTCG GACTGT AATTGCACCTGTATT CCC
commercial assay or kit	FuGENE HD Transfection Reagent	Promega	E2312	Transfection reagent
commercial assay or kit	Dual-Luciferase® Reporter Assay System	Promega	E1910	Quantification of luciferase activity
commercial assay or kit	iScript cDNA synthesis kit	Bio-Rad	1708891	cDNA synthesis
commercial assay or kit	FastStart Universal SYBR Green Master	Roche Sigma	4913850001	Real time qPCR assays
commercial assay or kit	CytoTox-ONE™ Homogen Membrn Integrity Assay	Promega	G7891	Cytotoxicity assay

chemical compound, drug	Bacitracin	Sigma	B0125-250KU	water
chemical compound, drug	NTZ (Nitazoxanide)	Sigma	N0290-50MG	DMSO
chemical compound, drug	EGCG (-)-Epigallocatechin gallate	Sigma	E4268-100MG	water
chemical compound, drug	RUTIN HYDRATE	Sigma	R5143-50G	DMSO
chemical compound, drug	PX-12	Sigma	M5324-5MG	DMSO
chemical compound, drug	DTNB 5,5'-Dithiobis(2-nitrobenzoic acid)	Sigma	D218200-1G	DMSO
chemical compound, drug	EZ-Link Sulfo-NHS-LC-LC-Biotin	Life technologies	21338	
software, algorithm	ImaJ software	ImaJ	RRID:SCR_003070	
software, algorithm	Membrane Protein eXplorer	<a href="http://blanco.biomol.uci.edu/mpex/">http://blanco.biomol.uci.edu/mpex/</a>	RRID:SCR_014077	
software, algorithm	RaptorX	<a href="http://raptorx.uchicago.edu/">http://raptorx.uchicago.edu/</a>	RRID:SCR_018118	
software, algorithm	Jpred	<a href="http://www.compbio.dundee.ac.uk/jpred/">http://www.compbio.dundee.ac.uk/jpred/</a>	RRID:SCR_016504	

software, algorithm	MODELLER	<a href="http://salilab.org/modeller/modeller.html">http://salilab.org/modeller/modeller.html</a>	RRID:SCR_008395	
software, algorithm	Clustal X	<a href="http://www.clustal.org/clustal2/">http://www.clustal.org/clustal2/</a>	RRID:SCR_017055	
software, algorithm	Molecular Modelling Toolkit	<a href="http://dirac.cnrs-orleans.fr/MMTK.html">http://dirac.cnrs-orleans.fr/MMTK.html</a>		
software, algorithm	GROMACS	<a href="http://www.gromacs.org">http://www.gromacs.org</a>	RRID:SCR_014565	
software, algorithm	UCSF Chimera	<a href="http://plato.cgl.ucsf.edu/chimera/">http://plato.cgl.ucsf.edu/chimera/</a>	RRID:SCR_004097	
other	Hoechst 33342 stain	Thermo Fisher	H3570	10 µg/ml
other	STREPTAVIDIN AGAROSE RESIN	Thermo fisher	20353	
other	TRI-Reagent	Molecular Research Center Euromedex	TR118-200	RNA extraction

498

499 **Plasmids.** Plasmid pSVLD3 harboring a trimer of the HDV gt1 genome (accession number  
500 M21012.1), pCiL encoding the L protein, pCiS encoding the S protein (Komla-Soukha and Sureau,  
501 2006) and pT7HB2.7 encoding the three HBV envelope proteins were a gift from Camille Sureau  
502 (Sureau, 2010; Sureau et al., 1994). To induce the expression of L and S only, the pT7HB2.7 plasmid  
503 was modified at the M start codon and Kozak consensus sequence in order to silence the expression  
504 of M protein, resulting in pT7HB2.7Mless construct. The pCiM plasmid encoding the M protein was  
505 constructed by deleting the preS1 region from pCiL until the N-terminal methionine of preS2. All  
506 mutations in pT7HB2.7 plasmid were introduced by point directed mutagenesis. The pHCMV-VSV-G  
507 encoding the G protein from vesicular stomatitis virus (VSV) and pCAGGS-GP/wt-M encoding the Gn  
508 and Gc glycoproteins from Crimean-Congo hemorrhagic fever virus (CCHFV) were described  
509 previously (Freitas et al., 2020). The plasmid encoding the luciferase reporter under control of an HIV-  
510 1 long terminal repeat internal promoter (pLTR-luc) was a gift from Olivier Schwartz and was used as



511 described before (Lavillette et al., 2007). Mission shRNAs plasmids (Sigma), shRNAs sequences and  
512 oligonucleotides used for introducing mutations in HBV GPs are described in Supplementary file 1.

513

514 **Cells.** Huh7 human hepatocarcinoma cells and Huh7-NTCP cells, which were generated by  
515 transduction of Huh7 cells with a retroviral vector transducing the NTCP plasmid (pLX304NTCP,  
516 DNASU) and selected for blasticidin resistance, were grown in William's E medium (WME) (Gibco,  
517 France) supplemented with non-essential amino acids, 2 mM L-Glutamine, 10 mM HEPES buffer, 100  
518 U/mL of penicillin, 100 µg/mL of streptomycin and 10% fetal bovine serum. 293T human kidney cells  
519 (ATCC CRL-1573), CHO-K1 (CHO) Chinese hamster ovary cells (ATCC CCL-61) and CHO-pgsB-618  
520 cells (ATCC CRL-2241), which do not produce glycosaminoglycans, were grown in Dulbecco's  
521 modified minimal essential medium (DMEM, Gibco) supplemented with 100 U/mL of penicillin, 100  
522 µg/mL of streptomycin, and 10% fetal calf serum. Huh7-Tat and Huh7-NTCP-Tat indicator cells  
523 expressing HIV Tat were generated by transduction of Huh7 and Huh7-NTCP cells, respectively, with  
524 the LXSNT-tat retroviral vector and selected for G418 resistance. HepG2.2.15 human hepatoma cells  
525 were used to produce HBV virus, there were maintained in WME medium complemented with 10%  
526 fetal bovine serum. Authentication of purchased cell lines was performed by ATCC. Authentication of  
527 Huh7 cells was based on expression of human transferrin and serum albumin. Authentication of  
528 HepG2.2.15 cells was based on titration of released infectious HBV particles. All cell lines were  
529 certified mycoplasma-free, as per our monthly contamination testing.

530

531 **PDI inhibitors.** 5,5-Dithiobis(2-nitrobenzoic acid) (DTNB), Nitazoxanide (NTZ), (-)-Epigallocatechin 3-  
532 gallate (EGCG), Rutin, Bacitracin and PX-12 were purchased from Sigma-Aldrich and dissolved in  
533 DMSO, ethanol or water according to the manufacturer's instructions.

534

535 **Antibodies.** For western-blot analysis, HBs antigen and calnexin were detected with goat anti-HBV  
536 polyclonal antibody (murex, DiaSorin) coupled to horseradish peroxidase (HRP) and rabbit calnexin  
537 polyclonal antibody (Enzo), respectively. The rabbit anti-ERp46 (Abcam), mouse anti-ERp57 (Abcam),  
538 and mouse anti-ERp72 (Santa Cruz Biotechnology) antibodies were used for detecting protein  
539 disulfide isomerase proteins by flow cytometry and western blot. NTCP was detected with polyclonal  
540 NTCP/SLC10A1 antibody (Bioss Antibodies) coupled to PE for flow cytometry. Mouse anti-ERp57  
541 (Abcam), Rabbit anti-Rab5, anti-Rab7, anti-Rab11 and anti-Lamp1 (Cell Signaling Technology), and  
542 Donkey anti-Rabbit-Alexa-Fluor-488 and Donkey anti-Mouse-Alexa-Fluor-568 (Thermo Fisher)  
543 antibodies were used for immuno-fluorescence studies.

544

545 **shRNA-expressing stable cell lines.** 293T cells were seeded 24h prior to transfection with VSV-G  
546 plasmid, psPAX2 packaging plasmid, and pLKO.1 expression vector carrying shRNA against ERp46,  
547 ERp57, or ERp72 using calcium phosphate precipitation. Medium was replaced 16h post-transfection.  
548 Vector supernatants were harvested 24h later, filtered through a 0.45 µm filter. Stable knockdown of  
549 ERp72, ERp57 or ERp46 in Huh7-NTCP, Huh7-tat, and Huh7-NTCP-tat cells was performed by  
550 selection with puromycin after lentiviral transduction. The knockdown was validated by flow cytometry  
551 and western blot using antibodies against ERp46, ERp57 or ERp72.

552

553 **Cell-cell fusion assays.** Huh7 “donor” cells ( $2.5 \times 10^5$  cells/well seeded in six-well tissue culture dishes  
554 24 h prior to transfection) were co-transfected using FuGENE 6 transfection reagent (Promega) with 3  
555 µg of pT7HB2.7- wt or mutated glycoproteins and 50 ng of pLTR-luc reporter plasmid. For a positive  
556 control, cells were co-transfected with 3 µg of either pCAGGS-GP/wt-M, expressing CCHFV GPs, or 1  
557 µg of pHCMV-VSV-G and with 50 ng of the pLTR-luc plasmid. For negative controls, cells were co-  
558 transfected with 2 µg of an empty pHCMV plasmid and 50 ng of the pLTR-luc plasmid. Twelve hours  
559 later, transfected cells were detached with Versene (0.53 mM EDTA; Gibco), counted, and reseeded  
560 at the same concentration ( $10^5$  cells/well) in twelve-well plates. Huh7-Tat or Huh7-NTCP-Tat indicator  
561 cells, detached with EDTA and washed, were then added to the transfected cells ( $3 \times 10^5$  cells per  
562 well). After 24h of cocultivation, the cells were washed with PBS, incubated for 3 min in fusion buffer  
563 (130 mM NaCl, 15 mM sodium citrate, 10 mM MES [2-(N-morpholino)ethanesulfonic acid], 5 mM  
564 HEPES) at pH4, pH5 or pH7, and then washed three times with normal medium. The luciferase  
565 activity was measured 24h later using a luciferase assay kit according to the manufacturer’s  
566 instructions (Promega).

567

568 **HDV particles production and infection.** Huh7 cells were seeded in 10 cm plates at a density of  $10^6$   
569 cells per plate and were transfected with a mixture of 2.5 µg of pSVLD3 plasmid and 10 µg of plasmid  
570 allowing the expression of surface envelope glycoproteins of VSV or HBV using FuGENE 6  
571 transfection reagent (Promega), as described previously (Perez-Vargas et al., 2019). Transfected cells  
572 were grown for up to 9 days in primary hepatocyte maintenance medium containing 2% DMSO to slow  
573 cell growth.

574 The supernatants of virus producer cells were filtrated through 0.45 nm-pore filters and were analyzed  
575 by RTqPCR for detection of HDV RNA, using the primers described below. These supernatants were  
576 also used for infection experiments in Huh7-NTCP cells or PDI-down-regulated Huh7-NTCP cells,  
577 which were seeded in 48-well plates at a density of  $1.5 \times 10^4$  cells per well. Infected cells were cultured  
578 in primary hepatocyte maintenance medium containing 2% DMSO following infection. RTqPCR  
579 assays were used to assess infectivity of viral particles at 7 days post-infection.

580 For inhibition assays, drugs were incubated with cells for 2h at 37°C before virus addition or at  
581 different times post-infection and the infectivity was assessed 7 days post-infection by RT-qPCR.

582

583 **Binding assays.** HDV wt particles ( $10^7$  GE) were added to Huh7-NTCP cells and incubated for 1h at  
584 4°C. Unbound virions were removed by three washes with cold PBS, and RTqPCR was used to  
585 assess the amount of bound viral particles.

586

587 **RTqPCR detection of HDV RNAs in virus-producer and in infected cells.** Cells were washed with  
588 phosphate-buffer saline (PBS) and total RNA was extracted with TRI Reagent according to the  
589 manufacturer's instructions (Molecular Research Center). RNAs were reverse transcribed using  
590 random oligonucleotides primers with iScript (Bio-Rad). The following specific primers were used: for  
591 HDV RNA quantification, forward primer 5'-GGACCCCTTCAGCGAACA and reverse primer 5'-  
592 CCTAGCATCTCCTCTATCGCTAT. qPCR was performed using FastStart Universal SYBR Green  
593 Master (Roche) on a StepOne Real-Time PCR System (Applied Biosystems). As an internal control of  
594 extraction, *in vitro*-transcribed exogenous RNAs from the linearized Triplescript plasmid pTRI-Xef  
595 (Invitrogen) were added to the samples prior to RNA extraction and quantified with specific primers (5'-  
596 CGACGTTGTCACCGGGCACG and 5'-ACCAGGCATGGTGGTTACCTTTGC). All values of  
597 intracellular HDV RNAs were normalized to GAPDH gene transcription. For GAPDH mRNAs  
598 quantification, we used the forward 5'-AGGTGAAGGTCCGAGTCAACG and reverse 5'-  
599 TGGAAGATGGTGGTGGGATTTTC primers.

600

601 **Western-blot analyses.** The proteins from pelleted cell supernatants or extracted from total cell  
602 lysates were denatured in Lammeli buffer at 95°C for 5 min and were separated by sodium dodecyl  
603 sulfate polyacrylamide gel electrophoresis and then transferred to nitrocellulose membranes (GE  
604 Healthcare). Membranes were blocked with 5% nonfat dried milk in PBS and incubated at 4°C with a  
605 rabbit or mouse antibody diluted in PBS-0.01% milk, followed by incubation with a IRdye secondary  
606 antibody (Li-Cor Biosciences). Membranes visualization was performed using an Odyssey infrared  
607 imaging system CLx (LI-COR Biosciences).

608 For cell surface biotinylation, Huh7 cells were transfected into 10 cm plates with plasmid encoding wt  
609 or mutant HBV GPs. After 48h, the cell monolayers were rinsed three times with ice-cold PBS and  
610 overlaid with 0.5 ml biotin solution (0.5 mg sulpho-N-hydroxysuccinimide-biotin (Pierce) per ml of  
611 PBS, pH 7.2). The cells were then labeled for 30 min at 4°C. The biotin solution was removed and the  
612 cells were rinsed once with ice-cold 100 mM glycine solution and then incubated for 15 min with 100  
613 mM glycine at 4 °C to stop the reaction. The last washing step was performed with ice-cold PBS.  
614 Proteins were solubilized by the addition of 1 ml RIPA buffer and equivalent quantities of protein  
615 lysates from each sample (Nanodrop quantification, Thermofisher) were immunoprecipitated with

616 Biotin-agarose beads. Proteins were electrophoresed under reducing conditions in SDS-PAGE  
617 followed by electrophoretic transfer to nitrocellulose. Surface-biotinylated proteins were detected with  
618 anti-HBV antibody (murex) coupled to horseradish peroxidase (HRP) and enhanced  
619 chemiluminescence (ECL; Roche). The membranes of biotinylated samples were routinely re-probed  
620 with anti-calnexin antibody to confirm the absence of the intracellular protein calnexin. In addition, 10%  
621 of each lysate was denatured and loaded onto separate gels. Immunoblotting for calnexin on the  
622 membranes of lysate was done to confirm uniform protein loading.

623 Densitometry analysis (Image Lab BioRad software) was used to estimate the relative total amount of  
624 L, M and S mutant proteins, which were expressed relative of the wild type L, M and S total proteins.

625

626 **Flow cytometry.** The surface expression of NTCP, ERp46, ERp57 and ERp72 was quantified by  
627 FACS analysis from  $10^6$  live cells using antibodies added to cells for 1h at 4°C. After washing, the  
628 binding of antibody to the cell surface was detected using PE (Phycoerythrin)-conjugated anti-mouse  
629 antibodies.

630

631 **Immuno-fluorescence (IF), confocal microscopy imaging and image analysis.** Huh7-NTCP cells  
632 were grown on uncoated 14mm-diameter glass coverslips. Forty-eight hours after seeding, cells were  
633 washed with PBS, fixed with 3% paraformaldehyde in PBS for 15 min, quenched with 50mM NH<sub>4</sub>Cl  
634 and permeabilized with 0.1% Triton X-100 for 7min. Fixed cells were then incubated for 1h with  
635 primary antibodies in 1% BSA/PBS, washed and stained for 1 hr with the corresponding fluorescent  
636 Alexa Fluor conjugated secondary antibody (Alexa-Fluor-488 and Alexa-Fluor-568, Thermo Fisher) in  
637 1% BSA/PBS. Cells were washed three times with PBS, stained for nuclei with Hoechst 33342  
638 (Thermo Fisher) for 5 min, washed two times with PBS and mounted in Mowiol 40-88 (Sigma-Aldrich)  
639 prior to image acquisition with LSM-710 confocal microscope (Zeiss). Single section confocal images  
640 of 0.6µm of thickness were analyzed with the ImageJ software. The Pearson's correlation coefficients  
641 were calculated by using the JACoP plugin for ImageJ.

642

643 **Cytotoxicity assay.** The release of LDH from damaged cells was measured with CytoTox-ONE  
644 (Promega, MA, USA) homogeneous membrane integrity assay. Cells were grown in a 96-well flat-  
645 bottom culture plate in density of  $3 \times 10^3$  cells per well and treated with the different drugs for 2h or 24h.  
646 Maximum LDH release was determined by adding 2µl of CytoTox-ONE lysis solution to control wells  
647 for 10min. The assay was performed in 96-well plates by adding 100 µl of the sample supernatant and  
648 100 µl of CytoTox-ONE reagent, after which the plate was shaken for 10s. After 10min of incubation,  
649 50 µl CytoTox-One stop solution was added and the plate was shaken again for 10s. The fluorescence  
650 signal was measured at  $\lambda_{EX}=560$  nm,  $\lambda_{EM}=590$ . LDH-release was calculated as percentage of LDH  
651 released in the culture media of total LDH (media and lysates).

652

653 **Fusion peptide prediction.** The HBV surface sequence used was taken from the UniProt database,  
654 with accession number P03138. Hydropathy plots were obtained with Membrane Protein eXplorer  
655 software (Snider et al., 2009) using as input the reference sequence. Hydropathy plots were also used  
656 to evaluate the effect of residue mutations. Sequences with a propensity to partition into the lipid  
657 bilayer were identified using interfacial settings and pH=5.0.

658

659 **Contact prediction on the Cys rich region.** Contact prediction was performed using RaptorX (Wang  
660 et al., 2017, Teppa et al., 2020). RaptorX integrates evolutionary coupling and sequence conservation  
661 information through an ultra-deep neural network formed by two deep residual neural networks.  
662 RaptorX predicts pairs of residues, whose mutations have arisen simultaneously during evolution.

663

664 **Structural models and molecular dynamic simulation studies.** The HBV surface protein sequence  
665 was taken from the UniProt database, with accession number P03138. Secondary structure prediction  
666 was performed with Jpred (Cole et al., 2008). The S protein region 294-317 was modelled using  
667 MODELLER (Sali and Blundell, 1993). The template crystal structure of the Newcastle disease virus  
668 fusion protein (PDB code: 1G5G) was retrieved from the PDB database (Berman et al., 2000).  
669 Sequence alignment was generated with Clustal X (Larkin et al., 2007). The model evaluation was  
670 conducted using the Ramachandran plot (Ramachandran et al., 1963). The model of the wild-type  
671 sequence was further used to create two structural models with mutations using UCSF Chimera  
672 package (Pettersen et al., 2004). One model contains the double mutations T303C/G308C, which may  
673 create an extra disulfide bond. The overall effect of those mutations would be to "shift" the disulfide  
674 bridge of two amino acids towards the turn of the  $\beta$ -hairpin motif. After mutations, the models were  
675 energy minimized by applying Molecular Modelling Toolkit (MMTK) with Amber parameters for  
676 standard residues, and 100 steepest descent minimization steps with a step size of 0.02 Å. To  
677 investigate the stability of the disulfide bonds, molecular dynamic (MD) simulations of the three models  
678 were carried out by GROMACS version 2020 (Abraham et al., 2015) in conjunction with OPLS-AA/L  
679 all-atom force field. The models were immersed in the cubic boxes filled with water molecules with a  
680 minimal distance of 1.0 nm between the peptide surface and box. Each system was equilibrated to the  
681 desired temperature through a stepwise heating protocol in NVT ensemble followed by 100.0 ps  
682 equilibration in NPT ensemble with position restraints on the protein molecule. The final productive MD  
683 was performed for each system for 10 ns under periodic boundary conditions without any restraints on  
684 the protein with a time step of 2 fs at constant pressure (1 atm) and temperature (300 K). Coordinates  
685 were saved every 10 ps, yielding 1000 frames per MD trajectory. All the frames were further  
686 investigated to differentiate between allosteric and structurally stabilizing disulfides. Disulfide bonds  
687 were classified based on the five relevant torsion angles ( $\chi_1$ ,  $\chi_2$ ,  $\chi_3$ ,  $\chi_2'$  and  $\chi_1'$ ) (see Figure 4-figure

688 supplement 2), disulfides were treated as symmetrical. In this system, twenty conformational  
689 categories are possible (Marques et al., 2010; Schmidt and Hogg, 2007; Schmidt et al., 2006). The  
690 three central angles ( $\chi_2$ ,  $\chi_3$  and  $\chi_2$ ) define the basic shape: Spiral, Hook and Staple (Eklund et al.,  
691 1984). The  $\chi_3$  defines the orientationally motif: left-handed (LH) or right-handed (RH) if the sign is  
692 negative or positive, respectively (Eklund et al., 1984). The  $\chi_1$  and  $\chi_1'$  determines the sign of the  
693 nomenclature (Qi and Grishin, 2005).

694

695 ***In vivo* experiments.** All experiments were performed in accordance with the European Union  
696 guidelines for approval of the protocols by the local ethics committee (Authorization Agreement C2EA-  
697 15, “Comité Rhône-Alpes d’Ethique pour l’Expérimentation Animale”, Lyon, France - APAFIS#27316-  
698 2020060810332115 v4). Primary human hepatocytes (PHH, Corning, BD Gentest) were  
699 intrasplenically injected in NFRG mice (Azuma et al., 2007), a triple mutant mouse knocked-out for  
700 fumarylacetoacetate hydrolase ( $fah^{-/-}$ ), recombinase activating gene 2 ( $rag2^{-/-}$ ), interleukin 2 receptor  
701 gamma chain ( $IL2rg^{-/-}$ ). 48h after adeno-uPA conditioning (Bissig et al., 2010; Calattini et al., 2015).  
702 Mice were subjected to NTBC cycling during the liver repopulation process, as described previously  
703 (Calattini et al., 2015). Mice with human serum albumin (HSA) levels >15 mg/mL, as determined using  
704 a Cobas C501 analyzer (Roche Applied Science), were inoculated with virus preparations by intra-  
705 peritoneal injection. Sera were collected at different time points before and after infection. Mice were  
706 sacrificed 6 weeks post-infection.

707

708 **Statistical analysis.** Statistical analyses were performed using GraphPad Prism version 5.02 for  
709 Windows, GraphPad Software (San Diego California, USA). The Mann-Whitney or Wilcoxon tests  
710 were used for statistical comparisons. A p-value of 0.05 or less was considered as significant. When  
711 applicable, data are presented as mean  $\pm$  standard deviation and results of the statistical analysis are  
712 shown as follows: ns, not significant ( $P > 0.05$ ); \*,  $P < 0.05$ ; \*\*,  $P < 0.01$ ; and \*\*\*,  $P < 0.001$ .

713

714

## 715 **Acknowledgment**

716

717 We are grateful to Camille Sureau for the HBV GP expression constructs and for sharing the HDV  
718 infection assay. We thank Solène Denolly for helpful discussions.

719 We thank the “Plateforme de Thérapie Génique” in Nantes (France) for the production of the *in vivo*-  
720 certified lots of adeno-uPA vectors. We thank Jean-François Henry, Nadine Aguilera and Tiphaine  
721 Dorel from the animal facility (PBES, Plateau de Biologie Experimental de la Souris, UMS3444/CNRS,  
722 US8/Inserm, ENS de Lyon, UCBL), and Véronique Pierre for her technical help in handling of mice.  
723 We acknowledge the contribution of the ANIRA-Genetic Analysis and the PLATIM-Microscopy

724 facilities of SFR Biosciences (UMS3444/CNRS, US8/Inserm, ENS de Lyon, UCBL) for images  
725 quantifications, technical assistance and support. We thank Didier Décimo for support with the BSL3  
726 facility. We thank Didier Décimo for support with the BSL3 facility. We thank Omran Allatif for guidance  
727 with the statistical analysis.

728

729

### 730 **Funding**

731

732 This work was supported by the French “Agence Nationale de la Recherche sur le SIDA et les  
733 Hépatites Virales | Maladie Infectieuses Emergentes” (ANRS|MIE, grants ECTZ71388, ECTZ160643,  
734 ECTZ160726, ECTZ38814 and ECTZ41733), the Foundation FINOVI, the 2017 Call for Joriss  
735 Projects, the LabEx Ecofect (ANR-11-LABX-0048) of the “Université de Lyon”, within the program  
736 “Investissements d’Avenir” (ANR-11-IDEX-0007) operated by the French National Research Agency  
737 (ANR), and the LabEX CALSIMLAB (ANR-11-LABX-0037-01 and ANR-11-IDEX-0004-02).

738

739

### 740 **Competing interests**

741

742 The authors have declared that no competing interests exist.

743

744

### 745 **References**

746

747 Abell, B.A., and Brown, D.T. (1993). Sindbis virus membrane fusion is mediated by reduction of  
748 glycoprotein disulfide bridges at the cell surface. *J. Virol.* *67*, 5496–5501.

749 Abou-Jaoudé, G., and Sureau, C. (2007). Entry of hepatitis delta virus requires the conserved cysteine  
750 residues of the hepatitis B virus envelope protein antigenic loop and is blocked by inhibitors of thiol-  
751 disulfide exchange. *J. Virol.* *81*, 13057–13066.

752 Abraham, M.J., Murtola, T., Schulz, R., Páll, S., Smith, J.C., Hess, B., and Lindahl, E. (2015).  
753 GROMACS: High performance molecular simulations through multi-level parallelism from laptops to  
754 supercomputers. *SoftwareX* *1-2*, 19–25.

755 Apellániz, B., Huarte, N., Largo, E., and Nieva, J.L. (2014). The three lives of viral fusion peptides.  
756 *Chemistry and Physics of Lipids* *181*, 40–55.

757 Azuma, H., Paulk, N., Ranade, A., Dorrell, C., Al-Dhalimy, M., Ellis, E., Strom, S., Kay, M.A., Finegold,  
758 M., and Grompe, M. (2007). Robust expansion of human hepatocytes in Fah<sup>-/-</sup>/Rag2<sup>-/-</sup>/Il2rg<sup>-/-</sup>  
759 mice. *Nature Biotechnology* 25, 903–910.

760 Barbouche, R., Miquelis, R., Jones, I.M., and Fenouillet, E. (2003). Protein-disulfide isomerase-  
761 mediated reduction of two disulfide bonds of HIV envelope glycoprotein 120 occurs post-CXCR4  
762 binding and is required for fusion. *J Biol Chem* 278, 3131–3136.

763 Baumert, T.F., Meredith, L., Ni, Y., Felmlee, D.J., McKeating, J.A., and Urban, S. (2014). Entry of  
764 hepatitis B and C viruses - recent progress and future impact. *Curr Opin Virol* 4, 58–65.

765 Berman, H.M., Bhat, T.N., Bourne, P.E., Feng, Z., Gilliland, G., Weissig, H., and Westbrook, J. (2000).  
766 The Protein Data Bank and the challenge of structural genomics. *Nat. Struct. Biol.* 7 *Suppl*, 957–959.

767 Berting, A., Fischer, C., Schaefer, S., Garten, W., Klenk, H.D., and Gerlich, W.H. (2000). Hemifusion  
768 activity of a chimeric influenza virus hemagglutinin with a putative fusion peptide from hepatitis B virus.  
769 *Virus Res* 68, 35–49.

770 Bissig, K.-D., Wieland, S.F., Tran, P., Isogawa, M., Le, T.T., Chisari, F.V., and Verma, I.M. (2010).  
771 Human liver chimeric mice provide a model for hepatitis B and C virus infection and treatment. *J Clin*  
772 *Invest* 120, 924–930.

773 Blanchet, M., and Sureau, C. (2007). Infectivity determinants of the hepatitis B virus pre-S domain are  
774 confined to the N-terminal 75 amino acid residues. *J. Virol.* 81, 5841–5849.

775 Bremer, C.M., Bung, C., Kott, N., Hardt, M., and Glebe, D. (2009). Hepatitis B virus infection is  
776 dependent on cholesterol in the viral envelope. *Cell. Microbiol.* 11, 249–260.

777 Bremer, C.M., Sominskaya, I., Skrastina, D., Pumpens, P., El Wahed, A.A., Beutling, U., Frank, R.,  
778 Fritz, H.-J., Hunsmann, G., Gerlich, W.H., et al. (2011). N-terminal myristoylation-dependent masking  
779 of neutralizing epitopes in the preS1 attachment site of hepatitis B virus. *Journal of Hepatology* 55,  
780 29–37.

781 Calattini, S., Fusil, F., Mancip, J., Dao Thi, V.L., Granier, C., Gadot, N., Scoazec, J.-Y., Zeisel, M.B.,  
782 Baumert, T.F., Lavillette, D., et al. (2015). Functional and Biochemical Characterization of Hepatitis C  
783 Virus (HCV) Particles Produced in a Humanized Liver Mouse Model. *J. Biol. Chem.* 290, 23173–  
784 23187.



785 Chiu, J., and Hogg, P.J. (2019). Allosteric disulfides: Sophisticated molecular structures enabling  
786 flexible protein regulation. *J. Biol. Chem.* 294, 2949–2960.

787 Chojnacki, J., Anderson, D.A., and Grgacic, E.V.L. (2005). A hydrophobic domain in the large  
788 envelope protein is essential for fusion of duck hepatitis B virus at the late endosome. *J Virol* 79,  
789 14945–14955.

790 Cole, C., Barber, J.D., and Barton, G.J. (2008). The Jpred 3 secondary structure prediction server.  
791 *Nucleic Acids Res.* 36, W197–W201.

792 Delgado, C.L., Núñez, E., Yélamos, B., Gómez-Gutiérrez, J., Peterson, D.L., and Gavilanes, F.  
793 (2012). Spectroscopic characterization and fusogenic properties of preS domains of duck hepatitis B  
794 virus. *Biochemistry* 51, 8444–8454.

795 Delos, S.E., and White, J.M. (2000). Critical role for the cysteines flanking the internal fusion peptide  
796 of avian sarcoma/leukosis virus envelope glycoprotein. *J Virol* 74, 9738–9741.

797 Delos, S.E., Gilbert, J.M., and White, J.M. (2000). The central proline of an internal viral fusion peptide  
798 serves two important roles. *J Virol* 74, 1686–1693.

799 Diwaker, D., Mishra, K.P., and Ganju, L. (2013). Potential roles of protein disulphide isomerase in viral  
800 infections. *Acta Virol.* 57, 293–304.

801 Earp, L.J., Delos, S.E., Park, H.E., and White, J.M. (2004). The Many Mechanisms of Viral Membrane  
802 Fusion Proteins. In *Membrane Trafficking in Viral Replication*, M. Marsh, ed. (Berlin, Heidelberg:  
803 Springer Berlin Heidelberg), pp. 25–66.

804 Eklund, H., Cambillau, C., Sjöberg, B.M., Holmgren, A., Jörnvall, H., Höög, J.O., and Brändén, C.I.  
805 (1984). Conformational and functional similarities between glutaredoxin and thioredoxins. *EMBO J.* 3,  
806 1443–1449.

807 Epan, R.M. (2003). Fusion peptides and the mechanism of viral fusion. *Biochimica et Biophysica*  
808 *Acta (BBA) - Biomembranes* 1614, 116–121.

809 Fenouillet, E., Barbouche, R., and Jones, I.M. (2007). Cell entry by enveloped viruses: redox  
810 considerations for HIV and SARS-coronavirus. *Antioxid. Redox Signal.* 9, 1009–1034.

811 Freitas, N., Enguehard, M., Denolly, S., Levy, C., Neveu, G., Lerolle, S., Devignot, S., Weber, F.,  
812 Bergeron, E., Legros, V., et al. (2020). The interplays between Crimean-Congo hemorrhagic fever

813 virus (CCHFV) M segment-encoded accessory proteins and structural proteins promote virus  
814 assembly and infectivity. *PLoS Pathog.* 16, e1008850.

815 Glebe, D., Urban, S., Knoop, E.V., Cag, N., Krass, P., Grün, S., Bulavaite, A., Sasnauskas, K., and  
816 Gerlich, W.H. (2005). Mapping of the hepatitis B virus attachment site by use of infection-inhibiting  
817 preS1 lipopeptides and tupaia hepatocytes. *Gastroenterology* 129, 234–245.

818 Grgacic, E.V., and Schaller, H. (2000). A metastable form of the large envelope protein of duck  
819 hepatitis B virus: low-pH release results in a transition to a hydrophobic, potentially fusogenic  
820 conformation. *J Virol* 74, 5116–5122.

821 Gripon, P., Cannie, I., and Urban, S. (2005). Efficient inhibition of hepatitis B virus infection by  
822 acylated peptides derived from the large viral surface protein. *J. Virol.* 79, 1613–1622.

823 Harrison, S.C. (2015). Viral membrane fusion. *Virology* 479-480, 498–507.

824 van Hemert, F.J., Zaaijer, H.L., Berkhout, B., and Lukashov, V.V. (2008). Mosaic amino acid  
825 conservation in 3D-structures of surface protein and polymerase of hepatitis B virus. *Virology* 370,  
826 362–372.

827 Herrscher, C., Pastor, F., Burlaud - Gaillard, J., Dumans, A., Seigneuret, F., Moreau, A., Patient, R.,  
828 Eymieux, S., Rocquigny, H., Hourieux, C., et al. (2020). Hepatitis B virus entry into HEPG2-NTCP cells  
829 requires clathrin-mediated endocytosis. *Cellular Microbiology* 22.

830 Hogg, P.J. (2003). Disulfide bonds as switches for protein function. *Trends Biochem. Sci.* 28, 210–  
831 214.

832 Hogg, P.J. (2013). Targeting allosteric disulphide bonds in cancer. *Nature Reviews Cancer* 13, 425–  
833 431.

834 Huang, H.-C., Chen, C.-C., Chang, W.-C., Tao, M.-H., and Huang, C. (2012). Entry of Hepatitis B  
835 Virus into Immortalized Human Primary Hepatocytes by Clathrin-Dependent Endocytosis. *Journal of*  
836 *Virology* 86, 9443–9453.

837 Iwamoto, M., Saso, W., Sugiyama, R., Ishii, K., Ohki, M., Nagamori, S., Suzuki, R., Aizaki, H., Ryo, A.,  
838 Yun, J.-H., et al. (2019). Epidermal growth factor receptor is a host-entry cofactor triggering hepatitis B  
839 virus internalization. *Proceedings of the National Academy of Sciences* 116, 8487–8492.

840 Jain, S., McGinnes, L.W., and Morrison, T.G. (2007). Thiol/disulfide exchange is required for  
841 membrane fusion directed by the Newcastle disease virus fusion protein. *J. Virol.* *81*, 2328–2339.

842 Key, T., Sarker, M., de Antueno, R., Rainey, J.K., and Duncan, R. (2015). The p10 FAST protein  
843 fusion peptide functions as a cystine noose to induce cholesterol-dependent liposome fusion without  
844 liposome tubulation. *Biochim. Biophys. Acta* *1848*, 408–416.

845 Komla-Soukha, I., and Sureau, C. (2006). A tryptophan-rich motif in the carboxyl terminus of the small  
846 envelope protein of hepatitis B virus is central to the assembly of hepatitis delta virus particles. *J Virol*  
847 *80*, 4648–4655.

848 Korba, B.E., Montero, A.B., Farrar, K., Gaye, K., Mukerjee, S., Ayers, M.S., and Rossignol, J.-F.  
849 (2008). Nitazoxanide, tizoxanide and other thiazolides are potent inhibitors of hepatitis B virus and  
850 hepatitis C virus replication. *Antiviral Research* *77*, 56–63.

851 Larkin, M.A., Blackshields, G., Brown, N.P., Chenna, R., McGettigan, P.A., McWilliam, H., Valentin, F.,  
852 Wallace, I.M., Wilm, A., Lopez, R., et al. (2007). Clustal W and Clustal X version 2.0. *Bioinformatics*  
853 *23*, 2947–2948.

854 Lavillette, D., Bartosch, B., Nourrisson, D., Verney, G., Cosset, F.-L., Penin, F., and Pécheur, E.-I.  
855 (2006). Hepatitis C virus glycoproteins mediate low pH-dependent membrane fusion with liposomes. *J.*  
856 *Biol. Chem.* *281*, 3909–3917.

857 Lavillette, D., Pécheur, E.-I., Donot, P., Fresquet, J., Molle, J., Corbau, R., Dreux, M., Penin, F., and  
858 Cosset, F.-L. (2007). Characterization of fusion determinants points to the involvement of three  
859 discrete regions of both E1 and E2 glycoproteins in the membrane fusion process of hepatitis C virus.  
860 *J. Virol.* *81*, 8752–8765.

861 Le Duff, Y., Blanchet, M., and Sureau, C. (2009). The pre-S1 and antigenic loop infectivity  
862 determinants of the hepatitis B virus envelope proteins are functionally independent. *J. Virol.* *83*,  
863 12443–12451.

864 Leistner, C.M., Gruen-Bernhard, S., and Glebe, D. (2008). Role of glycosaminoglycans for binding and  
865 infection of hepatitis B virus. *Cell Microbiol* *10*, 122–133.

866 Le Seyec, J., Chouteau, P., Cannie, I., Guguen-Guillouzo, C., and Gripon, P. (1999). Infection Process  
867 of the Hepatitis B Virus Depends on the Presence of a Defined Sequence in the Pre-S1 Domain.  
868 *Journal of Virology* *73*, 2052–2057.

869 Lin, A.H., and Cannon, P.M. (2002). Use of pseudotyped retroviral vectors to analyze the receptor-  
870 binding pocket of hemagglutinin from a pathogenic avian influenza A virus (H7 subtype). *Virus Res* 83,  
871 43–56.

872 Ma, J., Wang, S., Wang, Z., and Xu, J. (2015). Protein contact prediction by integrating joint  
873 evolutionary coupling analysis and supervised learning. *Bioinformatics* 31, 3506–3513.

874 Macovei, A., Radulescu, C., Lazar, C., Petrescu, S., Durantel, D., Dwek, R.A., Zitzmann, N., and  
875 Nichita, N.B. (2010). Hepatitis B virus requires intact caveolin-1 function for productive infection in  
876 HepaRG cells. *J. Virol.* 84, 243–253.

877 Macovei, A., Petrareanu, C., Lazar, C., Florian, P., and Branza-Nichita, N. (2013). Regulation of  
878 hepatitis B virus infection by Rab5, Rab7, and the endolysosomal compartment. *J. Virol.* 87, 6415–  
879 6427.

880 Mangold, C.M., Unckell, F., Werr, M., and Streeck, R.E. (1995). Secretion and antigenicity of hepatitis  
881 B virus small envelope proteins lacking cysteines in the major antigenic region. *Virology* 211, 535–  
882 543.

883 Marques, J.R.F., da Fonseca, R.R., Drury, B., and Melo, A. (2010). Conformational characterization of  
884 disulfide bonds: A tool for protein classification. *Journal of Theoretical Biology* 267, 388–395.

885 Martin, I., Ruyschaert, J.-M., and Epand, R.M. (1999). Role of the N-terminal peptides of viral  
886 envelope proteins in membrane fusion. *Adv Drug Deliv Rev* 38, 233–255.

887 Müller, J., Naguleswaran, A., Müller, N., and Hemphill, A. (2008). *Neospora caninum*: Functional  
888 inhibition of protein disulfide isomerase by the broad-spectrum anti-parasitic drug nitazoxanide and  
889 other thiazolides. *Experimental Parasitology* 118, 80–88.

890 Ni, Y., Sonnabend, J., Seitz, S., and Urban, S. (2010). The Pre-S2 Domain of the Hepatitis B Virus Is  
891 Dispensable for Infectivity but Serves a Spacer Function for L-Protein-Connected Virus Assembly.  
892 *Journal of Virology* 84, 3879–3888.

893 Ni, Y., Lempp, F.A., Mehrle, S., Nkongolo, S., Kaufman, C., Fälth, M., Stindt, J., Königer, C., Nassal,  
894 M., Kubitz, R., et al. (2014). Hepatitis B and D viruses exploit sodium taurocholate co-transporting  
895 polypeptide for species-specific entry into hepatocytes. *Gastroenterology* 146, 1070–1083.

896 Pacello, F., D’Orazio, M., and Battistoni, A. (2016). An ERp57-mediated disulphide exchange  
897 promotes the interaction between *Burkholderia cenocepacia* and epithelial respiratory cells. *Sci Rep* 6,  
898 21140.

899 Perez-Vargas, J., Amirache, F., Boson, B., Mialon, C., Freitas, N., Sureau, C., Fusil, F., and Cosset,  
900 F.-L. (2019). Enveloped viruses distinct from HBV induce dissemination of hepatitis D virus in vivo.  
901 *Nature Communications* 10.

902 Pettersen, E.F., Goddard, T.D., Huang, C.C., Couch, G.S., Greenblatt, D.M., Meng, E.C., and Ferrin,  
903 T.E. (2004). UCSF Chimera--a visualization system for exploratory research and analysis. *J Comput*  
904 *Chem* 25, 1605–1612.

905 Qi, Y., and Grishin, N.V. (2005). Structural classification of thioredoxin-like fold proteins. *Proteins* 58,  
906 376–388.

907 Ramachandran, G.N., Ramakrishnan, C., and Sasisekharan, V. (1963). Stereochemistry of  
908 polypeptide chain configurations. *Journal of Molecular Biology* 7, 95–99.

909 Rey, F.A., and Lok, S.-M. (2018). Common Features of Enveloped Viruses and Implications for  
910 Immunogen Design for Next-Generation Vaccines. *Cell* 172, 1319–1334.

911 Richard, C., Liuzzo, J.P., and Moscatelli, D. (1995). Fibroblast Growth Factor-2 Can Mediate Cell  
912 Attachment by Linking Receptors and Heparan Sulfate Proteoglycans on Neighboring Cells. *Journal of*  
913 *Biological Chemistry* 270, 24188–24196.

914 Rigg, R.J., and Schaller, H. (1992). Duck hepatitis B virus infection of hepatocytes is not dependent on  
915 low pH. *J. Virol.* 66, 2829–2836.

916 Rodríguez-Crespo, I., Gómez-Gutiérrez, J., Nieto, M., Peterson, D.L., and Gavilanes, F. (1994).  
917 Prediction of a putative fusion peptide in the S protein of hepatitis B virus. *J Gen Virol* 75 ( Pt 3), 637–  
918 639.

919 Rodríguez-Crespo, I., Núñez, E., Gómez-Gutiérrez, J., Yélamos, B., Albar, J.P., Peterson, D.L., and  
920 Gavilanes, F. (1995). Phospholipid interactions of the putative fusion peptide of hepatitis B virus  
921 surface antigen S protein. *J Gen Virol* 76 ( Pt 2), 301–308.

922 Rodríguez-Crespo, I., Núñez, E., Yélamos, B., Gómez-Gutiérrez, J., Albar, J.P., Peterson, D.L., and  
923 Gavilanes, F. (1999). Fusogenic activity of hepadnavirus peptides corresponding to sequences  
924 downstream of the putative cleavage site. *Virology* 261, 133–142.

925 Rosenthal, P.B., Zhang, X., Formanowski, F., Fitz, W., Wong, C.H., Meier-Ewert, H., Skehel, J.J., and  
926 Wiley, D.C. (1998). Structure of the haemagglutinin-esterase-fusion glycoprotein of influenza C virus.  
927 *Nature* 396, 92–96.

928 Ruiz-Olmedo, M.I., González-Hernández, I., Palomares-Alonso, F., Franco-Pérez, J., González F., M.  
929 de L., and Jung-Cook, H. (2017). Effect of nitazoxanide on albendazole pharmacokinetics in  
930 cerebrospinal fluid and plasma in rats. *Saudi Pharmaceutical Journal* 25, 413–418.

931 Sali, A., and Blundell, T.L. (1993). Comparative protein modelling by satisfaction of spatial restraints.  
932 *J. Mol. Biol.* 234, 779–815.

933 Salisse, J., and Sureau, C. (2009). A Function Essential to Viral Entry Underlies the Hepatitis B Virus  
934 “a” Determinant. *Journal of Virology* 83, 9321–9328.

935 Schmidt, B., and Hogg, P.J. (2007). Search for allosteric disulfide bonds in NMR structures. *BMC*  
936 *Struct. Biol.* 7, 49.

937 Schmidt, B., Ho, L., and Hogg, P.J. (2006). Allosteric disulfide bonds. *Biochemistry* 45, 7429–7433.

938 Schulze, A., Gripon, P., and Urban, S. (2007). Hepatitis B virus infection initiates with a large surface  
939 protein-dependent binding to heparan sulfate proteoglycans. *Hepatology* 46, 1759–1768.

940 Siegler, V.D., and Bruss, V. (2013). Role of transmembrane domains of hepatitis B virus small surface  
941 proteins in subviral-particle biogenesis. *J Virol* 87, 1491–1496.

942 Snider, C., Jayasinghe, S., Hristova, K., and White, S.H. (2009). MPEX: a tool for exploring membrane  
943 proteins. *Protein Sci.* 18, 2624–2628.

944 Stockis, A., Deroubaix, X., Lins, R., Jeanbaptiste, B., Calderon, P., and Rossignol, J.F. (1996).  
945 Pharmacokinetics of nitazoxanide after single oral dose administration in 6 healthy volunteers.  
946 *International Journal of Clinical Pharmacology and Therapeutics* 34, 349–351.

947 Sureau, C. (2010). The use of hepatocytes to investigate HDV infection: the HDV/HepaRG model.  
948 *Methods Mol. Biol.* 640, 463–473.

949 Sureau, C., Guerra, B., and Lee, H. (1994). The middle hepatitis B virus envelope protein is not  
950 necessary for infectivity of hepatitis delta virus. *J. Virol.* 68, 4063–4066.

951 Turano, C., Coppari, S., Altieri, F., and Ferraro, A. (2002). Proteins of the PDI family: unpredicted non-  
952 ER locations and functions. *J. Cell. Physiol.* 193, 154–163.

953 Wang, S., Sun, S., Li, Z., Zhang, R., and Xu, J. (2017). Accurate De Novo Prediction of Protein  
954 Contact Map by Ultra-Deep Learning Model. *PLoS Comput. Biol.* *13*, e1005324.

955 White, J.M., and Whittaker, G.R. (2016). Fusion of Enveloped Viruses in Endosomes. *Traffic* *17*, 593–  
956 614.

957 Wouters, M.A., Lau, K.K., and Hogg, P.J. (2004). Cross-strand disulphides in cell entry proteins:  
958 poised to act. *Bioessays* *26*, 73–79.

959 Yan, H., Zhong, G., Xu, G., He, W., Jing, Z., Gao, Z., Huang, Y., Qi, Y., Peng, B., Wang, H., et al.  
960 (2012). Sodium taurocholate cotransporting polypeptide is a functional receptor for human hepatitis B  
961 and D virus. *Elife* *1*, e00049.

962 Yan, H., Liu, Y., Sui, J., and Li, W. (2015). NTCP opens the door for hepatitis B virus infection.  
963 *Antiviral Res.* *121*, 24–30.

964 Zhou, B., Baldus, I.B., Li, W., Edwards, S.A., and Gräter, F. (2014). Identification of allosteric  
965 disulfides from prestress analysis. *Biophys. J.* *107*, 672–681.

966

967 **Figure legends**

968

969 **Figure 1. HBV GP fusion trigger is independent of acid pH, HSPG and NTCP.** (A) Huh7 “donor”  
970 cells transfected with the pT7HB2.7 plasmid allowing expression of HBV GPs (HBV) and a luciferase  
971 marker gene driven by the HIV-1 promoter were co-cultured with either Huh7-tat (H-tat) or Huh7-  
972 NTCP-tat (N-tat) “indicator” cells that express the HIV Tat protein. After 24h of co-culture, the cells  
973 were treated at pH4 (or pH 5 for VSV-G) vs. pH7 for 3 minutes. The luciferase activity induced by  
974 fusion between donor and indicator cells was then measured 24h later. A control plasmid that does not  
975 allow GP expression (Empty) was used to determine the background of luciferase expression. The  
976 CCHFV Gn/Gc (CCHFV) or VSV-G (VSV) GPs were used as positive controls for fusion at low pH.  
977 Fusion mediated by HBV GPs with Huh7-tat cells was taken as 100%. The bars represent the means  
978 (N=3). Error bars correspond to standard deviation. See the raw data of individual experiments in  
979 Figure 1-figure supplement 1. (B) Results of cell-cell fusion assays performed as above-described in  
980 the presence of heparin at the indicated concentrations throughout the co-coculture. No cytotoxicity  
981 could be detected in these conditions (Figure 1-figure supplement 2). The graphs represent the  
982 average of two independent experiments. Fusion mediated by HBV GPs with mock-treated Huh7 cells  
983 was taken as 100%. (C) CHO “donor” cells transfected with the pT7HB2.7 plasmid and a luciferase  
984 marker gene driven by the HIV-1 promoter were co-cultured with either Huh7-tat (H-tat), CHO-tat  
985 (CHO wt), or CHO-pgsB618-tat (pgsB618) “indicator” cells that express the HIV Tat protein. The  
986 luciferase activity induced by fusion between donor and indicator cells was then measured 24h later. A  
987 control plasmid that does not allow GP expression (Empty) was used to determine the background of  
988 luciferase expression. Fusion mediated by HBV GPs with Huh7-tat was taken as 100%. The graphs  
989 represent the average of two independent experiments. (D) Huh7 “donor” cells transfected plasmids  
990 allowing expression of L, M or S HBV GPs alone, both L and S GPs (noM) or all HBV GPs (Wt) and a  
991 luciferase marker gene driven by the HIV-1 promoter were co-cultured with Huh7-tat or Huh7-NTCP-  
992 tat “indicator” cells that express HIV Tat protein. Cell co-cultures were then processed as above  
993 described to determine cell-cell fusion activity. Fusion mediated by HBV GP at pH7 with Huh7-tat cells  
994 was taken as 100%. The bars represent the means (N=3). Error bars correspond to standard  
995 deviation. (E) Detection of HBV GPs at the cell surface by biotinylation. Transfected Huh7 cells were  
996 biotinylated for 30 min at 4°C and then processed biochemically. Cell lysates were subjected to  
997 streptavidin pull-down prior to western blot analysis using anti-HBsAg antibody (Murex). The molecular  
998 weight markers (kDa) are shown to the right. Calnexin detection was used as control for cytoplasmic  
999 protein marker, showing the integrity of cell membrane, as shown in this representative western blot.  
1000 (F) Relative GPs expression at the cell surface as compared to Wt, quantified by adding the L+M+S  
1001 signals from western blot analyses. The results are expressed as mean  $\pm$  SD (N=3). No statistical



1002 differences could be found using the Mann-Whitney test (p-value >0.05). See also the quantification of  
1003 total HBV GP expression in the Figure 1-figure supplement 4.

1004

1005 **Figure 2. Functional analysis of predicted HBV fusion peptides.** (A) Sequence of HBV L protein  
1006 showing the amino acid color code and boxes for the localization of the two predicted fusion peptides  
1007 in preS1 and in preS2. (B) Sequence of the two predicted fusion peptides showing the positions that  
1008 were mutated (bold). (C, D) Huh7 cells were co-transfected with pSVLD3 plasmid coding for HDV  
1009 RNPs and plasmids coding for wt or mutant HBV GPs. The FW/AA and FW/EE are double alanine  
1010 mutants at position F52 and W66. As control, pSVLD3 was co-transfected with an empty plasmid  
1011 (referred to as “noGP”). At day 9 post-transfection, the cell supernatants were harvested, filtered and  
1012 the extracellular RNA was extracted and purified before quantifying HDV RNAs by RTqPCR HDV RNA  
1013 levels in GE (genome equivalent) are expressed as means  $\pm$  SD (N=3) per mL of cell supernatants.  
1014 (E, F) HDV particles were used to infect Huh7-NTCP cells, which were grown for 7 days before total  
1015 intracellular RNA was purified. The results of HDV RNA quantification by RTqPCR are expressed after  
1016 normalization with GAPDH RNAs as means  $\pm$  SD (N=3) per mL of cell lysates containing  $10^6$  cells. (G,  
1017 H) Huh7 “donor” cells co-expressing wt or mutant HBV GPs and a luciferase marker gene driven by  
1018 the HIV-1 promoter were co-cultured with either Huh7-tat (H-tat) or Huh7-NTCP-tat (N-tat) “indicator”  
1019 cells that express HIV Tat protein. After 24h, the cells were treated at pH4 or pH7 for 3 minutes. The  
1020 luciferase activity induced by the fusion between the donor and indicator cells was measured 24h  
1021 later. Fusion mediated by wt GP at pH7 with Huh7-NTCP-tat cells was taken as 100%. The bars  
1022 represent the means (N=5). Error bars correspond to standard deviations. (I, J) Quantification of wt  
1023 and mutant GPs at cell surface by western blot analyses (see examples in Figure 2-figure supplement  
1024 2). The results show the relative GPs expression of preS1 (I) and preS2 (J) mutants compared to Wt,  
1025 as indicated, and are expressed as means  $\pm$  SD (N=3). No statistical differences could be found using  
1026 the Mann-Whitney test (p-value >0.05).

1027

1028 **Figure 3. DTNB, a thiol-specific oxidizing reagent, inhibits HBV membrane fusion.** (A) DTNB (2  
1029 mM) was added to the cell supernatant containing HDV particles at the onset of infection (0h) or at the  
1030 indicated times post-infection and was removed 8hr later. VSV- $\Delta$ p, *i.e.*, HDV particles generated with  
1031 VSV-G GP rather than HBV, were used as control for a virus entry process that is not affected by  
1032 DNTB. As negative control, pSVLD3 was co-transfected with an empty plasmid (referred to as  
1033 “noGP”). At 7 days post-infection, HDV RNAs were extracted from infected cells and quantified by  
1034 RTqPCR. The results are expressed after normalization with GAPDH RNAs as means  $\pm$  SD (N=3) per  
1035 mL of cell lysates containing  $10^6$  cells. The results of infection in the absence of DTNB are shown  
1036 [DTNB(-)]. (B) Huh7 “donor” cells co-expressing HBV GPs and a luciferase marker gene driven by the  
1037 HIV-1 promoter were co-cultured with Huh7-NTCP-tat “indicator” cells that express HIV Tat protein.

1038 Different concentrations of DTNB were added at 0h vs. at 16h after initiating the cell co-culture, as  
1039 indicated. No cytotoxicity could be detected in these conditions (Figure 1-figure supplement 2). The  
1040 luciferase activity induced by fusion between donor and indicator cells was then measured 24h later.  
1041 Fusion mediated by HBV GPs without DTNB was taken as 100%. The graphs represent the average  
1042 of four independent experiments. **(C, D)** Huh7 cells transfected with pUC19 (noGP) or the pT7HB2.7  
1043 (HBV) plasmids were incubated with DMSO (0) or increasing doses of DTNB (0.5, 1 and 2 mM) for  
1044 16h prior to incubation with biotin for 30 min at 4°C. Biotin was omitted from one sample (-) and served  
1045 as a negative control for non-specific binding of proteins to streptavidin. Cells were subsequently lysed  
1046 and the biotinylated surface proteins were captured by streptavidin agarose. Total **(C)** and biotin-  
1047 labelled proteins **(D)** were then analyzed by western blot using anti-HBsAg (Murex) and anti-calnexin  
1048 antibodies. Calnexin detection was used as control for cytoplasmic protein marker, showing the  
1049 integrity of cell membrane, as shown in these representative western blots. The molecular weight  
1050 markers (kDa) are shown to the left.

1051

1052 **Figure 4. Disulfides conformation models.** **(A)** Cysteine-rich regions on the “a” determinant  
1053 (residues 261-324) of the HBV S GP. Four sub-regions that are rich in cysteine are coloured: I (blue),  
1054 II (green), III (yellow) and IV (red). Jpred secondary structure prediction different from random-coil is  
1055 indicated:  $\beta$ -strand (arrow) and  $\alpha$ -helix (zigzag line). **(B)** Probability of contacts predicted by RaptorX  
1056 between the four cysteine-rich regions. The probabilities higher than 0.7 are highlighted in red (see  
1057 also Figure 4-figure supplement 1). **(C)** Predominant disulfide conformations obtained by molecular  
1058 dynamics simulation of the modelled 294-317 region of the HBV surface protein. Note that the  $\beta$ -  
1059 strand on the wt sequence (left) adopts a loop conformation with an allosteric disulfide conformer  
1060 between the C301-C310 bond, which is specifically classified as a -/+RHHook conformation. The  
1061 T303C/G308C double mutant (right) may generate an additional disulfide bond, resulting in two  
1062 structural disulfides of +/-RHStaple and -/+LHSpiral conformations that form the C301-310 and C303-  
1063 C308 bonds, respectively.

1064

1065 **Figure 5. Evidence for a functional role of the CSD in the region 294-317 of the HBV S GP.** **(A)**  
1066 Huh7 cells were co-transfected with pSVLD3 plasmid coding for HDV RNPs and plasmids coding for  
1067 wt, single or double mutant (TG/CC) HBV GPs. As control, pSVLD3 was co-transfected with an empty  
1068 plasmid (referred to as “noGP”). At day 9 post-transfection, the cell supernatants were harvested,  
1069 filtered and the extracellular RNA was extracted and purified before quantifying HDV RNAs by  
1070 RTqPCR. HDV RNA levels in GE (genome equivalent) are expressed as means  $\pm$  SD (N=4) per mL of  
1071 cell supernatants. **(B)** HDV particles were used to infect Huh7-NTCP cells, which were grown for 7  
1072 days before total intracellular RNA was purified. The results of HDV RNA quantification by RTqPCR  
1073 are expressed after normalization with GAPDH RNAs as means  $\pm$  SD (N=4) per mL of cell lysates

1074 containing  $10^6$  cells. (C) Detection of GP mutants at the cell surface by biotinylation. Huh7 cells  
1075 expressing wt or mutant HBV GPs were biotinylated for 30 min at 4°C and then processed  
1076 biochemically. Cell lysates were subjected to streptavidin pull-down prior to western blot analysis  
1077 using anti-HBsAg antibody (Murex). The molecular weight markers (kDa) are shown to the left.  
1078 Calnexin detection was used as control for cytoplasm protein marker, showing the integrity of cell  
1079 membrane, as shown in this representative western blot. The relative quantification of cell surface GP  
1080 expression compared to wt were quantified from western blot analyses (means  $\pm$  SD; N=3) are shown  
1081 below. See the quantification of total HBV GP expression in the Figure 1-figure supplement 4. (D)  
1082 Huh7 “donor” cells co-expressing wt or mutant HBV GPs and a luciferase marker gene driven by the  
1083 HIV-1 promoter were co-cultured with either Huh7-tat (H-tat) or Huh7-NTCP-tat (N-tat) “indicator” cells  
1084 that express HIV Tat protein. After 24h, the cells were treated at pH4 or pH7 for 3 minutes. The  
1085 luciferase activity induced by the fusion between the donor and indicator cells was measured 24h  
1086 later. Fusion mediated by wt GP at pH7 with Huh7-NTCP-tat cells was taken as 100%. The bars  
1087 represent the means (N=4). Error bars correspond to standard deviations.  
1088

1089 **Figure 6. PDI inhibitors in HBV entry.** (A) HDV particles harboring wt or TG/CC mutant  
1090 (T330C/G308C) HBV GPs were incubated with Huh7 or Huh7-NTCP cells that were pre-treated for 2h  
1091 with the indicated inhibitors that block different PDI proteins or with DMSO, used as vehicle. Binding of  
1092 either virus particles to the cells was quantified by RTqPCR and expressed after normalization with  
1093 GAPDH RNAs as mean  $\pm$  SD (N=3) per mL of cell lysates containing  $10^6$  cells. (B) HDV or (C) HBV  
1094 particles were used to infect Huh7-NTCP cells that were pre-incubated for 2h with the indicated  
1095 inhibitors that block different PDI proteins or with DMSO, used as vehicle. Infected cells were grown  
1096 for 7 days before total intracellular RNA or DNA was purified. The results of HDV RNA and HBV DNA  
1097 quantification by RTqPCR and qPCR, respectively, are expressed after normalization with GAPDH  
1098 RNAs as means  $\pm$  SD (N=3) per mL of cell lysates containing  $10^6$  cells. (D) Huh7 “donor” cells co-  
1099 expressing HBV GPs and a luciferase marker gene driven by the HIV-1 promoter were co-cultured  
1100 with Huh7-NTCP-tat “indicator” cells that express HIV Tat protein. The indicated PDI inhibitors were  
1101 added when “donor” and “indicator” cells were mixed for co-cultures and the luciferase activity induced  
1102 by cell-cell fusion was measured 24h later. DMSO was used as vehicle. Fusion mediated by HBV GPs  
1103 without inhibitor was taken as 100%. The graphs represent the average of four independent  
1104 experiments. The PDI inhibitors were used at the following concentrations: NTZ, 30  $\mu$ g/mL; EGCG, 5  
1105  $\mu$ M; Rutin, 5  $\mu$ M; Bacitracin, 5 mM; PX-12, 30  $\mu$ g/mL. No cytotoxicity could be detected in these  
1106 conditions (Figure 1-figure supplement 2).

1107  
1108 **Figure 7. ERp57 down-regulation inhibits in HBV entry.** (A) Intracellular (upper panels) and cell-  
1109 surface (lower panels) staining of ERp46, ERp57 and ERp72 PDI members. Huh7-NTCP cells were

1110 subjected to flow cytometry analysis, in order to evaluate the expression of the indicated PDIs. Cells  
1111 stained with secondary antibody only (No primary) were used to provide the background of flow  
1112 cytometry analyses. **(B)** HDV or **(C)** HBV particles were used to infect Huh7-NTCP cells in which the  
1113 indicated PDIs were down-regulated by lentiviral vectors carrying shRNA (see Figure 7-figure  
1114 supplement 1 and Figure 7-figure supplement 2). Naïve Huh7-NTCP cells were used as controls.  
1115 Infected cells were grown for 7 days before total intracellular RNA or DNA was purified. The results of  
1116 HDV RNA and HBV DNA quantification by RTqPCR and qPCR, respectively, are expressed after  
1117 normalization with GAPDH RNAs as means  $\pm$  SD (N=3) per mL of cell lysates containing  $10^6$  cells. **(D)**  
1118 Huh7 “donor” cells co-expressing HBV GPs and a luciferase marker gene driven by the HIV-1  
1119 promoter were co-cultured with Huh7-NTCP-tat “indicator” cells that express HIV Tat protein in which  
1120 the indicated PDI were down-regulated by lentiviral vectors carrying shRNA. After 24h, the cells were  
1121 treated at pH4 or pH7 for 3 minutes. The luciferase activity induced by the fusion between donor and  
1122 indicator cells was measured 24h later. Fusion mediated by HBV GPs at pH7 with naïve Huh7-NTCP-  
1123 tat cells (Ctrl) was taken as 100%. A control plasmid that does not allow GP expression (Empty) was  
1124 used to determine the background of luciferase expression. The bars represent the means (N=3).  
1125 Error bars correspond to standard deviations.

1126

1127 **Figure 8. Intracellular localization of ERp57 in Huh7-NTCP cells.** Huh7-NTCP cells were grown on  
1128 glass cover slides and fixed 48hrs after seeding. **(A)** Endogenous ERp57 with Rab5, Rab7, Rab11 or  
1129 Lamp1 were immune-stained, and the colocalization of ERp57 (red channels) with Rab5, Rab7,  
1130 Rab11 or Lamp1 (green channels) was analyzed by confocal microscopy. Scale bars of panels and  
1131 zooms from squared area represent 10  $\mu$ m and 2  $\mu$ m, respectively. **(B)** The degree of colocalization  
1132 between ERp57 and the different cell markers was assessed by determining the Pearson’s correlation  
1133 coefficients with the JACoP plugin of ImageJ. Results are expressed as the mean of 6 individual cells.  
1134 Error bars correspond to standard deviations.

1135

1136 **Figure 9. *In vivo* assessment of ERp57 inhibition.** **(A)** 4-8 weeks old NOD-FRG mice were  
1137 engrafted with primary human hepatocytes (PHH). After ca. 2-3 months, the animals displaying HSA  
1138 levels  $>15$  mg/mL were randomly split in 4 different groups (N=3 to N=5 animals, see Table in the  
1139 inset) that were infected with HBV ( $10^8$  GE/mouse), using the displayed NTZ treatment schedule. **(B)**  
1140 At different time points post-infection, blood samples (50  $\mu$ l) were collected and the viremia in sera  
1141 was monitored by qPCR (GE/mL of serum). The graphs show the results of viremia (means  $\pm$  SD) of  
1142 HBV. See results of individual mice in Figure 9-figure supplement 1.

1143

1144 **Legends to figure supplements**

1145

1146 **Figure 1-figure supplement 1. HBV GP fusion trigger is independent of acid pH and NTCP.** Huh7  
1147 “donor” cells transfected with the pT7HB2.7 plasmid allowing expression of HBV GPs (HBV) and a  
1148 luciferase marker gene driven by the HIV-1 promoter were co-cultured with either Huh7-tat (H-tat) or  
1149 Huh7-NTCP-tat (N-tat) “indicator” cells that express the HIV Tat protein. After 24h of co-culture, the  
1150 cells were treated at pH4 (or pH5 for VSV-G) vs. pH7 for 3 minutes. The luciferase activity induced by  
1151 fusion between donor and indicator cells was then measured 24h later. A control plasmid that does not  
1152 allow GP expression (Empty) was used to determine the background of luciferase expression. The  
1153 CCHFV Gn/Gc (CCHFV) or VSV-G GPs (VSV) were used as positive controls for fusion at low pH.  
1154 Results from three independent experiments expressed as ratios of luciferase activities of the different  
1155 conditions relative to that of the control conditions.

1156

1157 **Figure 1-figure supplement 2. Results of cell survival after drug treatments.** The indicated drugs  
1158 were used as described in Figure 1B (Heparin), Figure 3 (DNTB), and Figure 6 (NTZ, EGCG, Rutin,  
1159 Bacitracin and PX-12). Cell supernatants were collected immediately after treatment (Post-treatment)  
1160 or after a further incubation at 37°C of the treated cells (Post-incubation). Cell toxicity assessment was  
1161 performed with the LDH (CytoTox-ONE Promega) using the indicated positive and negative controls of  
1162 the kit. Error bars correspond to standard deviations.

1163

1164 **Figure 1-figure supplement 3. Characterization of “noM” HDV particles.** (A) Huh7 cells were co-  
1165 transfected with pSVLD3 plasmid coding for HDV RNPs and with plasmids encoding either the wt HBV  
1166 GPs (Wt) or only L and S (noM). As control, pSVLD3 was co-transfected with an empty plasmid  
1167 (referred to as “noGP”). At day 9 post-transfection, the cell supernatants were harvested, filtered and  
1168 the extracellular RNA was extracted and purified before quantifying HDV RNAs by RTqPCR. HDV  
1169 RNA levels in GE (genome equivalent) are expressed as means  $\pm$  SD (N=4) per mL of cell  
1170 supernatants. (B) HDV or noM particles were used to infect Huh7-NTCP cells, which were grown for 7  
1171 days before total intracellular RNA was purified. The results of HDV RNA quantification by RTqPCR,  
1172 are expressed after normalization with GAPDH RNAs as means  $\pm$  SD (N=4) per mL of cell lysates  
1173 containing  $10^6$  cells.

1174

1175 **Figure 1-figure supplement 4. Total protein expression.** (A) Cell lysates of Huh7 cells expressing  
1176 the indicated wt or mutant GPs from Figure 1 (left) and Figure 5 (right) were subjected to western blot  
1177 analysis, using anti-HBsAg antibody (Murex). The molecular weight markers (kDa) are shown to the  
1178 left. Calnexin detection was used as control for cytoplasmic protein marker, as shown in these  
1179 representative western blots. The black dots indicate dimers of S, as described in the literature

1180 (Huovila et al., 1992), which are formed in the pre-Golgi compartment (B) Relative GPs expression  
1181 compared to Wt, quantified from western blot using anti-HBsAg antibody. The results are expressed  
1182 as mean  $\pm$  SD (N=3).

1183

1184 **Figure 2-figure supplement 1. Prediction of fusion peptides within S protein by using Wimley-**  
1185 **White Interfacial Hydrophobicity Scale. (A)** The hydropathy profile (black curve) and its smoothed  
1186 approximation (green curve). The interface scale measures a residue's free energy of transfer within  
1187 an unfolded polypeptide chain, from water to a phosphocholine bilayer. The five predicted regions with  
1188 high propensity to interact with the lipid surface of the cell membrane are indicated with horizontal red  
1189 bars, the four putative transmembrane regions are indicated with horizontal brown bars. The two  
1190 regions indicated with red arrows were considered as putative fusogenic peptides. The preS1, preS2  
1191 and S regions are represented above the curve. (B) Impact of mutations in predicted putative  
1192 fusogenic segments. The table reports the Gibbs free energy ( $\Delta G$ ) of the two presumed fusogenic  
1193 segments computed for WT and mutants. A negative  $\Delta G$  indicates that a peptide is favoured for  
1194 partitioning from water to lipid bilayer, so it may be suspected as fusogenic. A dash indicates that the  
1195 region is no longer expected to interact with lipid bilayer and hence to be fusogenic.

1196

1197 **Figure 2-figure supplement 2. Cell surface and intracellular detection of preS1 and preS2 HBV**  
1198 **GP mutants. (A, B)** Huh7 cells expressing wt or mutant HBV GPs from Figure 2 were biotinylated for  
1199 30 min at 4°C and then processed biochemically. Cell lysates were subjected to streptavidin pull-down  
1200 prior to western blot analysis using anti-HBsAg antibody (Murex). The molecular weight markers (kDa)  
1201 are shown to the left. Calnexin detection was used as control for cytoplasm protein marker, showing  
1202 the integrity of cell membrane. (C, D) Detection and quantification of total GP expression. Cell lysates  
1203 of Huh7 cells expressing the indicated wt or mutant GPs from Figure 2 were subjected to western blot  
1204 analysis using anti-HBsAg antibody (Murex). The molecular weight markers (kDa) are shown to the  
1205 left. Calnexin detection was used as control for cytoplasmic protein marker, as shown in these  
1206 representative western blots. The results show the relative GPs expression compared to Wt of preS1  
1207 (C) and preS2 mutants (D), as indicated, and are expressed as mean  $\pm$  SD (N=3).

1208

1209 **Figure 3-figure supplement 1. Effect of DTNB on HDV entry.** Different concentrations of DTNB  
1210 were added to the cell supernatant containing HDV particles at the onset of infection (0h) or at 16  
1211 hours post-infection. At 7 days post-infection virus HDV RNA from cells were extracted and quantified  
1212 by RTqPCR. The results are expressed after normalization with GAPDH RNAs as means  $\pm$  SD (N=3)  
1213 per mL of cell lysates containing  $10^6$  cells.

1214

1215

1216 **Figure 4-figure supplement 1. Contact map prediction for the L protein by RaptorX.** (A) The  
1217 symmetric NxN matrix, where N is the length of the L protein, represents the probability of two  
1218 residues being in contact. Higher probabilities are represented by darker colors. The green square  
1219 highlights the “a” determinant containing the four cysteine-reach regions illustrated in Figure 4A and in  
1220 (C) on the sequence. (B) A zoom of the green square where contacts between residues in the four  
1221 cysteine-reach regions are delimited by five distinguished boxes. (C) Colors of the boxes pair with the  
1222 links connecting the cysteine-reach regions.

1223

1224 **Figure 4-figure supplement 2. Geometry of a disulphide bond.** The five  $\chi$  angles used to classify a  
1225 disulfide bond conformers are labelled across the bond. MD simulations (see Methods) confirmed the  
1226 stability of the bond as an allosteric disulfide, specifically on a -/+RH Hook conformation. While only  
1227 three out of the twenty possible configurations, namely -RH Staple, -LH Hook and -/+RH Hook, are  
1228 identified as allosteric disulfide bonds (Hogg, 2013; Schmidt and Hogg, 2007), the -/+RH Hook  
1229 conformation is more stressed than other geometries, due to stretching of the S-S bond and bending  
1230 of the neighboring bond angles (Zhou et al., 2014).

1231

1232 **Figure 7-figure supplement 1. Down-regulation of PDI family members.** (A-C) Naïve Huh7-NTCP  
1233 cells (Ctrl+) or shRNA-expressing Huh7-NTCP cells were subjected to flow cytometry (left) and  
1234 western blot (right) analyses, in order to evaluate the expression levels of the indicated PDIs [(A),  
1235 ERp46; (B), ERp57; (C), ERp72] before or after down-regulation. Huh7-NTCP cells stained with  
1236 secondary antibody only (Neg) were used to provide the background of flow cytometry analyses.

1237

1238 **Figure 7-figure supplement 2. NTCP expression in target cells.** (A) Huh7-NTCP and Huh7-NTCP-  
1239 tat cells were subjected to flow cytometry analysis, in order to evaluate the expression of NTCP at  
1240 intracellular and cell surface levels, as indicated. Cells stained with secondary antibody only (Neg)  
1241 were used to provide the background of flow cytometry analyses. (B) Huh7-NTCP and (C) Huh7-  
1242 NTCP-tat cells were subjected to flow cytometry analysis, in order to evaluate the expression of NTCP  
1243 after the stable expression of shRNAs targeting the indicated PDIs. Non-transduced cells were used  
1244 as positive control (Ctrl+) and cells stained with secondary antibody only (Neg) were used to provide  
1245 the background of flow cytometry analysis.

1246

1247 **Figure 9-figure supplement 1.** (A) NTZ at 30  $\mu\text{g}/\text{mL}$  was added to the cell supernatant 2h before  
1248 infection (2h-) vs. at the onset of infection (0h), at 4h (4h+) or at 16h (16h+) post-infection. DMSO was  
1249 used as control vehicle. At 7 days post-infection, HDV RNAs were extracted from cells and quantified  
1250 by RTqPCR. The results are expressed after normalization with GAPDH RNAs as means  $\pm$  SD (N=4)

1251 per mL of cell lysates containing  $10^6$  cells. **(B-E)** Study of NTZ effect in HBV *in vivo*. 4-8 weeks old  
1252 NOD-FRG mice were engrafted with primary human hepatocytes (PHH). After *ca.* 2-3 months, the  
1253 animals displaying HSA levels >15 mg/mL were split in 4 groups that were infected with HBV ( $10^8$   
1254 GE/mouse) with or without NTZ. See schedule in Figure 9A. At different time points post-infection,  
1255 blood samples (50  $\mu$ l) were collected and the viremia in sera was monitored by qPCR on the HBV  
1256 genome (GE/mL of serum) The graphs show the results of viremia for individual mice within each  
1257 group. **(B)** Group #1: mice were infected and inoculated with DMSO, **(C)** Group #2: mice were infected  
1258 and inoculated with NTZ (100 mg/kg), **(D)** Group #3: mice were only inoculated with NTZ (100 mg/kg)  
1259 and **(E)** Group #4: mice were only inoculated with DMSO (used as control vehicle of NTZ).  
1260



1261 **Legend to Supplementary file**

1262

1263 **Supplementary file 1. Oligonucleotide sequences used for shRNAs and mutagenesis.** The  
1264 sequences correspond to the oligonucleotides used to generate the lentiviral vectors carrying shRNA  
1265 against the indicated PDIs in Figure 7 or the HBV GP mutants described in Figure 2 (preS1 and preS2  
1266 mutants) and in Figures 4 and 5 (CSD mutants).

1267

1268 **Legends to the source data files**

1269

1270 **Figure 1-source data 1. HBV GP fusion trigger is independent of acid pH and NTCP.** The values  
1271 correspond to the data expressed in the graphs displayed in Figure 1A, 1D and 1F.

1272

1273 **Figure 1-source data 2. HBV GP fusion trigger is independent of acid pH and NTCP.** These  
1274 images are the original and uncropped gels that correspond to the blots displayed in Figure 1E. The  
1275 vertical bars correspond to samples that were not described in the Results section.

1276

1277 **Figure 2-source data 1. Functional analysis of predicted HBV fusion peptides.** The values  
1278 correspond to the data expressed in the graphs displayed in Figure 2C, 2D, 2E, 2F, 2I and 2J.

1279

1280 **Figure 2-source data 2. Functional analysis of predicted HBV fusion peptides.** The values  
1281 correspond to the data expressed in the graphs displayed in Figure 2G.

1282

1283 **Figure 2-source data 3. Functional analysis of predicted HBV fusion peptides.** The values  
1284 correspond to the data expressed in the graphs displayed in Figure 2H.

1285

1286 **Figure 3-source data 1. DTNB, a thiol-specific oxidizing reagent, inhibits HBV membrane  
1287 fusion.** The values correspond to the data expressed in the graphs displayed in Figure 3A and 3B.

1288

1289 **Figure 3-source data 2. DTNB, a thiol-specific oxidizing reagent, inhibits HBV membrane  
1290 fusion.** These images are the original and uncropped gels that correspond to the blots displayed in  
1291 Figure 3C.

1292

1293 **Figure 3-source data 3. DTNB, a thiol-specific oxidizing reagent, inhibits HBV membrane  
1294 fusion.** These images are the original and uncropped gels that correspond to the blots displayed in  
1295 Figure 3D.

1296

1297 **Figure 5-source data 1. Evidence for a functional role of the CSD in the region 294-317 of the  
1298 HBV S GP.** The values correspond to the data expressed in the graphs displayed in Figure 5A-5C.

1299

1300 **Figure 5-source data 2. Evidence for a functional role of the CSD in the region 294-317 of the  
1301 HBV S GP.** The values correspond to the data expressed in the graphs displayed in Figure 5D.

1302

1303 **Figure 5-source data 3. Evidence for a functional role of the CSD in the region 294-317 of the**  
1304 **HBV S GP.** These images are the original and uncropped gels that correspond to the blots displayed  
1305 in Figure 5C. The vertical bars correspond to samples that were not described in the Results section.

1306

1307 **Figure 6-source data 1. PDI inhibitors in HBV entry.** The values correspond to the data expressed  
1308 in the graphs displayed in Figure 6A-6D.

1309

1310 **Figure 7-source data 1. ERp57 down-regulation inhibits in HBV entry.** The values correspond to  
1311 the data expressed in the graphs displayed in Figure 7B-7D.

1312

1313 **Figure 9-source data 1. *In vivo* assessment of ERp57 inhibition.** The values correspond to the  
1314 data expressed in the graphs displayed in Figure 9B.

1315

1316

1317

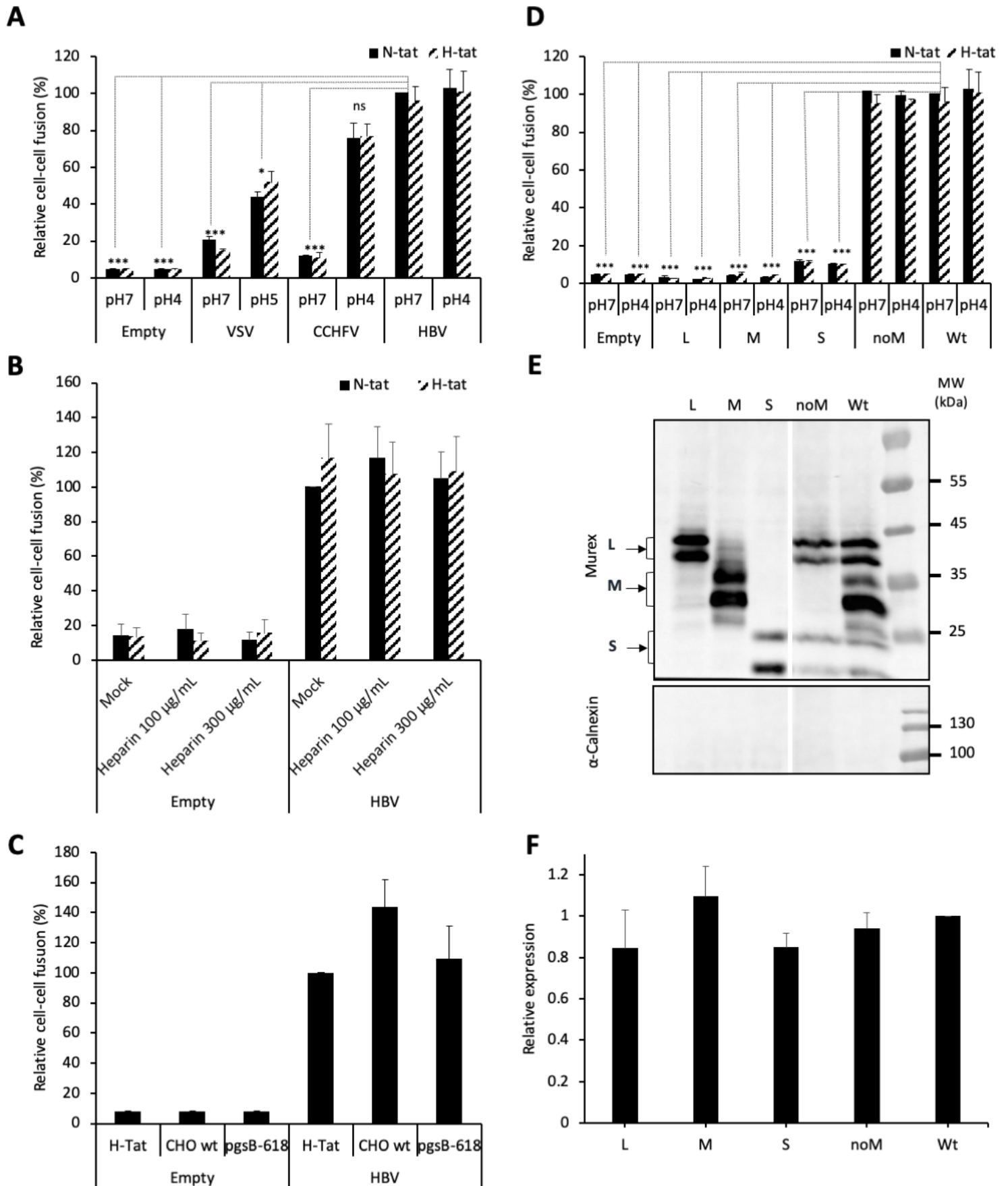


Figure 1. Pérez-Vargas et al.

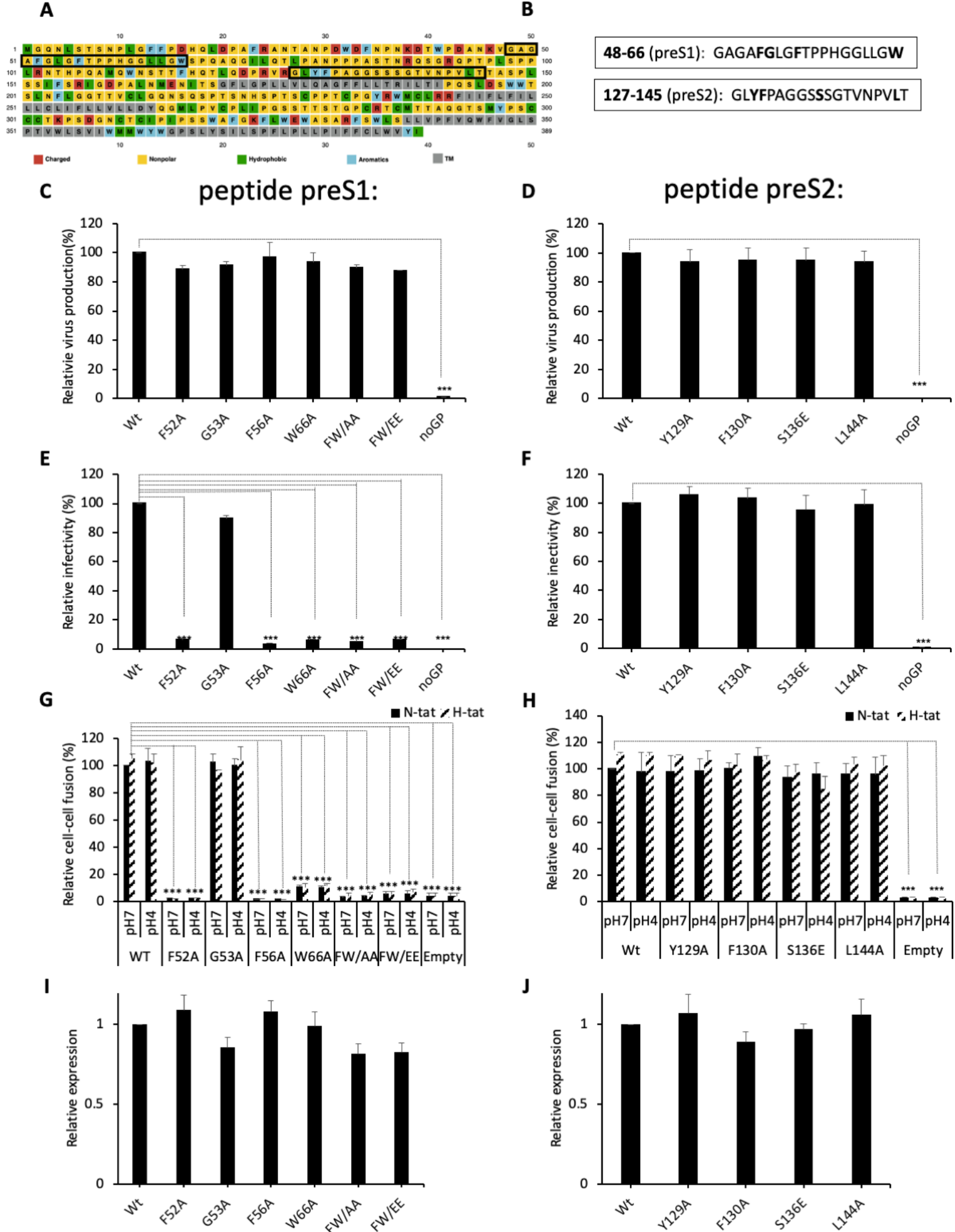


Figure 2. Pérez-Vargas et al.

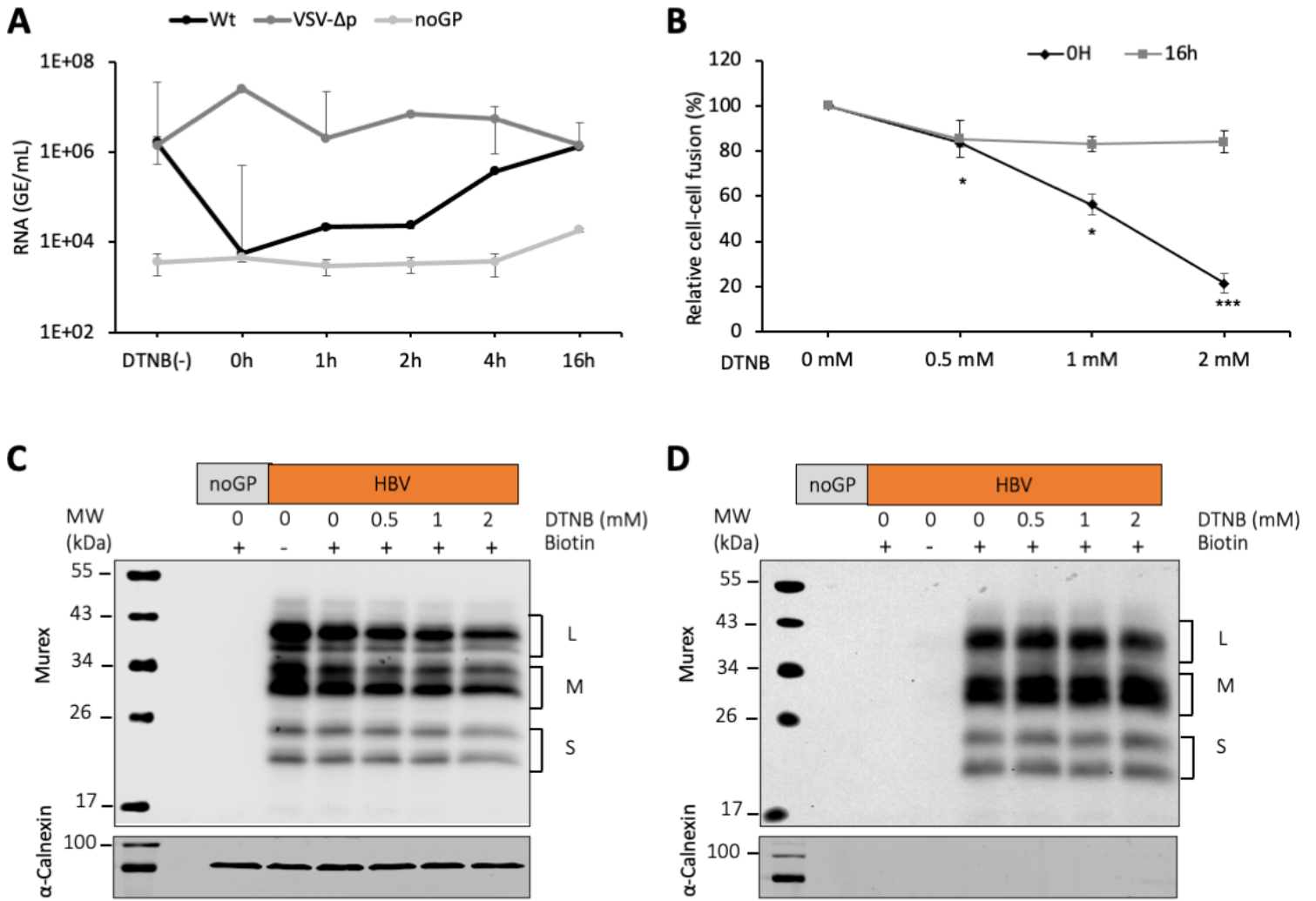
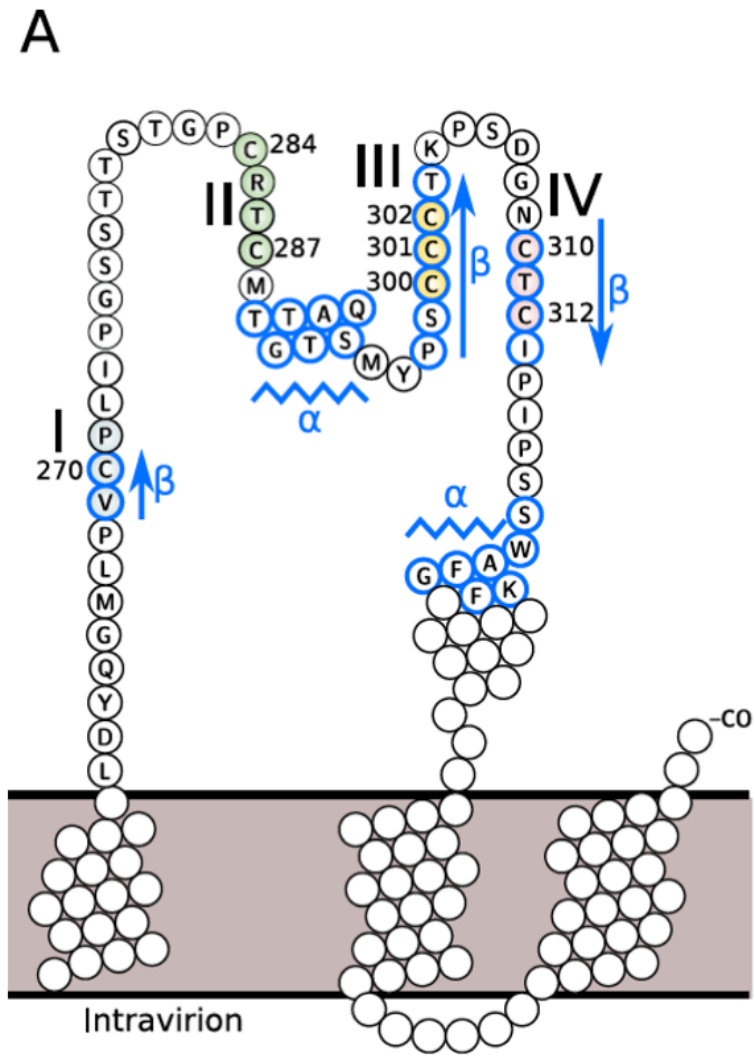


Figure 3. Pérez-Vargas et al.



**B**

	II				III			IV			
	284	285	286	287	300	301	302	310	311	312	
I	269	0.30	0.18	0.19	0.28	0.38	0.39	0.30	0.38	0.39	0.45
	C270	0.47	0.23	0.26	0.43	0.53	0.58	0.47	0.57	0.40	0.57
	271	0.29	0.20	0.22	0.31	0.35	0.35	0.29	0.35	0.34	0.35
II	C284					0.60	0.58	0.52	0.64	0.45	0.62
	285					0.40	0.38	0.30	0.36	0.27	0.34
	286					0.44	0.36	0.28	0.38	0.35	0.39
	C287					0.58	0.50	0.40	0.49	0.35	0.58
III	C300								0.49	0.43	<b>0.83</b>
	C301								0.62	0.54	<b>0.84</b>
	C302								<b>0.87</b>	<b>0.78</b>	<b>0.84</b>

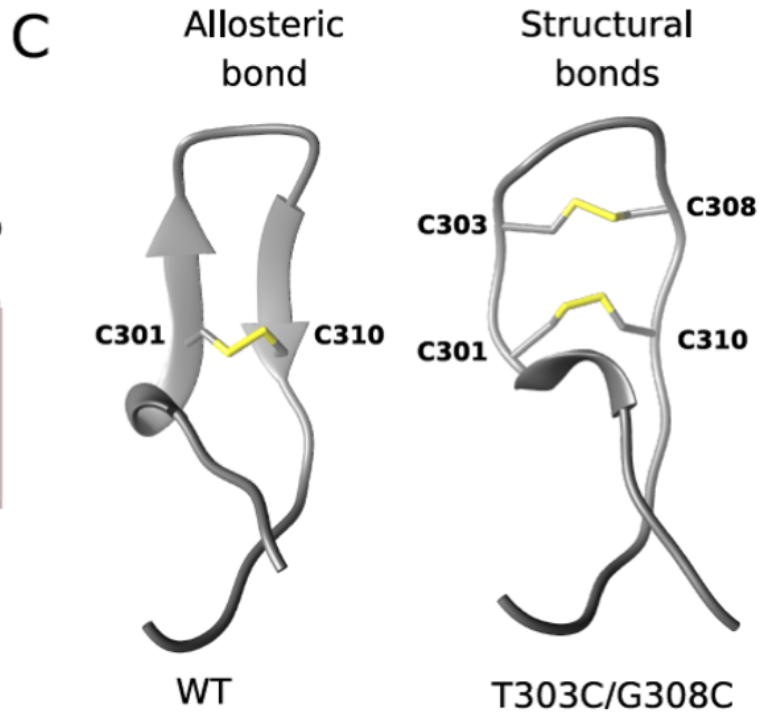


Figure 4. Pérez-Vargas et al.

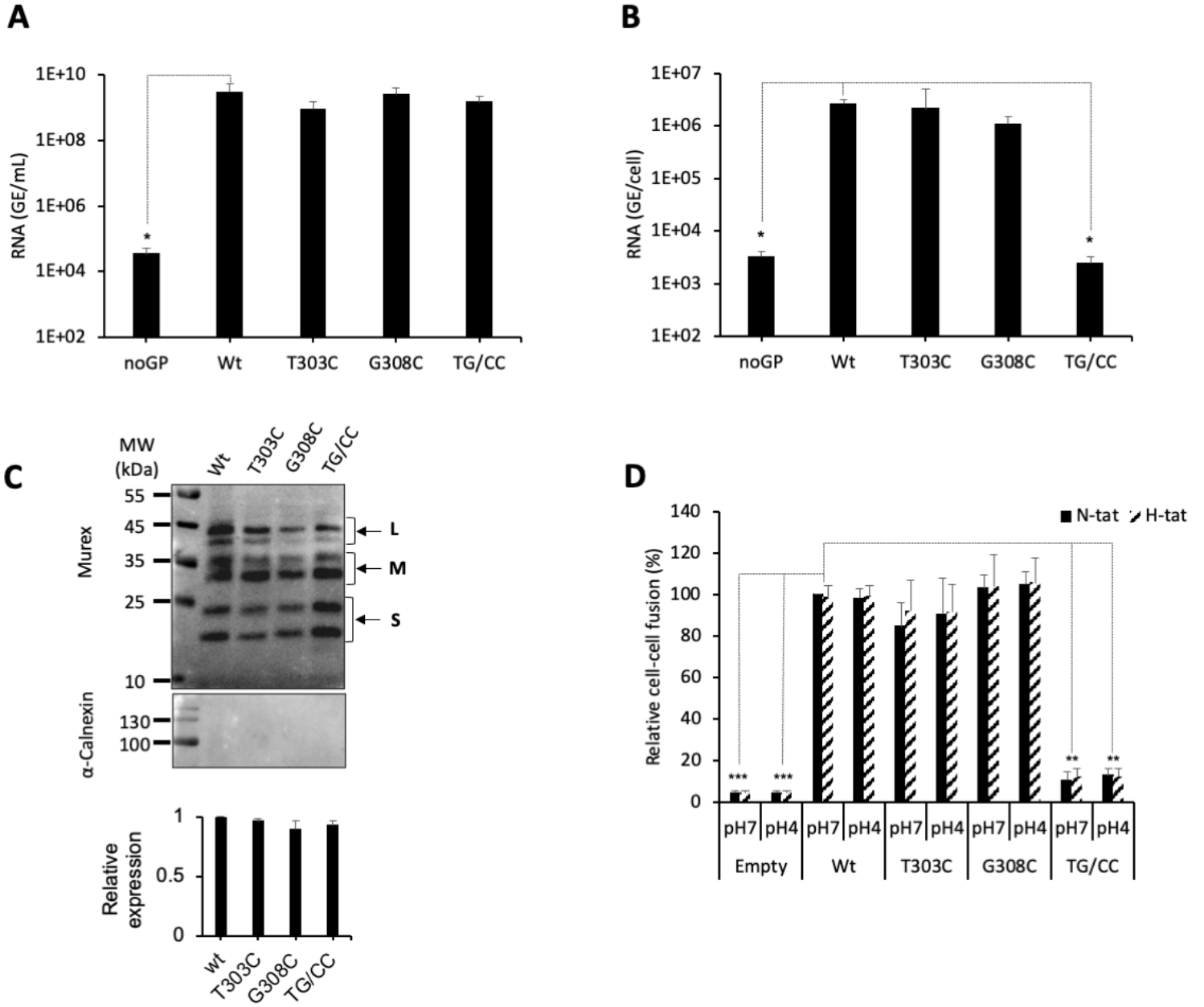


Figure 5. Pérez-Vargas et al.



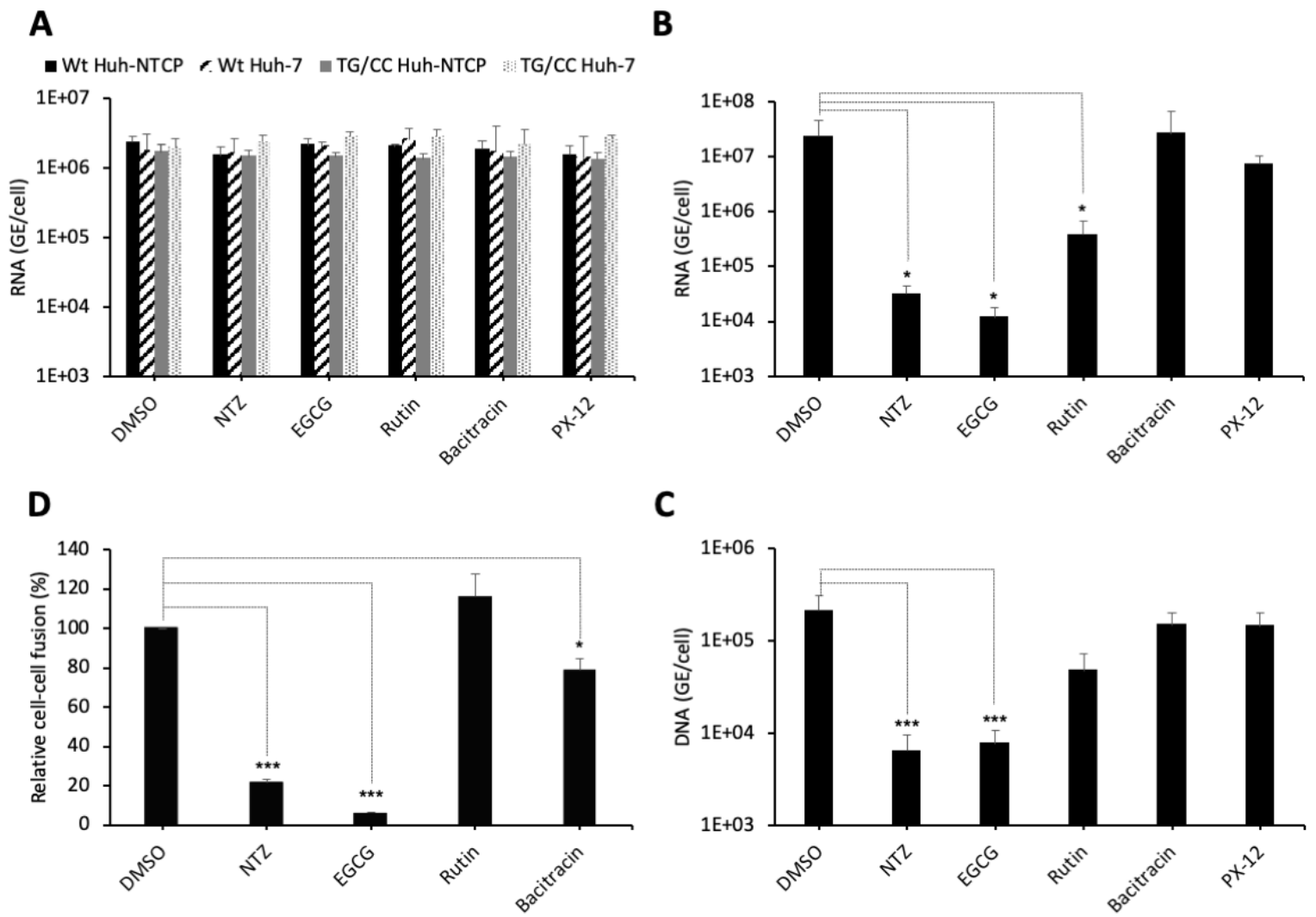


Figure 6. Pérez-Vargas et al.

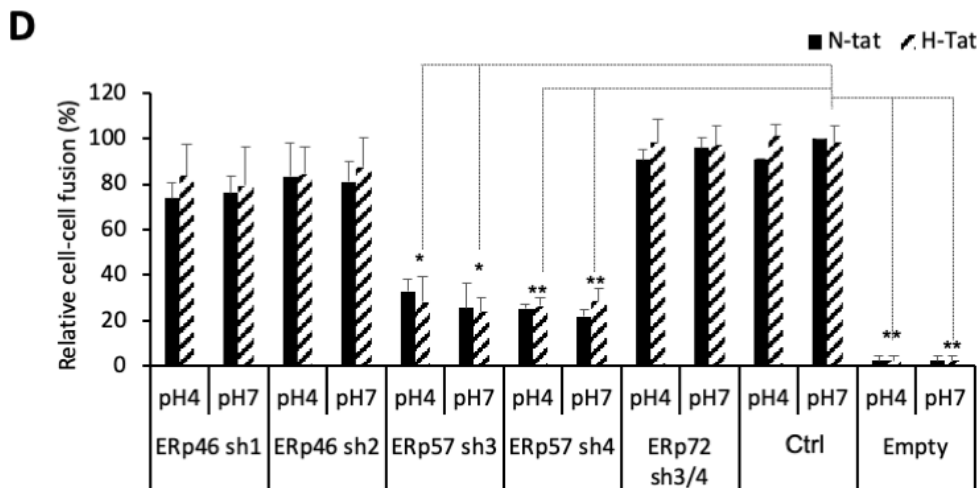
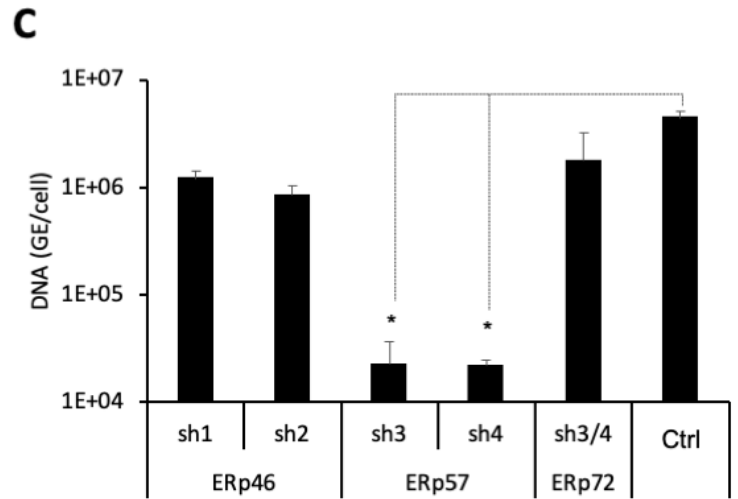
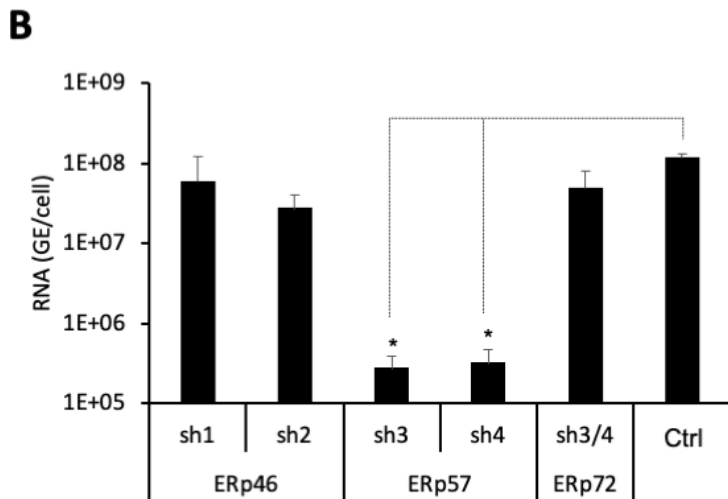
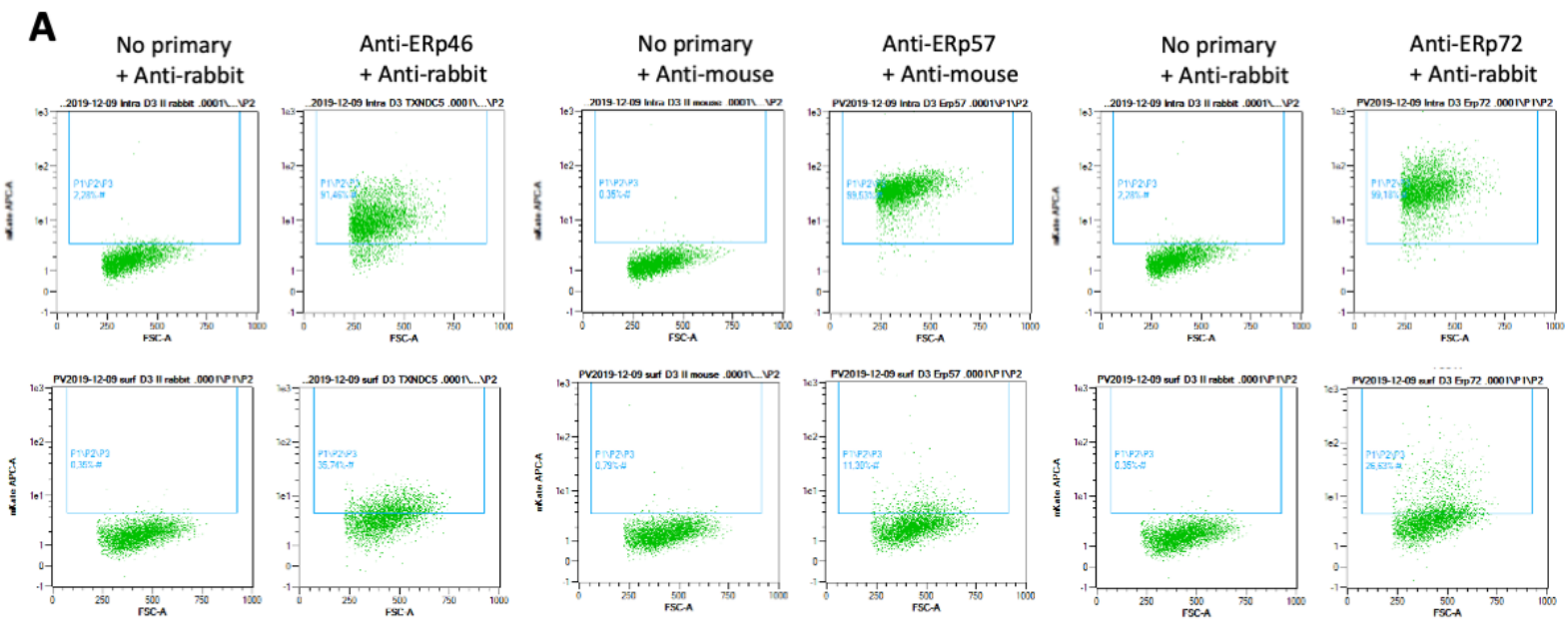


Figure 7. Pérez-Vargas et al.

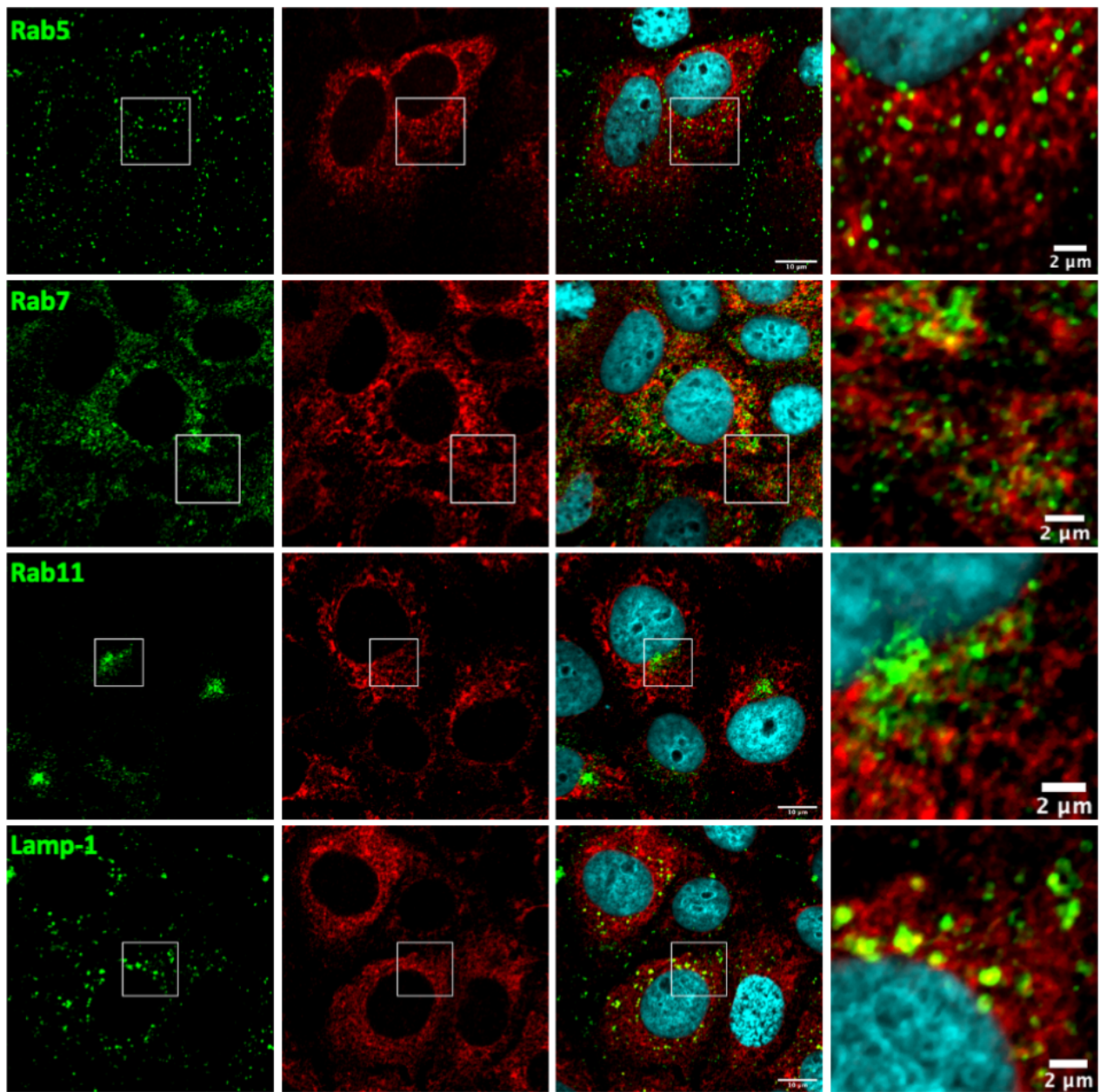
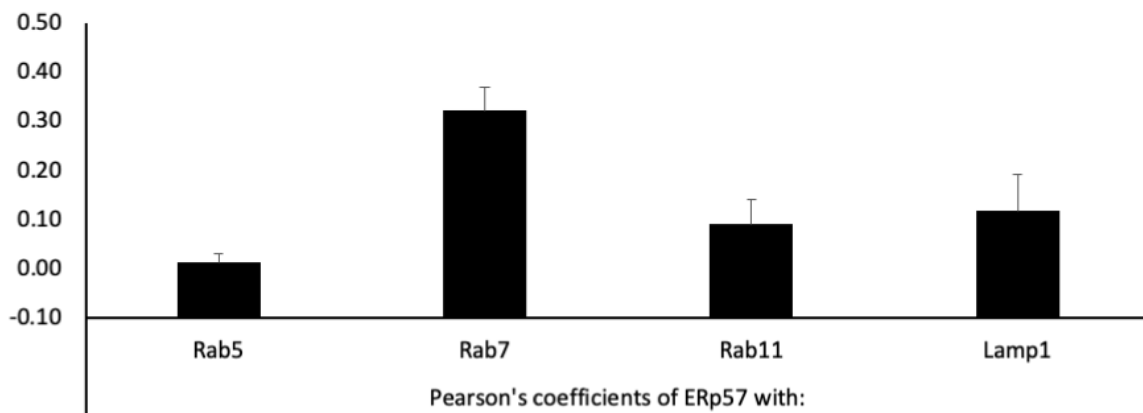
**A****B**

Figure 8. Pérez-Vargas et al.

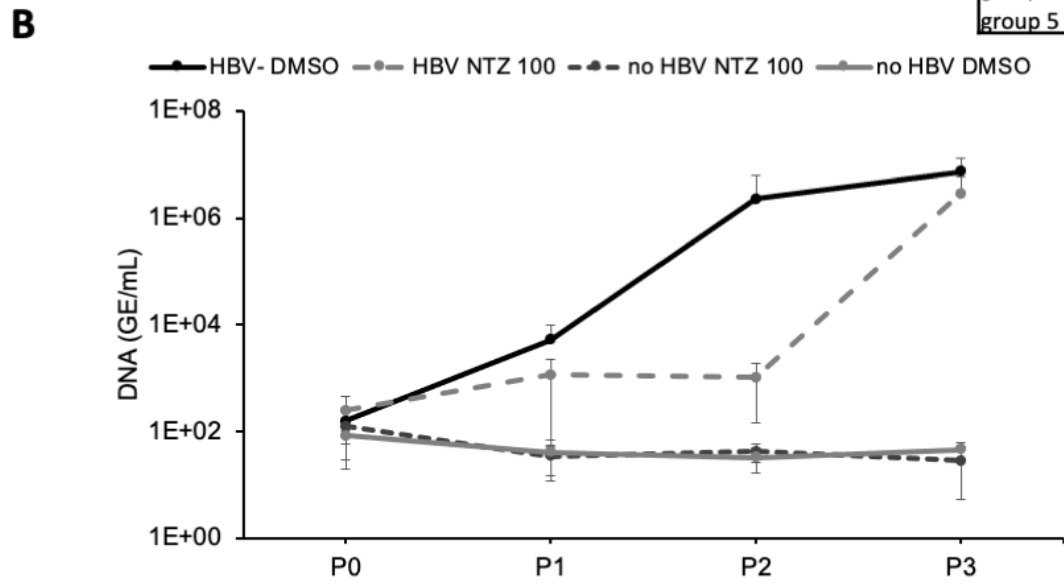
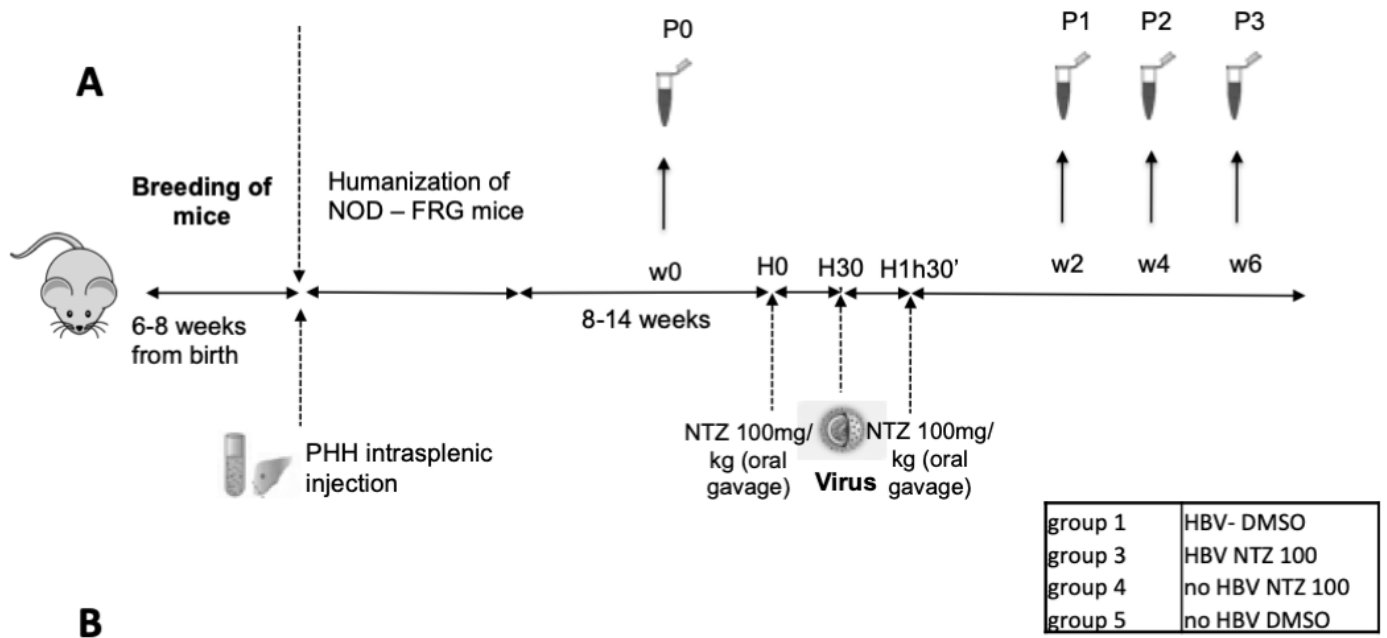


Figure 9. Pérez-Vargas et al.

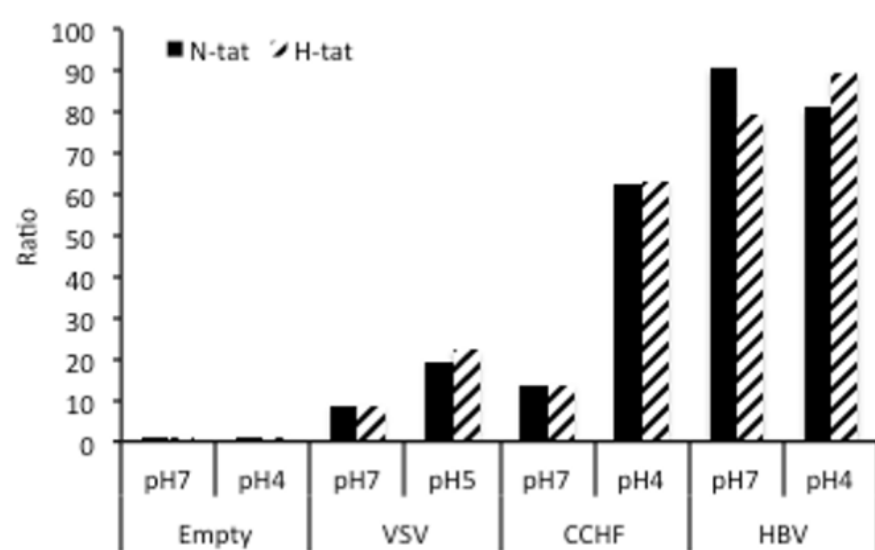
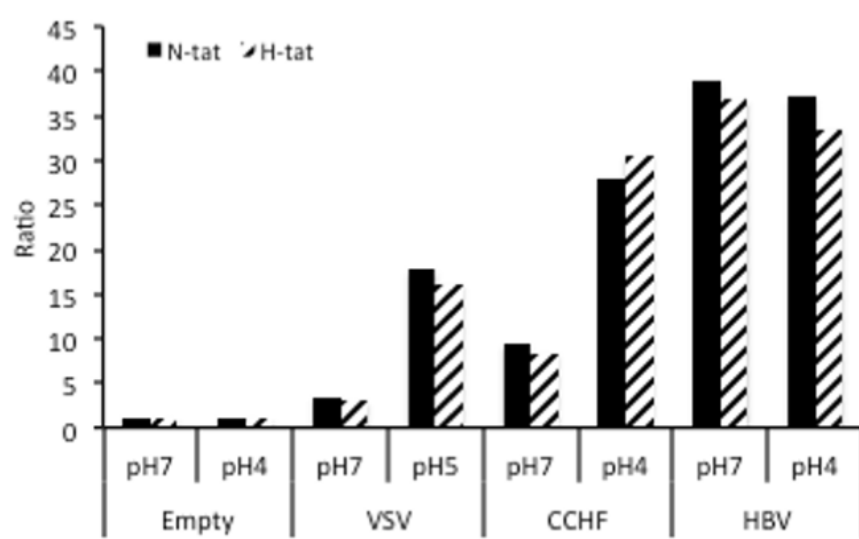
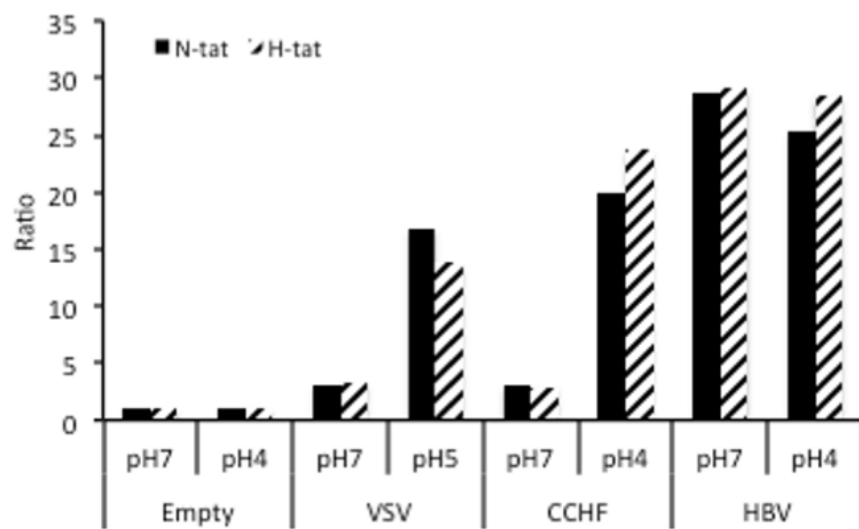


Figure 1-figure supplement 1

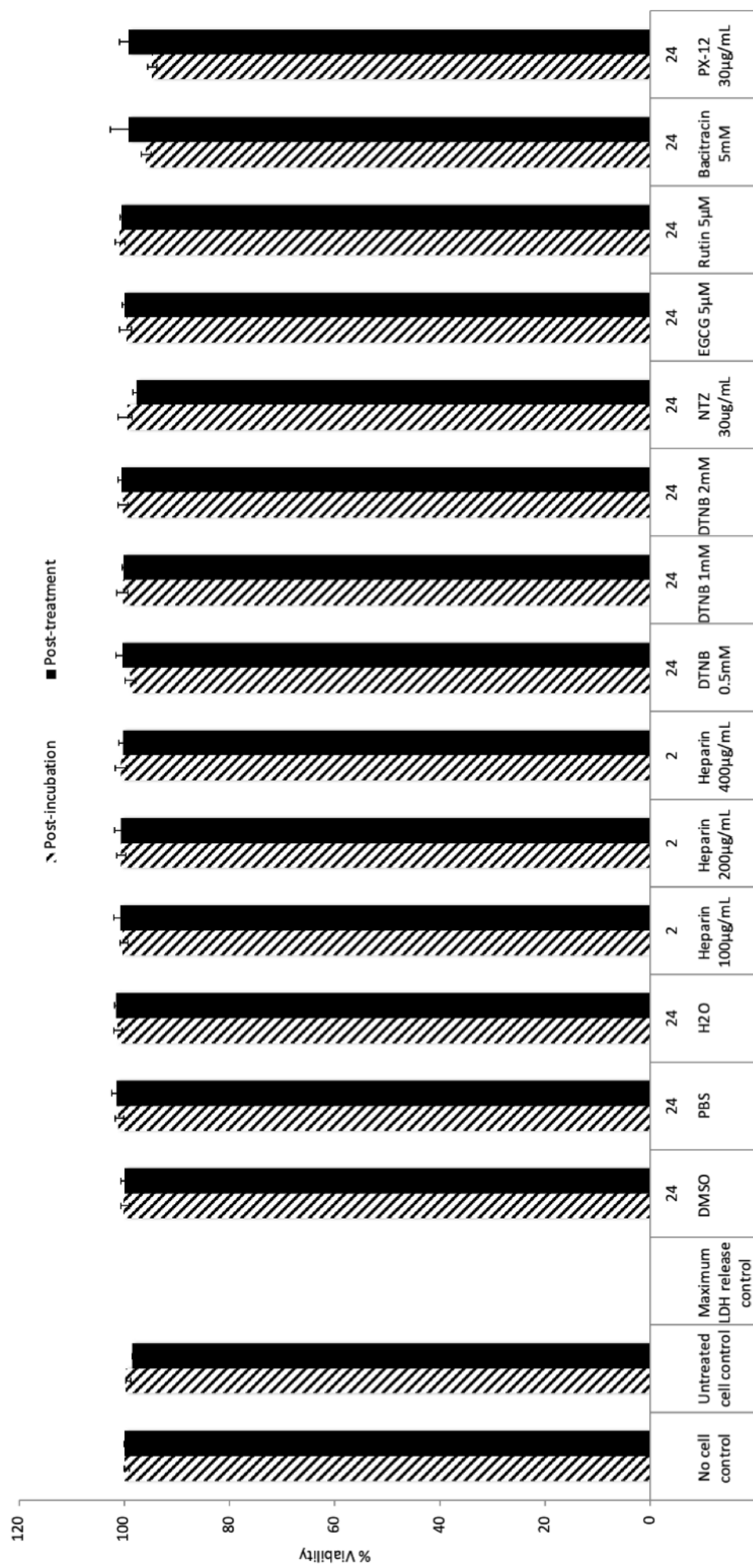


Figure 1-figure supplement 2

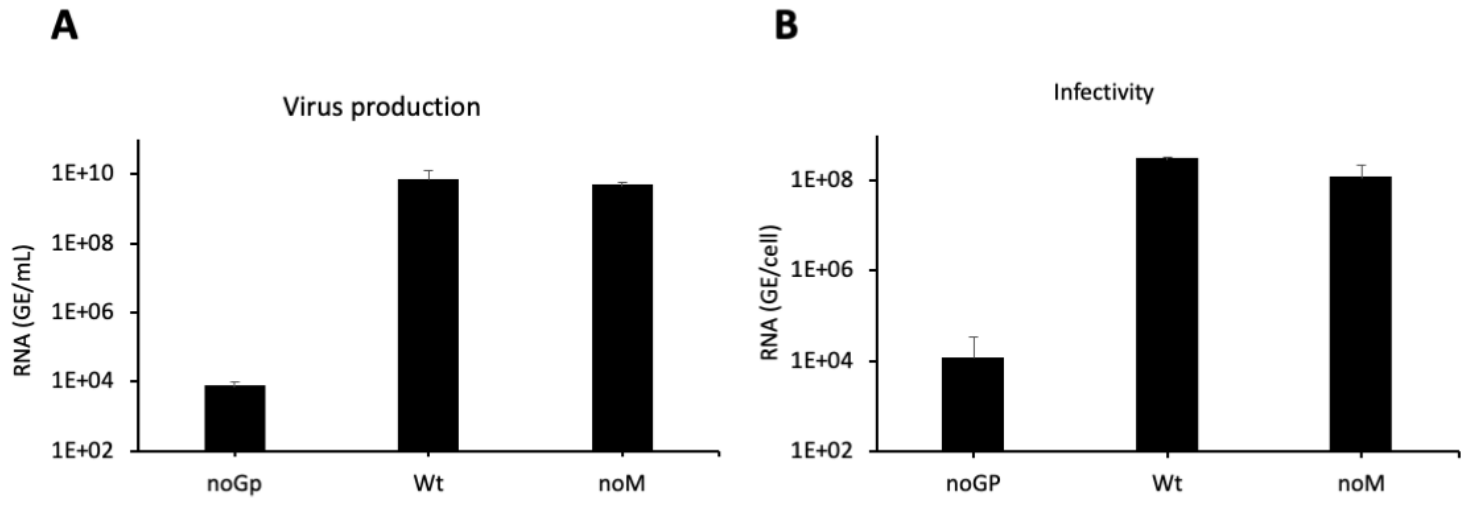


Figure 1-figure supplement 3

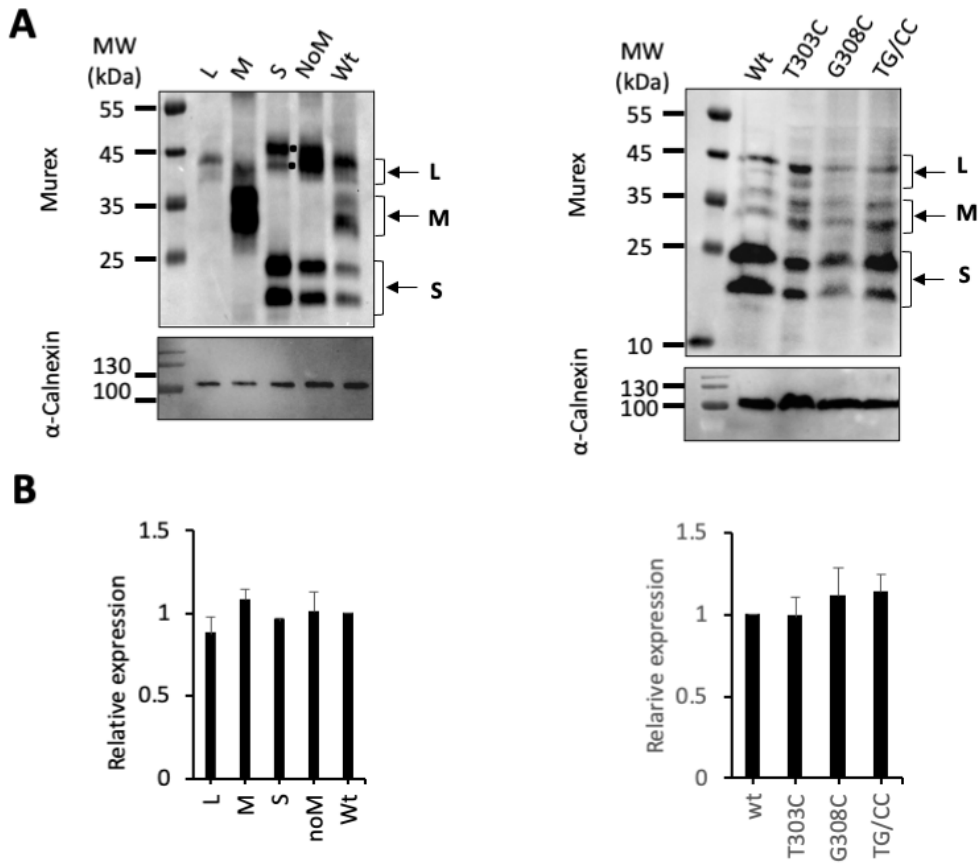
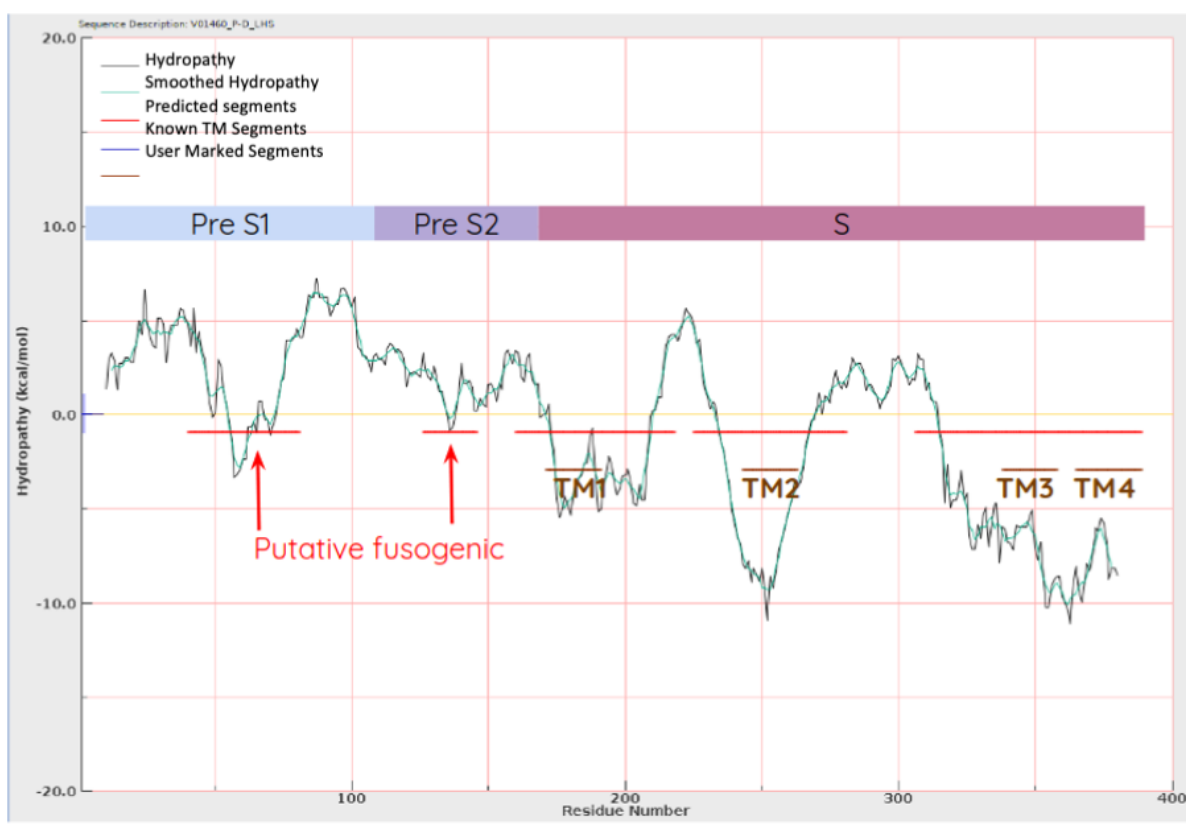


Figure 1-figure supplement 4



**A****B**

First fusion candidate			Second fusion candidate		
	$\Delta G$ (Kcal/mol)	Predicted region		$\Delta G$ (Kcal/mol)	Predicted region
wt	-3.38	48-66	wt	-0.85	127-145
F52A	-2.08	48-66	Y129A	-	-
G53A	-3.22	48-66	F130A	-	-
F56A	-2.08	48-66	S136E	-	-
W66A	-1.46	47-65	L144A	-0.12	127-145
F52A/W56A	-0.16	61-79			
F52E/W56E	-	-			

Figure 2-figure supplement 1

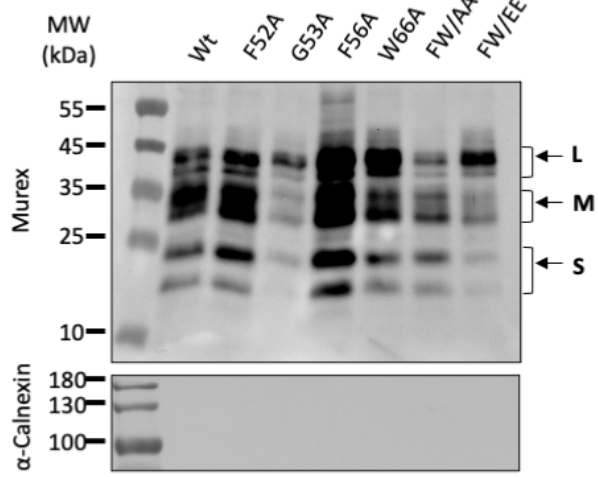
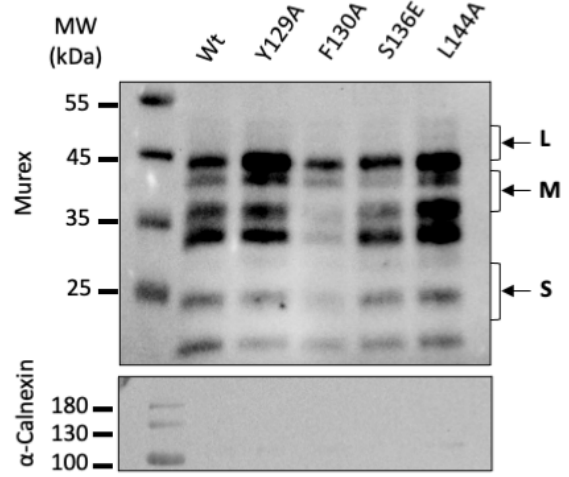
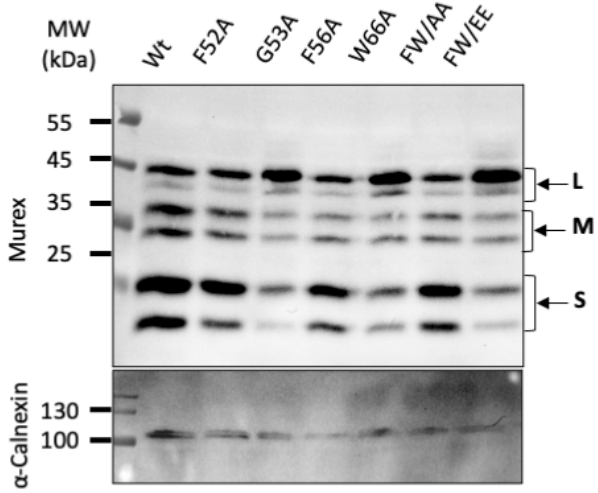
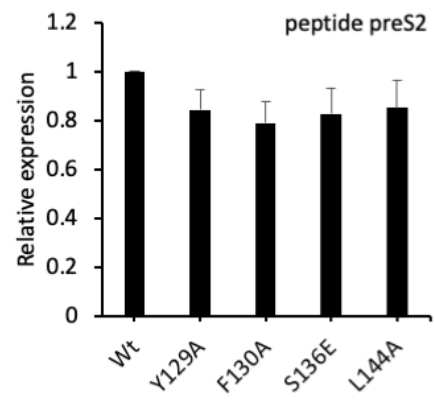
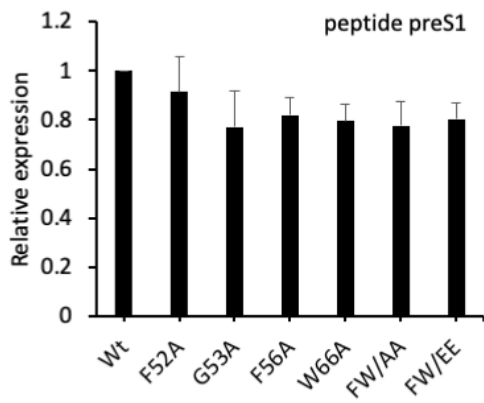
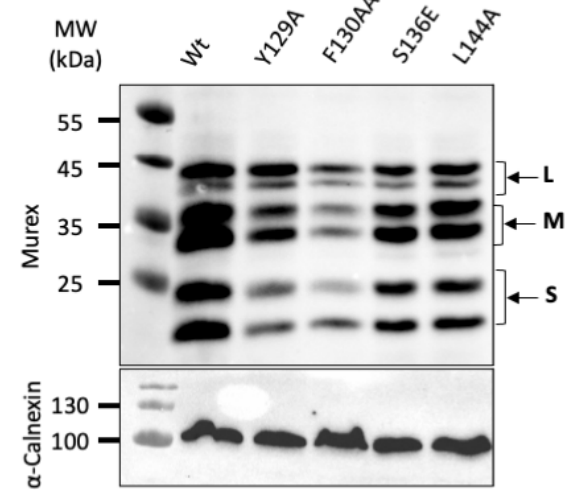
**A****B****C****D**

Figure 2-figure supplement 2

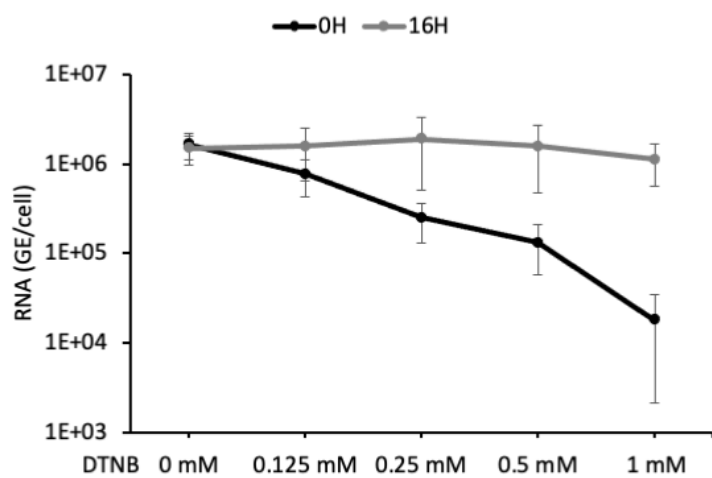
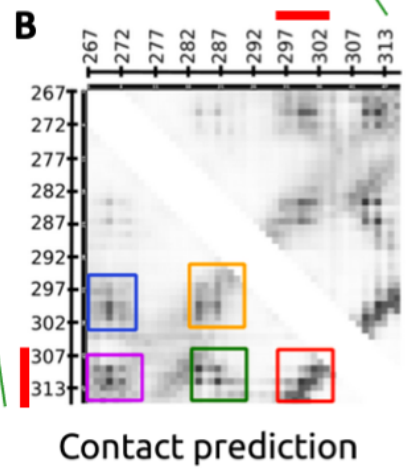
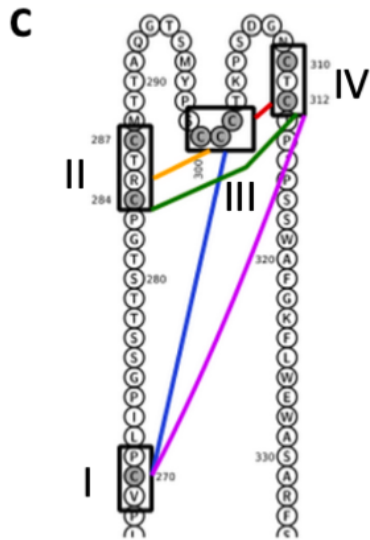
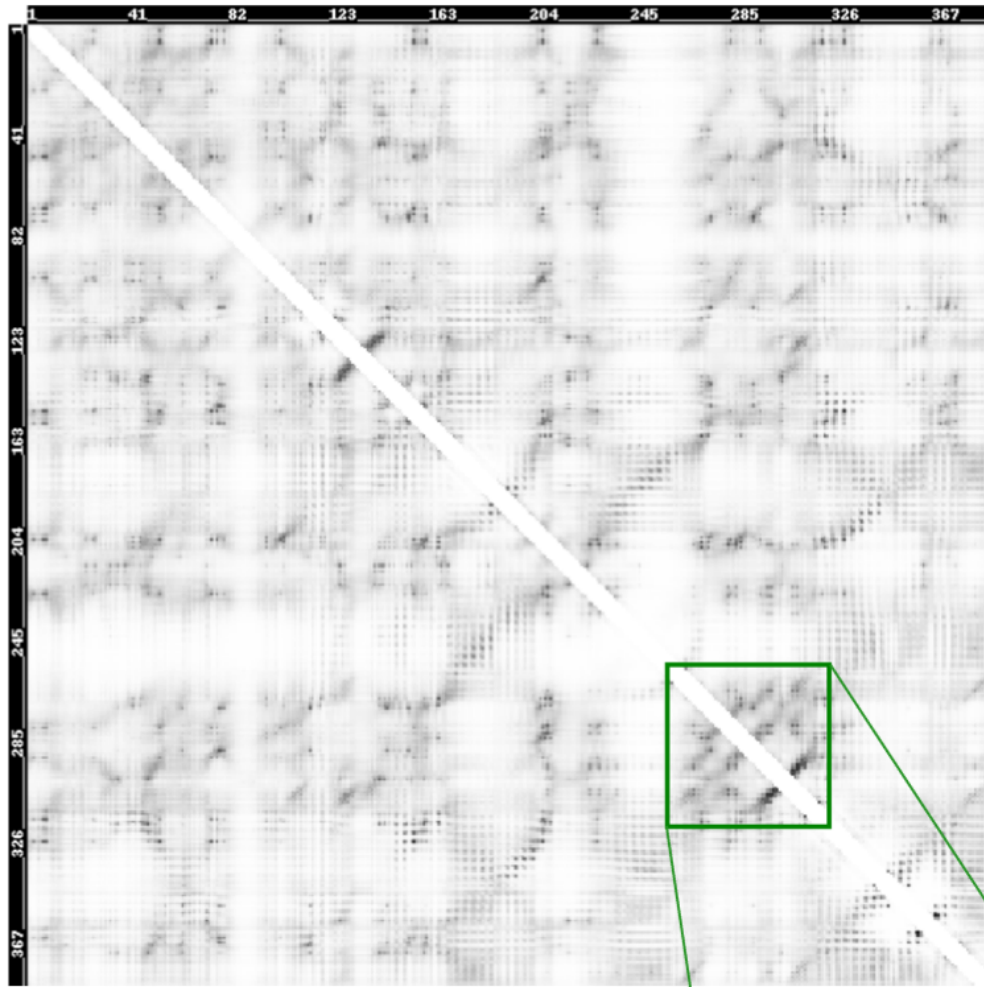


Figure 3-figure supplement 1

**A**

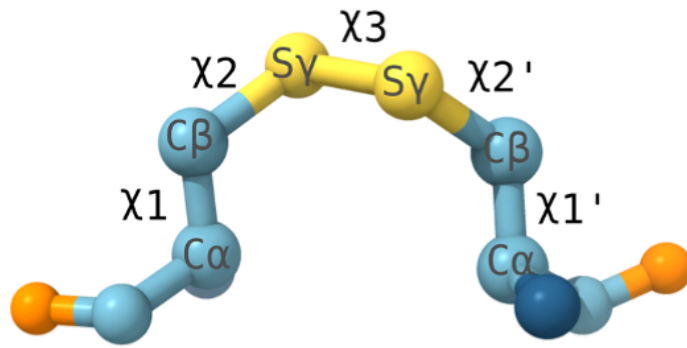


Figure 4-figure supplement 2

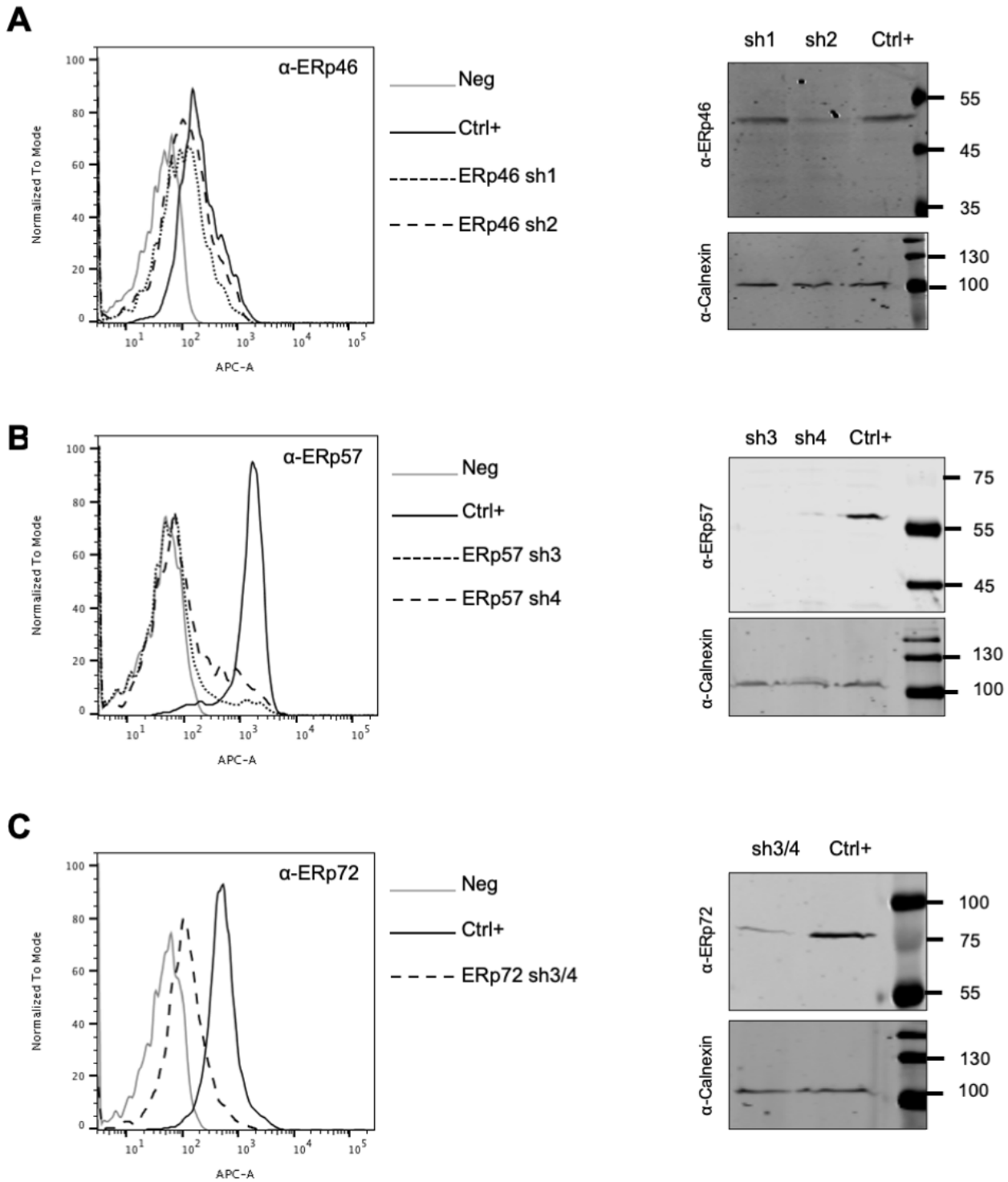


Figure 7-figure supplement 1

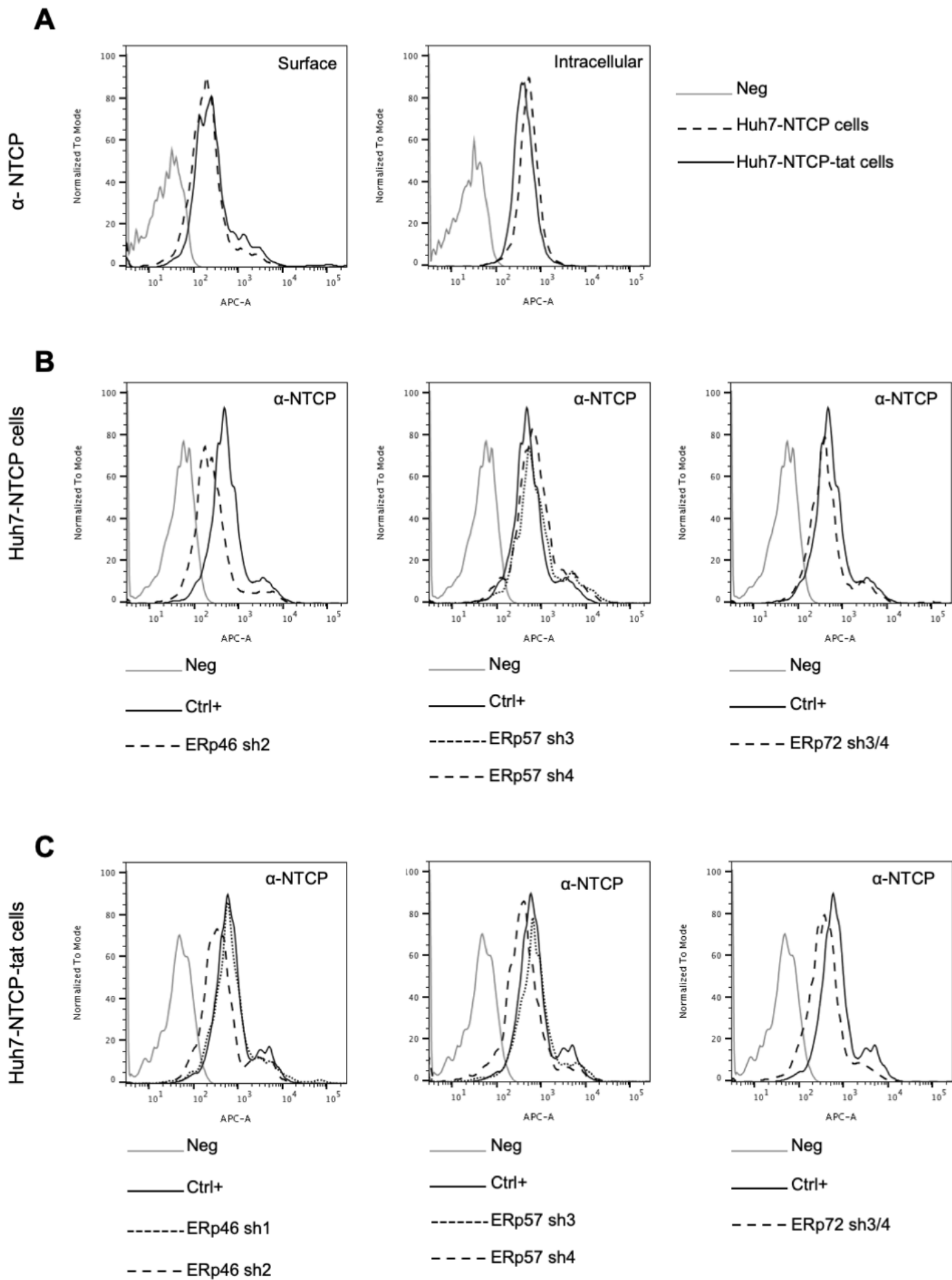


Figure 7-figure supplement 2

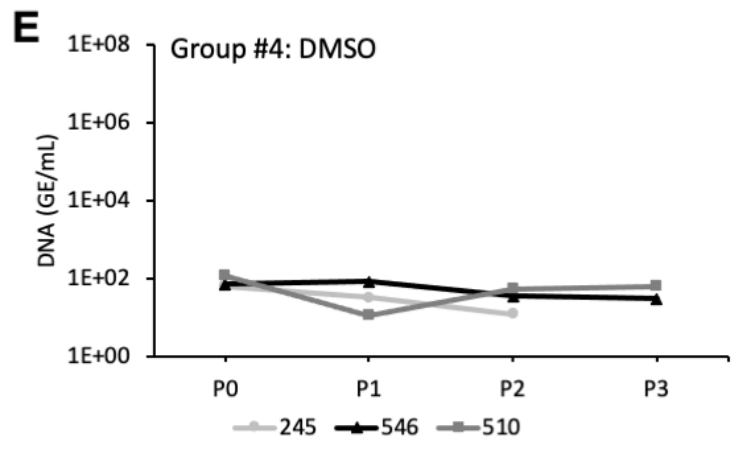
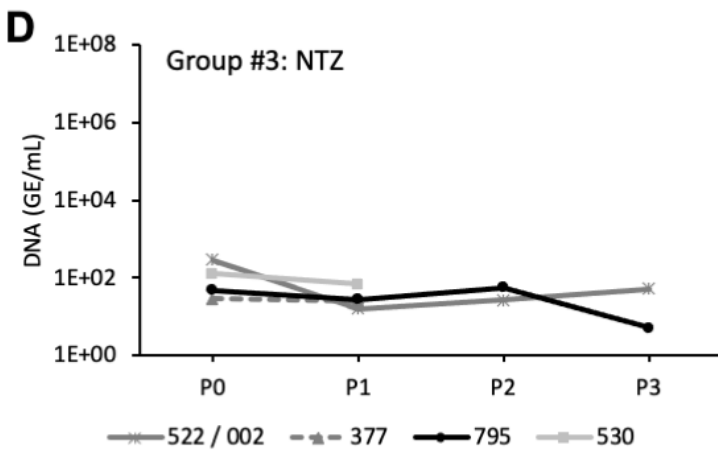
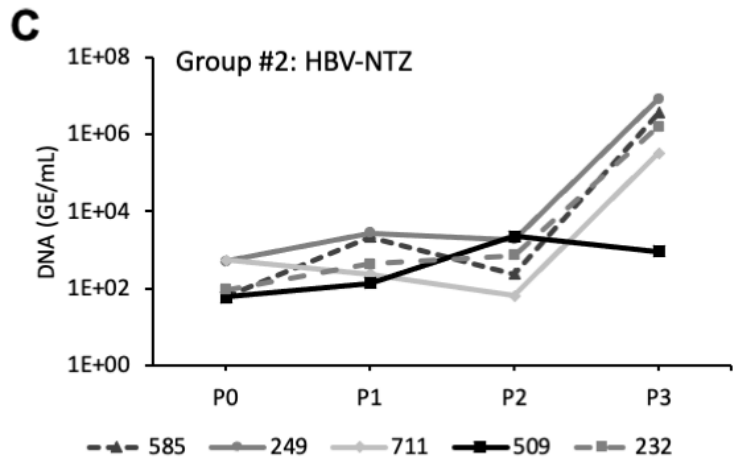
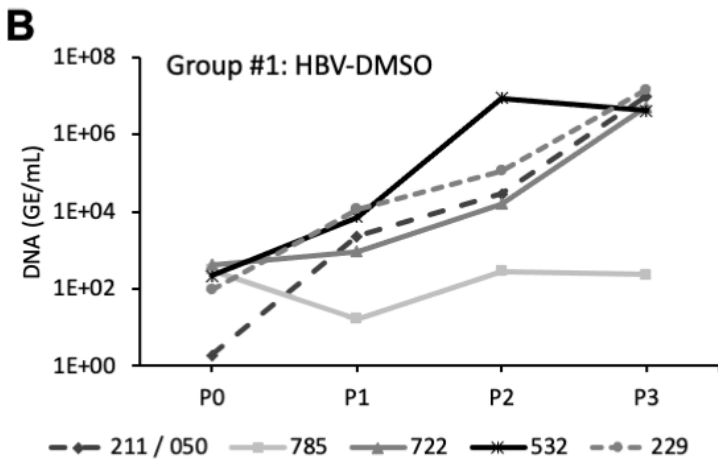
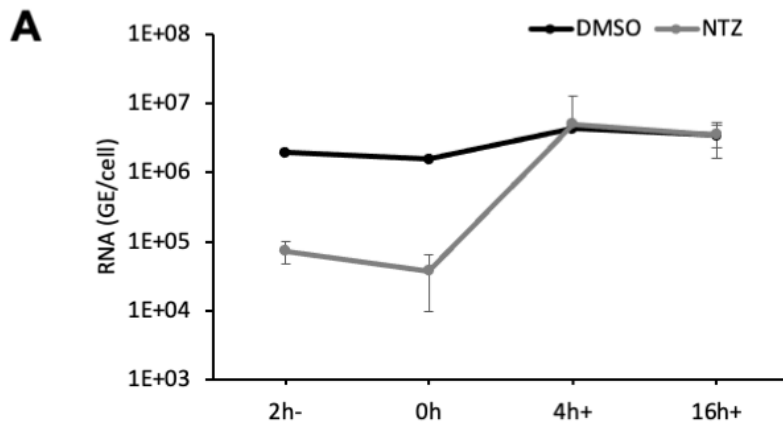


Figure 9-figure supplement 1